UAVs Employment in the Next Generation Wireless Communication Systems

by

Hamzih Alsmadi

Graduate Program

in

Department of Electrical and Computer Engineering

A thesis submitted in partial fulfillment of the requirements

for the degree of Doctor of Philosophy (Ph.D.)

The Faculty of Graduate Studies

Lakehead University

Thunder Bay, Ontario, Canada

August 2023

Examining Committee Membership

The following served on the Examining Committee for this thesis. The decision of the Examining Committee is by majority vote.

External Examiner: Rami Mustafa A Mohammad, Associate Professor
Dept. of Computer Information Systems,
College of Computer Science and Information Technology
Imam Abdulrahman Bin Faisal University, Dammam, Saudi Arabia

Internal Members: Apparao Dekka, Assistant Professor
Dept. of Electrical and Computer Engineering
Lakehead University, Canada

Shafiqul Hai, Assistant Professor
Dept. of Electrical and Computer Engineering
Lakehead University, Canada

Supervisor: Salama Ikki, Professor
Dept. of Electrical Engineering and Computer
Lakehead University, Canada

Declaration

I hereby declare that I am the sole author of this thesis. This is a true copy of the thesis, including any required final revisions, as accepted by my examiners.

I understand that my thesis may be made electronically available to the public.

Dedication

With profound gratitude and a heavy heart, I dedicate this thesis to my late father, '**Mohammad Alsmadi**'. He was not only my mentor but also a constant source of inspiration, always pushing me to reach greater heights in life. Though he may no longer be physically present, his influence remains etched in my heart, fueling my determination to make him proud.

To my mother for her prayers and Dua.

To my wife and daughters for their support and endless love.

To my sisters, brothers and friends for their support.

To everyone who believes in me, I dedicate this thesis.

Acknowledgements

"Firstly, I extend my heartfelt gratitude to Allah (SWT) for providing me with the strength and capability to complete this work, "Alhamdulillah".

The successful completion of this thesis is attributed to the unwavering support and guidance of numerous individuals, to whom I extend my humble thanks. I express my deepest appreciation to my supervisor, Dr. Salama Ikki. His trust in my abilities by agreeing to supervise this research, coupled with his consistent support, invaluable advice, and motivation throughout my Ph.D. tenure, played a pivotal role in my academic journey. His expert advice in designing the research questions and methodology was critical to the realization of this work. The constructive critique he provided served as a catalyst in refining my thoughts and elevating my work to greater heights. I would also like to extend my heartfelt thanks to the committee members, Dr.Rami Mustafa, Dr. Shafiqul Hai and Dr. Apparao Dekka, for their willingness to review this work. Their insightful comments have undeniably aided in enhancing this thesis. Last but not least, my family is my priority and the most important in my life, my sincere appreciation and respect to all of you, especially my parents. I would like to say that you are the main source of inspiration in my life. Last, but certainly not least, I offer profound thanks to my late father, my mother, my father-in-law, and my mother-in-law. Their wisdom, compassion, unwavering support, and selfless sacrifices have consistently guided me. Their steadfast presence was crucial to my journey. Equally, I could not have reached this milestone without the support of my wife, Ameera Alsaradgeh, and my daughters Retal, Talien, Larien, and Aryam. Their strength and encouragement enabled me to fulfill my commitments and achieve what I initially set out to do. A special word of gratitude goes to my brother, Dr. Malek, as well as to all my siblings and friends for their enduring love, support, and prayers. Life, with its myriad challenges, has taught me invaluable lessons in my quest to reach my goals. These challenges helped me to forge strong working relationships and learn the importance of self-encouragement and resilience. I am truly grateful for the growth I have experienced and the achievements I have accomplished during this journey.

Abstract

New network architectures of communication systems are required to support and connect the next generation of wireless networks. This thesis focuses on unmanned aerial vehicles (UAVs) as integral components of future wireless networks. Specifically, this work addresses the optimization problem of association between the wireless access points (WAPs) and UAVs, aiming to maximize the total weighted sum rate. This optimization problem is subjected to fulfilling quality of service (QoS), number of links, available bandwidth, fairness, and coverage constraints. To address this challenge, a centralized algorithm with reduced complexity is proposed for solving the association problem. The results demonstrate that this algorithm's solution offers excellent performance compared to suboptimal alternatives and approach the exhaustive search technique while significantly reducing computational complexity.

Furthermore, the channel assignment in the context of UAVs-supported wireless networks is investigated. By selecting from a pool of channels provided by a main core network, a joint optimization problem is formulated. The objective here is to find an optimal solution for the association problem between WAPs and UAVs, maximizing the total weighted sum rate using a max-min total sum data rate optimization approach. This formulation incorporates considerations of QoS, a maximum number of links, and available bandwidth constraints. It is important to note that the formulated problems are Non-deterministic polynomial time (NP)-hard and become computationally intensive as the number of WAPs increases.

In addition, this work analyzes the effects of hardware impairments (HWIs) on UAVs and ground station (GS) communication systems since HWIs are inherent in practical communication systems. To this end, the average ergodic capacity of the system is derived by considering the Rician fading channel conditions between the UAV and the GS. The analysis considers the average over a random three-dimensional trajectory movement, including the angle of arrival and the distance between the UAVs and the GS. Additionally, asymptotic analysis is conducted for cases where the transmit power of the UAVs and the

number of GS antennas become exceptionally large. Extensive MATLAB simulations are provided to validate the gained results.

In the same context, this thesis further investigates the employment of UAVs-assisted over-the-air computation (OAC) communication systems. OAC is a technique that enables data aggregation from numerous nodes with limited bandwidth. UAVs can serve as fusion centers (FCs) in OAC, allowing for rapid data aggregation from massive number of sensors. Nonetheless, the presence of HWIs and imperfect Channel State Information (CSI) pose challenges to OAC. While prior studies assumed ideal hardware and perfect CSI, this study investigates the joint impact of HWIs and imperfect CSI on the average square error (MSE) performance of OAC. By considering a common channel estimation approach that utilizes reference signals from the FC, a closed-form expression for MSE is derived, revealing the negative impact of HWIs and channel estimation error. Analytical and simulation results demonstrated the presence of MSE floors, even at high signal-to-noise ratio (SNR) levels, indicating the need for system designs to mitigate the effects of HWIs and the significance of accurate channel estimation.

Table of Contents

List of Tables

List of Figures

Abbreviations

5G fifth-generation 1, 27, 29, 32

5G+ fifth-generation and beyond 1, 27, 28

6G sixth-generation 55, 72

ADCs analog-to-digital converters 19

ATG air-to-ground 18, 28, 104

AWGN additive white Gaussian noise 21, 22, 76–78, 90–92

BSs base stations 2, 27, 29, 32, 34, 55–57, 72

CSI channel state information xvi, 5, 7, 30, 88, 89, 92–94, 97–103

DACs digital-to-analog converters 19

EVM error vector magnitude 22, 23, 76

FC fusion center 89–92, 94, 97, 101, 103

FCs fusion centers 87

GS ground station xv, xvi, 5, 6, 27, 29, 31–35, 73–75, 77–86, 103

HWI hardware impairment xv, xvi, 4–7, 19, 21, 22, 30–33, 73, 76–78, 81–86, 88, 89, 91, 92, 94, 97–103

I/Q in-phase/quadrature-phase 19, 20, 30, 76

ILP integer linear programming 9, 10, 60

IM index modulation 1

IoT Internet of things 3, 31, 36, 73, 87

LAPs low-altitude platforms 36

LO local oscillator 19, 20

LoS line-of-sight 3, 18, 19, 24, 25, 27–29, 36, 39, 50, 56, 74, 75, 79, 80, 104

LTE long-term evolution 23

mMIMO massive multiple-input multiple-output 1, 32

mmWave millimeter wave 1

MSE mean squared error 4–7, 88, 89, 92–95, 97–103

NFP network flying platform 30, 32

NLoS Non-line-of-sight 18, 19

NOMA non-orthogonal multiple access 1, 31, 36

NP Non-deterministic polynomial time 30, 35, 41, 56, 60, 61

OAC over-the-air computation 4, 87–89, 91, 97, 101, 103

OTA over-the-air 5, 6, 33

PAMP power amplifier 20, 21

PDF probability density function 79, 80, 89, 95

PL path loss 6, 18, 19, 24, 38–40, 50, 59

QAM quadrature amplitude modulation 23

QoS quality-of-service 28–31, 34, 36, 38–40, 56, 58, 59, 72, 104

RF radio frequency xv, 19–21, 23, 76

SC small cell 36

SCs small cells 30, 35, 36, 56

SDNR received signal-to-distortion plus noise ratio 78

SINR signal to interference and noise ratio xiii, 35, 38–42, 44–46, 50, 53, 58, 102

SNR signal-to-noise ratio xiii, 31, 59–64, 68

THz terahertz 1

UAV unmanned aerial vehicle xv, xvi, 4–6, 18, 19, 23, 25–28, 31–33, 35, 36, 38–40, 42, 44–49, 53, 56–58, 60, 62–67, 72–75, 77–80, 82, 86–90, 101–105

UAVs unmanned aerial vehicles xiii, xv, 2–6, 18, 25–30, 32, 35–39, 41–53, 56–65, 67–70, 72, 73, 87, 101–105

UDN ultra-dense network 1

WAP wireless access point 4, 32, 36, 38–40, 44–46, 48, 49, 57, 58, 60–62, 64–66

WAPs wireless access points xiii, xv, 4–6, 32, 35–39, 41–53, 56–70, 102–104

Chapter 1

Introduction

1.1 Introduction and Motivation

Since 2020, the global deployment of fifth-generation (5G) wireless communication networks has provided advanced features such as massive connectivity, ultra-reliability, and guaranteed low latency. However, it is anticipated that 5G alone will not be able to meet the growing demands beyond 2030 [4, 6]. Consequently, fifth-generation and beyond (5G+) cellular networks are expected to address the challenges and expectations associated with near-future communication networks and cater to high-end user requirements. 5G+ networks will be expected to increase the potential number of connected devices, network coverage, and availability while also extending the battery life of mobile devices by reducing power consumption. Therefore, developing new technologies is crucial to achieving these objectives [7, 8]. The progression of mobile networks can be observed in Fig. 1.1.

To meet the performance expectations and overcome the limitations of current terrestrial cellular systems, new technologies can be utilized in 5G+ wireless communication alongside existing techniques. These include massive multiple-input multiple-output (mMIMO) [9, 10], millimeter wave (mmWave) communications [11], ultra-dense network (UDN), index modulation (IM), non-orthogonal multiple access (NOMA), terahertz (THz)

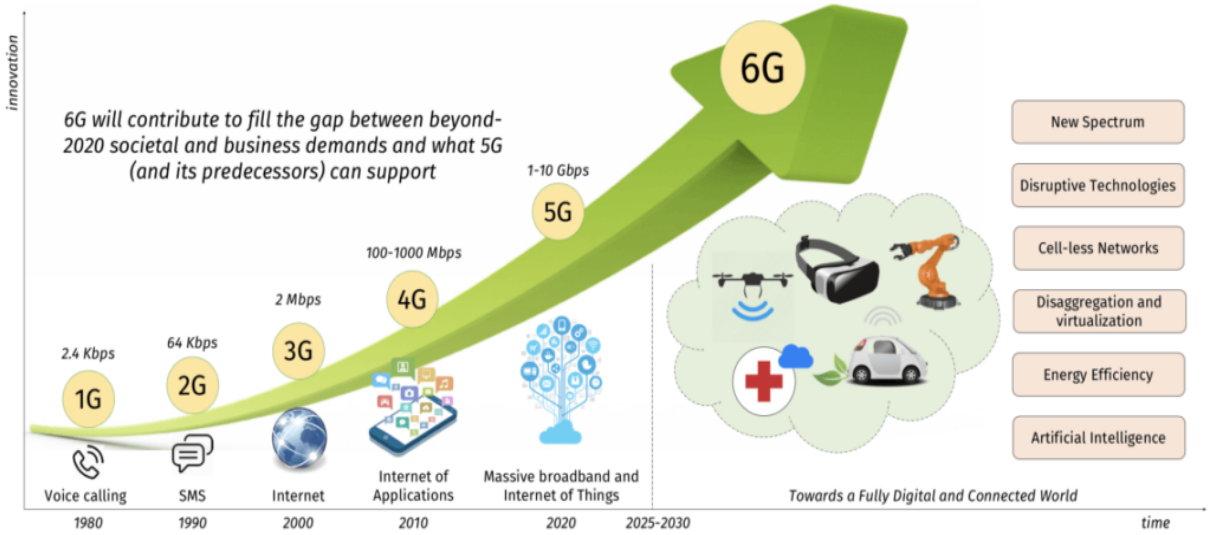

Figure 1.1: The progression of mobile networks [4].

communications, alternative/advanced waveforms, and novel antenna technologies [12,13]. Along with these technologies, unmanned aerial vehicles (UAVs) have emerged as a remarkable addition. They provide a unique avenue to address various challenges and offer innovative solutions in the field [14].

In wireless communication networks, UAVs can be effectively utilized as flying base stations (BSs). The implementation of flying BSs offers numerous advantages, including mobility, versatility, cost-effectiveness, and the ability to adjust altitude, which have contributed to increasing the popularity of UAVs. Therefore, UAVs can serve the purpose of providing connectivity in terrestrial wireless networks. Depending on factors such as coverage area and weather conditions, UAVs can hover at altitudes ranging from a few hundred meters to 20 kilometers. This capability allows UAVs to enhance network coverage and provide additional capacity in urban areas or extend network coverage to remote rural regions that are challenging to reach [15–17]. The freedom of navigation and ability to circumvent obstacles enhances the ability of UAVs to establish reliable communication links with ground users. Consequently, UAVs have garnered considerable attention from both academia and industry as promising solutions to achieve comprehensive network coverage [18, 19] in dense environments.

UAVs have the potential to serve in low power networks, particularly in applications like the Internet of things (IoT), where devices operate at low power levels and communicate over short distances. In this context, UAVs can function as wireless relays, enhancing the connectivity and coverage of ground-based wireless devices [20–23]. Additionally, in certain locations and countries, the cost of building an entire cellular infrastructure can be prohibitively high. Consequently, opting for UAVs instead of costly towers and infrastructure emerges as a favorable alternative.

Besides the features and benefits of UAVs, it is accompanied by several challenges [24]. One of the main challenges that face using the UAVs is the association with the users. Secondly, both fixed-wing and rotary-wing UAVs must adhere to strict constraints regarding size, weight, and power. These limitations inherently restrict communication, sensing, and endurance capabilities. Thirdly, strong line-of-sight (LoS) links between the air and ground components unavoidably result in significant interference [25]. However, this interference can be effectively utilized to extract valuable target information, including details such as location, velocity, and direction. Finally, the introduction of flexible UAVs placement and trajectory introduces an additional degree of optimization, making the design of the system more complex. Moreover, unlike conventional UAVs-enabled communications that primarily focus on maximizing data rates, UAVs-assisted systems require the incorporation of sensing performance metrics, such as detection probability and estimation/recognition accuracy, as well as efficient cooperative mechanisms. This entails considerations of sensing signal processing, including echo signal processing and clutter interference suppression [26]. Consequently, designing UAVs-assisted systems to achieve high situational awareness and coordination among the UAVs presents a new and challenging problem that needs to be addressed.

1.2 Objectives and Contributions

The significance of this topic, coupled with the existing gaps in the current literature, impelled us to pursue the following objectives:

1. Investigating the association problem between wireless access points(WAPs) and UAVs and proposing low complexity algorithms to maximize the total weighted sum rate of the system where each wireless access point (WAP) is granted a certain weight under practical operational conditions, such as allowing each WAP to connect with more than one unmanned aerial vehicle (UAV) and dealing with WAPs distributed in different coverage areas.

2. Exploring the joint optimization problem of channel assignment, utilizing the available pool channels provided by the main core network. Furthermore, addressing the issue of fairness among WAPs by finding the maximum minimum total sum data rates, ensuring equitable allocation of resources and promoting fairness in the system.

3. Studying the ergodic capacity performance of UAV wireless communication systems under the impact of HWIs and providing mathematical expressions for the average ergodic capacity considering the averaging over the channel parameters.

4. Studying the combined effect of channel estimation errors, including both amplitude and phase estimation errors, as well as HWIs on the performance of UAV-assisted over-the-air computation (OAC) systems. In addition, developing mathematical frameworks to quantify the average mean squared error (MSE).

This study treats some of the important challenges of using UAVs in wireless systems, and it presents new techniques and solutions for improving the system performance. The main contributions of the study can be summarized as follows:

1. A resource allocation algorithm that maximizes the total weighted sum rate is proposed. Furthermore, the complexity analysis of the presented algorithm is conducted. This algorithm considers practical operational conditions including allowing each WAP to connect with multiple UAVs, managing WAPs distributed across different coverage areas, and ensuring fairness between WAPs is studied. The obtained results here have been published in [27].

2. A novel algorithm is proposed for low complexity, high spectral efficiency, and fair resource allocation in UAV networks. This algorithm aims to achieve fairness among WAPs by finding the maximum minimum total sum data rate. This algorithm considers the utilization of channels assigned from a pool of channels provided by the core network. The obtained results here have been published in [28].

3. The ergodic capacity performance of UAV wireless communication systems under the effect of the HWIs is investigated. Analytical expressions are obtained for the average ergodic capacity while averaging over the Rician parameter and the distance between the UAVs and the ground station (GS). Furthermore, an asymptotic analysis of the system performance is conducted, specifically examining the behavior of the system when the transmitted power and the number of GS antennas become very large. This analysis provides valuable insights into the system's performance characteristics and its scalability under high-power and multi-antenna configurations. The obtained results here have been published in [29].

4. The performance of the UAV-assisted over-the-air (OTA) computation systems under joint effects of imperfect CSI and non-ideal transceivers is studied. More specifically, the influence of these factors on the average MSE is analyzed. Furthermore, mathematical frameworks of the average MSE are obtained. This analysis provides a deeper understanding of the impact of these factors on the overall system performance and helps in designing robust and efficient UAV-assisted OTA computation systems.

1.3 Thesis Organization

The organization of the remaining sections of the thesis is as follows:

Chapter 2 introduces some relevant background on UAVs wireless communication systems. First, it explores the core concepts of integer linear programming (ILP) and the Hungarian algorithm with illustrative examples. Next, the classification of UAVs is

studied focusing on their unique characteristics and functionalities. Also, various models relevant to UAV-assisted wireless communication systems are explained, including UAV-based path loss (PL), HWIs, and fading channel distribution. Finally, the related work section is introduced.

Chapter 3 presents a resource allocation algorithm for UAV networks, aimed at resolving the association problem between WAPs and UAVs while considering practical operational conditions to maximize the system total sum rate. The chapter begins with an introduction, followed by the presentation of the system model and problem formulation. Subsequently, the proposed algorithm is thoroughly explained, along with an analysis of its complexity and evaluation of its performance.

Chapter 4 introduces a less complex algorithm to Max-min the resource allocation between WAPs and UAVs taking into account the utilization of channels assigned from a pool of channels provided by the core network to maximize minimum total sum data rates. The chapter begins with an introduction, then it presents the system model and discusses the problem formulation. Subsequently, the proposed algorithm is thoroughly explained, including an analysis of its complexity and performance evaluation.

Chapter 5 studies the impact of HWIs on the ergodic capacity performance of UAV-GS wireless communication systems. The chapter begins with an introduction. Then, the considered UAV-GS system model is then presented, followed by a detailed discussion on the signal model considering the presence of HWIs at the transmitter and receiver. Furthermore, the chapter analyzes the system performance, providing an approximation of the average ergodic capacity in the presence of HWIs. Asymptotic analysis is also conducted to gain further insights. The analytical findings are validated through simulations, and the results are thoroughly discussed.

Chapter 6 studies the joint impact of channel estimation errors and HWIs on the MSE performance of UAV-assisted OTA computation communication systems. The chapter begins with some context for the study. The UAV-assisted OTA computation system model is then explained, followed by a discussion on the signal model considering non-ideal

transceivers. Additionally, the chapter investigates the system performance by providing an approximation of the average MSE under the presence of HWIs for both perfect and imperfect CSI. The theoretical results are further validated by computer simulations, and the obtained results are presented.

Chapter 7 serves as a summary of the obtained results, along with highlighting potential avenues for future research in this field.

1.4 List of Publications

1. Hamzih Alsmadi, Huda Alsheyab, Malek Alsmadi, Emad Mohammed, Yazan Alomari and Salama Ikki, "Less Complex and Higher Spectral Efficiency Resource Allocation Algorithm for Unmanned Aerial Vehicles Networks," *IEEE Canadian Journal of Electrical and Computer Engineering* vol. 45, no. 3, 279–284, 2022. I am the main contributor to this work and played a leading role in the theoretical modeling and planning of the publication.

2. H. Alsmadi, E. Saleh, M. Alsmadi and S. Ikki, "Capacity Analysis of UAV Communications Under the Non-ideal Transceiver Effects," *IEEE Communications Letters*, doi: 10.1109/LCOMM.2023.3287945. I am the main contributor to this work and played a leading role in the theoretical modeling and planning of the publication.

3. Hamzih Alsmadi, Emad Saleh, Malek Alsmadi, and Salama Ikki, "Hardware Impairments Effects on Over the Air System Assisted by Unmanned Aerial Vehicle," *IEEE Transactions on Vehicular Technology*, Submitted, 2023. I am the main contributor to this work and played a leading role in the theoretical modeling and planning of the publication.

4. Hamzih Alsmadi, Huda Alsheyab, Malek Alsmadi, and Salama Ikki, "Less Complex Algorithm to Max-Min the Resource Allocation for Unmanned Aerial Vehicles Networks," *IEEE VTC2022-Spring*, Helsinki, Finland, 2022. I am the main contributor

to this work and played a leading role in the theoretical modeling and planning of the publication.

Chapter 2

Background and Preliminaries

2.1 Integer Linear Programming (ILP)

A mathematical optimization or feasibility problem in which some or all of the decision variables are integers is known as an integer programming problem. A common subcategory of integer programming is integer linear programming (ILP), which has a linear objective function and may have additional constraints apart from requiring that certain variables be integers. Integer programming falls into the category of NP-complete problems. One of Karp's 21 NP-complete problems is the specific case of 0-1 ILP, in which the unknowns are binary and only the constraints must be satisfied. It takes exponentially long to be solved in the worst case. Therefore, the ILP technique can help solve optimization problems, where the computational complexity depends on the number of constraints and variables [30]. The ILP can be written as:

$$\begin{aligned} \text{Objective:} \quad & \min_{w} \quad rw, \\ \text{subject to} \quad & Kw \leq v, \\ & w \geq 0, \end{aligned} \tag{2.1}$$

where K is a $m \times n$ matrix , r is an n-dimensional row vector, v is an m-dimensional column vector, and w is an n-dimensional column vector of unknown variables.

Table 2.1: Monthly demand for each product

Product	Month 1	Month 2	Month 3
P1	100	120	110
P2	80	70	90
P3	75	85	80

Table 2.2: Production capacity per machine per month

Machine	P1	P2	P3
M1	70	60	50
M2	50	60	70

Many algorithms, such as the branch and bound method and the cutting plane method, are used to solve ILP problems. The branch and bound method manages optimization by segmenting the solution space, setting bounds, and eliminating non-optimal subsets, thus identifying the best solution. In contrast, the cutting plane method tackles these problems by progressively refining the solution space using additional linear constraints, known as cutting planes. This method is particularly effective when traditional methods prove inefficient due to the complexity of the problem [31, 32].

2.1.1 Integer Linear Program Example

This section provides an illustrative example to clarify the formulation of the optimization problem. Suppose a company produces three products (P1, P2, P3) using two machines (M1, M2). The company has forecast the demand for each product for the next three months, knows the production capacity of each machine per month, and knows the storage capacity for its products. it is also assumed that each machine cannot operate for more than 160 hours per month owing to maintenance requirements. The goal is to plan production for the next three months to meet demand without exceeding either machine's production capacity, operation hours, and storage capacity while also minimizing the unused production capacity based on the details outlined in tables 2.1-2.5.

Table 2.3: Max operation hours per machine per month

Machine	**Max Hours**
M1	160
M2	160

Table 2.4: Time in hours to produce one unit of each product

Product	**Time**
P1	1.5
P2	2
P3	2.5

Table 2.5: Storage capacity

Product	**Capacity**
P1	100
P2	100
P3	100

- The decision variables are defined as:

  1. x_{ijk} = units of product i produced by machine j in month k.
  2. s_{ik} = units of product i stored in month k.

- The objective function targets minimizing the unused production capacity (Z) and is given as:

$$\text{minimize } Z = \sum_i \sum_j \sum_k (C_{ijk} - x_{ijk}).$$

- The constraints can be summarized as:

  1. Production Capacity (C): The production cannot exceed the machine capacity.

$$x_{ijk} \leq C_{ijk} \quad \forall i, j, k.$$

  2. Operating Hours (T): The operation hours of each machine should not exceed

160 hours.

$$\sum_i (x_{ijk} \cdot T_i) \leq 160 \quad \forall j, k.$$

3. Demand (D): The production plus any stored units from the previous month should meet the demand.

$$x_{ijk} + s_{ik-1} = D_{ik} + s_{ik} \quad \forall i, k.$$

4. Storage: The storage cannot exceed 100 units.

$$s_{ik} \leq 100 \quad \forall i, k.$$

5. Non-negativity and Integer Constraints:

$$x_{ijk}, s_{ik} \geq 0 \quad \text{and integer} \quad \forall i, j, k.$$

The comprehensive problem formulation is expressed as follows:

$$\begin{aligned}
\textbf{Objective:} \quad & \min \quad Z = \sum_i \sum_j \sum_k (C_{ijk} - x_{ijk}). \\
\textbf{subject to:} \quad & x_{ijk} \leq C_{ijk} \quad \forall i, j, k. \\
& \sum_i (x_{ijk} \cdot T_i) \leq 160 \quad \forall j, k. \\
& x_{ijk} + s_{ik-1} = D_{ik} + s_{ik} \quad \forall i, k. \\
& s_{ik} \leq 100 \quad \forall i, k. \\
& x_{ijk}, s_{ik} \geq 0 \quad \text{and integer} \quad \forall i, j, k.
\end{aligned}$$

2.2 Hungarian Algorithm

The Hungarian algorithm, also known as the Munkres algorithm, efficiently solves the assignment problem in polynomial time. This algorithm has numerous applications in combinatorial optimization, such as the Traveling Salesman problem [33]. The Hungarian algorithm comprises four steps. The first two steps are executed once, while the third and fourth steps are repeated until an optimal assignment is found. The input for the algorithm is an $n \times n$ square matrix with non-negative elements. The steps are as follows:

1. Subtract row minima: subtract the smallest entry in each row from each entry in that row.

2. Subtract column minima: Subtract the smallest entry in each column from each entry in that column.

3. Cover all zeros with a minimum number of lines: using the smallest possible number of lines, draw lines over rows and columns in order to cover all zeros in the matrix. If the number of lines is equal to the number of rows in the square matrix, stop here. Now, choose a set of zeros so each row and column has only one selected zero. Remove any dummy rows or columns that have been added. The zeros in the final matrix correspond to the optimal assignment in the original matrix. If this condition is not met, proceed to step four.

4. Create additional zeros: Find the smallest element, denoted as c, that is not covered by a line. Subtract c from all uncovered elements in the matrix, and add it to any element that is covered twice. Then, return to step three.

Finally, it is worth mentioning that the worst-case time complexity for the Hungarian algorithm is $O(n^3)$. The following example illustrates these steps.

2.2.1 Hungarian Algorithm Example

Assuming that there is five people $(P_1, P_2, P_3, P_4, P_5)$ and five jobs $(X_1, X_2, X_3, X_4, X_5)$. Considering that one job can only be assigned to one person. The matrix shows the cost of assigning each person to each job. The objective of this problem is to minimize the total cost of the job-person assignment. The original cost matrix size is 5×5, and it's given in table 2.6.

Table 2.6: Job-Person assignment cost matrix

	P_1	P_2	P_3	P_4	P_5
X_1	12	40	13	35	18
X_2	83	65	76	92	90
X_3	70	38	70	67	99
X_4	84	45	28	90	39
X_5	61	88	85	10	16

The following steps show how to find the lowest cost of the job-person assignment problem.

1. Step 1: subtract row minima - this step subtracts the minimum value of each row from all other values in that row. The resulting matrix is shown in table 2.7.

Table 2.7: The matrix after row minima subtraction

	P_1	P_2	P_3	P_4	P_5	
X_1	0	28	1	23	6	(-12)
X_2	18	0	11	27	25	(-65)
X_3	32	0	32	29	61	(-38)
X_4	56	17	0	62	11	(-28)
X_5	51	78	75	0	6	(-10)

2. Step 2: subtract column minima - this step subtracts the minimum value of each column from all other values in that column. The resulting matrix is shown in table 2.8.

Table 2.8: The matrix after column minima subtraction

	P_1	P_2	P_3	P_4	P_5
X_1	0	28	1	23	0
X_2	18	0	11	27	19
X_3	32	0	32	29	55
X_4	56	17	0	62	5
X_5	51	78	75	0	0
					-6

3. Step 3: cover all zeros with a minimum number of lines - this step draws the minimum number of lines required to cover all zeros in the matrix. As illustrated below, four lines are necessary for complete coverage as shown in table 2.9.

Table 2.9: Zero-covered matrix

	P_1	P_2	P_3	P_4	P_5	
X_1	0	28	1	23	0	x
X_2	18	0	11	27	19	
X_3	32	0	32	29	55	
X_4	56	17	0	62	5	x
X_5	51	78	75	0	0	x
		x				

4. Step 4: create additional zeros - this step, since the number of lines drawn is less than five, selects the smallest uncovered number, which is 11. Then, it subtracts this number from all uncovered elements and adds it to the elements that are covered twice. The resulting matrix is table 2.10.

Table 2.10: The matrix after additional zero creation

	P_1	P_2	P_3	P_4	P_5
X_1	0	39	1	23	0
X_2	7	0	0	16	8
X_3	21	0	21	18	44
X_4	56	28	0	62	5
X_5	51	89	75	0	0

Now, depending on the result, the algorithm revisits step 3 again

5. Step 3: cover all zeros with a minimum number of lines - this step draws the minimum number of lines required to cover all zeros in the matrix. The updated matrix is presented in table 2.11.

Table 2.11: Updated zero covered matrix

	P_1	P_2	P_3	P_4	P_5	
X_1	0	39	1	23	0	x
X_2	7	0	0	16	8	
X_3	21	0	21	18	44	
X_4	56	28	0	62	5	
X_5	51	89	75	0	0	x
		x	x			

6. Step 4: create additional zeros - this step, since the number of lines drawn is less than five, selects the smallest uncovered number, which is 5. Then, it subtracts this number from all uncovered elements and add it to the elements that are covered twice. The resulting matrix is shown in table 2.12.

Table 2.12: The matrix after new additional zero creation

	P_1	P_2	P_3	P_4	P_5
X_1	0	44	6	23	0
X_2	2	0	0	11	3
X_3	16	0	21	13	39
X_4	51	28	0	57	0
X_5	51	94	80	0	0

Now, depending on the result, the algorithm revisits step 3 again.

7. Step 3: cover all zeros with a minimum number of lines There are 5 lines required to cover all zeros as shown in table 2.13

Table 2.13: The matrix after coverage of new zeros

	P_1	P_2	P_3	P_4	P_5	
X_1	0	44	6	23	0	x
X_2	2	0	0	11	3	x
X_3	16	0	21	13	39	x
X_4	51	28	0	57	0	x
X_5	51	94	80	0	0	x

Now that there are five lines and each row and column has a zero. Then, these zeros cover the optimal assignment as in table 2.14.

Table 2.14: The candidate cost matrix

	P_1	P_2	P_3	P_4	P_5
X_1	0	44	6	23	0
X_2	2	0	0	11	3
X_3	16	0	21	13	39
X_4	51	28	0	57	0
X_5	51	94	80	0	0

Based on this, the corresponding optimal values can be calculated from the original cost matrix, as shown in Table.2.15.

Table 2.15: The cost matrix.

	P_1	P_2	P_3	P_4	P_5
X_1	12	40	13	35	18
X_2	83	65	76	92	90
X_3	70	38	70	67	99
X_4	84	45	28	90	39
X_5	61	88	85	10	16

Finally, the optimal value found to be 12+76+38+39+10= 175.

2.3 UAV-based Path Loss Model

Considering that UAVs are distributed in a horizontal parallel plane relative to the users at a specific height h_d above ground level, the air-to-ground (ATG) -PL channel model is employed. This is in contrast to conventional terrestrial communications, which typically utilize the log distance PL model. As a result, the wireless link between UAVs and users primarily exhibits a vertical orientation. Consequently, the following subsection focuses on discussing the ATG -PL.

2.3.1 Air-to-Ground Path Loss Model

This work uses the ATG -PL model from [15], which has been commonly assumed in the literature. This ATG model considers two propagation scenarios:

1. LoS receivers, where the sub-cell sites are positioned in LoS or near- LoS conditions with respect to the UAVs.

2. Non-line-of-sight (NLoS) receivers, where the sub-cell site coverage relies on reflections and refractions for signal propagation.

The probability of LoS is the crucial factor influencing PL in the ATG model. This probability is determined by the surrounding circumstances as well as the orientation of the UAVs and sub-cell Sites. The probability of LoS can be formulated as in [34]

$$P(\text{LoS}) = \frac{1}{1 + \alpha \exp[-\beta(\frac{180}{\pi}\theta - \alpha)]}, \tag{2.3}$$

where α and β are constants related to the environment (rural, urban, etc.), and $\theta = \arctan\left(\frac{h_D}{s}\right)$ is the angle between the user and the UAV, where $s = \sqrt{(x - x_D)^2 + (y - y_D)^2}$ represents the horizontal distance between the user and the UAV. The location of the user and UAV are denoted as (x, y) and (x_D, y_D, h_D), respectively. The average PL is given as

in [34]

$$PL(d)|_{\text{dB}} = 10\log\left(\frac{4\pi f_c d}{c}\right)^{\gamma} + \eta_{\text{LoS}}\, P(\text{LoS}) + \eta_{\text{NLoS}}\, P(\text{NLoS}), \tag{2.4}$$

where $PL(d)|_{\text{dB}}$ represents the free space PL in dB, the carrier frequency is f_c, c is the speed of light, γ is the PL exponent, and $d = \sqrt{{h_D}^2 + s^2}$ is the distance between the UAV and user. η_{LoS} and η_{NLoS} represent the additional losses of the LoS and NLoS links, and $P(\text{NLoS}) = 1 - P(\text{LoS})$.

2.3.2 Hardware Impairments

In practical wireless communication systems, the presence of HWIs is a common occurrence. These HWIs arise due to the numerous electrical devices and circuits involved in the physical transceiver implementations, causing various forms of signal distortion. Consequently, the distortions of the signal result in a mismatch between the intended signal and the actual transmitted signal [5, 35]. To provide a clearer depiction of the imperfect radio frequency (RF) components responsible for these HWIs, refer to Fig. 2.1. This figure illustrates how the real and imaginary components of the original baseband complex signal, denoted as x, are separated into in-phase/quadrature-phase (I/Q) signals. Subsequently, after undergoing some signal processing, these signals are up-converted to the desired RF and transmitted. As a consequence, instead of transmitting the original signal x, a modified signal $\tilde{x}$ is sent over the channel.

Throughout the transmission process, the signal undergoes distortion at various stages due to imperfections in the hardware. Initially, at the transmitter, the intended signal x is processed by digital-to-analog converters (DACs) to convert the digital signal into an analog one. Similarly, at the receiver, analog-to-digital converters (ADCs) are employed for the reverse conversion process. However, these conversions introduce sampling frequency offset distortions and quantization errors. The adoption of low-resolution ADCs exacerbates these distortions, as high-resolution ADCs would result in increased overhead and power consumption. Subsequently, the I/Q signals are filtered and mixed with their respective versions that are 90 degrees out of phase, referred to as the local oscillator

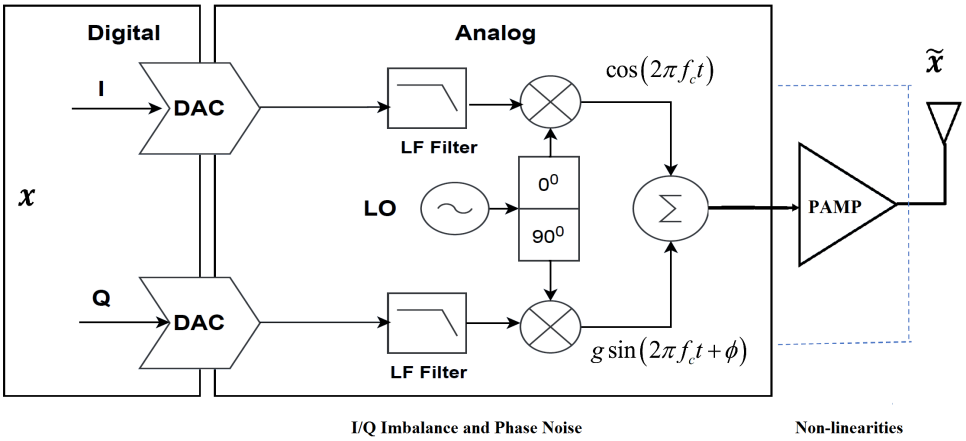

Figure 2.1: The RF transmitter block diagram in the communication systems.

(LO). The LO frequency corresponds to the carrier frequency (f_c) of the RF signal. This mixing process further contributes to the overall distortion experienced by the signal.

The second source of distortion occurs due to imperfections in the I/Q mixer, LO, and phase shifter, collectively referred to as I/Q imbalance and phase noise. In an ideal scenario, the LO should provide a precise 90-degree phase shift between the I/Q branches of the signal, with equal gain. However, due to non-idealities in the LO, there may be a phase imbalance between the I/Q branches of the transmitter and/or receiver signals as the provided phase shift deviates from the intended 90 degrees. These imperfections also leads to gain mismatch, also known as amplitude imbalance, which are slight variations in the amplitudes of the I/Q branches of the signal at the transmitter and/or receiver. Fig. 2.1 provides an illustration of these effects, where ϕ represents the phase difference and g denotes the gain mismatch between the I/Q branches.

In this figure, the I signal is represented by $\cos(2\pi f_c t)$, and the Q signal is represented by $g\sin(2\pi f_c t + \phi)$. Consequently, the combined impact of gain and phase imbalances is referred to as I/Q imbalance, as the I/Q branches are not identical and exhibit different gains. This I/Q imbalance can significantly degrade the system's performance.

Finally, both the power amplifier (PAMP) at the transmitting end and the low noise amplifier at the receiving end are vital components in the RF chain. Conventionally, these components are engineered to achieve maximum efficiency within their saturation

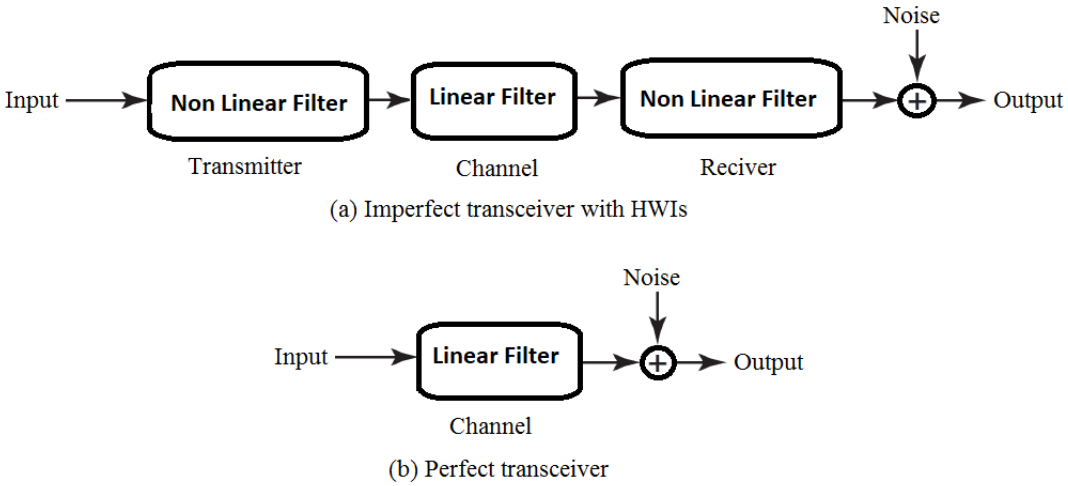

Figure 2.2: A communication system can be modeled with or without considering (HWIs). HWIs [5].

region. However, they also represent the principal sources of non-linear distortion in communication systems. In real-world scenarios, when the PAMP operates within its non-linear region, it induces both amplitude and phase distortions in the transmitted signal. A PAMP's non-linear distortion is typically defined by amplitude-to-amplitude and amplitude-to-phase distortion functions, as indicated in [36–38]. Consequently, $\tilde{x}$ emerges as the final RF signal for transmission rather than the original signal x.

2.3.3 Hardware Impairment Model

Wireless communication channels are typically represented as linear filters that receive an analog input signal from the transmitter. These filters introduce distortion, which is then measured at the receiver in the presence of additive white Gaussian noise (AWGN).

Fig. 2.2 depicts an analog channel with and without HWIs [5]. On the transmitter side, the non-ideal hardware output represents the HWIs and can be modeled as an additive distortion noise characterized in (2.5) [5, 39]

$$\tilde{x} = \sqrt{P\kappa_t}\, x + \eta_t. \tag{2.5}$$

Here, the actual transmitted signal is denoted as $\tilde{x}$ instead of the intended signal x, where $\mathbb{E}\{|x|^2\} = 1$. The transmitter's HWI factor is denoted as κ_t, which lies within the range $(0, 1)$. The complex transmitter additive distortion noise is represented by $\eta_t \sim \mathcal{CN}(0, (1 - \kappa_t)P)$, where P denotes the transmitted power. It is important to note that this distortion noise term is independent of the signal x.

The power of the distortion is directly proportional to the input power P [40–42], with the proportionality constant of $(1-\kappa_t)$. This distinguishes it from the conventional AWGN at the receiver, which remains independent of the input power. In scenarios with high signal-to-noise ratio (SNR), where the AWGN is negligible, the distortion noise becomes a significant limiting factor affecting performance. Similarly, the impaired signal at the receiver can be expressed as in (2.6)

$$y = \underbrace{\sqrt{P\kappa_r\kappa_t}\, h\, x}_{\text{Desired signal}} + \underbrace{\sqrt{\kappa_r}\, h\, \eta_t + \eta_r}_{\text{Distortion noise}} + \underbrace{w}_{\text{AWGN}} . \tag{2.6}$$

Here, h represents the complex channel gain between the transmitter and the receiver. The receiver's HWI factor is denoted as κ_r, while the complex receiver additive distortion noise is represented by $\eta_r \sim \mathcal{CN}\big(0, (1-\kappa_r)P\,|h|^2\big)$. Additionally, the AWGN is represented by $w \sim \mathcal{CN}(0, \sigma_w^2)$. Therefore, the power of the distortion is directly proportional to the input power P. In the case of perfect HWI, where there is no HWI, $\kappa_r = \kappa_t = 1$, $\eta_r = \eta_t = 0$, and the transmitted signal $\tilde{x}$ remains x.

The HWI factor κ_t plays a crucial role in determining the level of HWIs, and it is directly associated with the error vector magnitude (EVM). EVM is a widely used metric for quantifying the distortion level in practical transceiver hardware. It is defined as the square root of the ratio between the average distortion power and the average signal power [1]. Furthermore, the quality of the transmitted signal, including its modulation quality, is closely linked to the EVM. This implies that specific EVM requirements must be met to ensure a sufficiently high quality of the transmitted signal [2].

For the transmitted signal x in the model defined in equation (2.5), the EVM can be

Table 2.16: EVM requirements [1–3]

Modulation scheme	Required EVM	HWI factor κ_t
QPSK	17.5 %	0.970
16-QAM	12.5 %	0.984
64-QAM	8 %	0.994
256-QAM	3.5 %	0.999

expressed as in (2.7) [5]

$$\text{EVM} = \sqrt{\frac{\mathbb{E}\{\eta_t\}}{P\,\mathbb{E}\{|x|^2\}}} = \sqrt{\frac{(1-\kappa_t)P}{P}} = \sqrt{1-\kappa_t}. \tag{2.7}$$

Table 2.16, along with the relationship presented in equation (2.7), illustrates the direct correlation between hardware quality and the quality of the transmitted signal. For instance, according to the long-term evolution (LTE) standard, if 64-quadrature amplitude modulation (QAM) is to be supported, the transmitter hardware must satisfy the requirement EVM ≤ 0.08. This corresponds to $\kappa_t = 1 - \text{EVM}^2 \geq 0.994$. On the other hand, if the transmitter only needs to support 16-QAM modulation, the LTE standard specifies a requirement of EVM ≤ 0.125, corresponding to $\kappa_t \geq 0.984$ [1, 2]. While practical LTE transceivers typically support 64-QAM modulation, EVM values exceeding 0.08 can be of interest to UAV-based systems as they allow for more relaxed hardware design constraints. The EVM is a crucial metric that is commonly specified on the data sheets of RF transceivers. It provides valuable information about the quality and performance of the transceiver hardware.

2.4 Channel Models

Wireless communication systems rely on the inherent randomness of signal propagation, as signals spread in all directions and follow diverse paths before reaching their intended destination. This randomness introduces several challenges. One such challenge is the occurrence of fading, which arises from multiple copies of the transmitted signal reaching the receiver at different times and encountering varying levels of attenuation. Additionally,

factors like PL and shadowing deteriorate the transmitted signal due to the distance between the source and destination, as well as the presence of obstacles. The field of statistical modeling of fading channels has garnered significant attention since the advent of wireless communication systems. [43–53].

2.4.1 Rayleigh Fading Channel Distribution

The Rayleigh distribution is widely used as a model for multipath fading channels that lack a direct LoS path, often referred to as fast fading [54]. The probability density function of the Rayleigh distribution can be expressed as

$$f(x) = \frac{x}{\sigma^2} \exp\left(-\frac{x^2}{2\sigma^2}\right) \qquad x \geq 0, \tag{2.8}$$

where σ is the scale parameter of the distribution.

2.4.2 Ricean Fading Channel Distribution

Rician distribution is a statistical model that describes fast-fading channel realizations by incorporating two parts: a deterministic part representing the LoS signal, and a Rayleigh-distributed part representing the scattered signal. The Rician parameter, denoted as K_{Rc}, represents the power ratio between the LoS part and the Rayleigh-distributed part. The fading channel can be expressed as in [55–57]

$$\mathbf{g} = \sqrt{\frac{K_{Rc}}{K_{Rc}+1}}\bar{\mathbf{g}} + \sqrt{\frac{1}{K_{Rc}+1}}\mathbf{g}_{Ry}, \tag{2.9}$$

where the LoS channel part is represented by $\bar{\mathbf{g}} = [1, e^{-j\frac{2\pi d}{\lambda}\sin(\theta)}, \cdots, e^{-j(M-1)\frac{2\pi d}{\lambda}\sin(\theta)}]$, and the scattered channel part is represented by $\mathbf{g}_{Ry} \sim \mathcal{CN}(\mathbf{0}, \mathbf{I}_{\mathrm{M}})$. The antenna spacing is represented by d, the wavelength is represented by λ, and the arrival angle is represented by θ. It is worth mentioning that when $K_{Rc} = 0$, the Rician channel has only a Rayleigh distribution of the scattered signal. When $K_{Rc} \to \infty$, the Rician channel has LoS channel

part only. The probability density function of the Rician distribution can be expressed as [58]

$$f(x) = \frac{1}{2\sigma^2} \exp\left(-\frac{x^2+v^2}{2\sigma^2}\right) I_0\left\{\frac{xv}{\sigma^2}\right\} \qquad x \geq 0, \tag{2.10}$$

where v^2 represents the average power of the LoS part, σ^2 represents the power in the scattered component, and $I_0(v)$ denotes the modified Bessel function of the first kind. When studying UAV-assisted wireless communication systems, the most appropriate channel model is Rician fading because, in the open space, the LoS links for UAV communication are readily available. Where the Rician factor K_{Rc} incorporates the impact of scattering and reflections from the surrounding environment.

2.5 Classification of UAVs

UAVs are widely recognized with diverse attributes and characteristics which are employed to do different functionalities. So it is beneficial to categorize them based on these criteria such as UAV types, altitude, weight, size, controlling methods, structures and configuration, speed and power utilizing methods. This section provides an explanation of the UAV classifications.

2.5.1 Type-based Classification

UAVs can be classified into two main types based on their design: fixed-wing UAVs and rotary-wing UAVs. The difference is that fixed-wing crafts require forward motion to produce lift. Fixed-wing UAVs are more efficient because the lift surfaces are larger, and the speed of the lift surface is uniform. They are faster than rotary UAVs because they are optimized to fly in one direction, so they are streamlined in that direction, whereas rotary UAVs are designed for omnidirectional movement. Fixed-wing UAVs are more energy efficient because their lift surface faces less drag, and they have more inertia carrying them forward, allowing them to glide. Whereas rotary UAVs have very little inertia in

their propellers compared to the turbulent drag forces they face [59, 60].

2.5.2 Altitude-based Classification

Unlike conventional wireless communication systems, UAVs have the ability to adjust their altitude. By raising the UAVs altitude, a wider area can be covered [61]. Considering the altitude, UAVs can be categorized into high-altitude and low-altitude groups [62, 63]. A high-altitude UAV possesses the capability to remain in the stratosphere for extended periods, offering wider coverage. On the other hand, a low-altitude UAV operates within the troposphere for shorter durations, allowing for quick and effortless deployment. Low-altitude UAVs are characterized by their compact size and high mobility, contrasting with the quasi-stationary nature of high-altitude ones [64–66]. Moreover, the deployment of high-altitude UAV poses greater complexity compared to their original use-case of extending Internet coverage to vast regions lacking cellular networks. However, incorporating them into cellular communications introduces a higher vulnerability to network outages due to substantial inter-cell interference [67, 68].

2.5.3 Control Method-based Classification

UAVs can be categorized based on their controlling methods, which include manual control and autonomous control. These categories can be further subdivided into various types, such as full-control and semi-controlling methods [69]. Full and semi-controls can be organized into five types. The first type involves direct control by a pilot, commonly seen in manned aircraft and helicopters. In the second type, the operator can be located anywhere on the ground, remotely controlling the UAV. The third and fourth types involve the intelligent shifting of complete control from humans to software, achieved through embedded commands that enhance compatibility and efficiency. The fifth type holds significant importance in cooperative mission strategies where UAVs operate in swarms. These types of control methods are predominantly utilized in military applications.

2.6 Wireless Networking with UAVs

5G and 5G+ systems are expected to handle enormous amounts of data, necessitating a large amount of bandwidth. Meeting theses high-bandwidth demands requires the use of shorter wavelength waves and can be achieved through LoS propagation. However, maintaining LoS is more challenging than lower frequency propagation. Consequently, terrestrial systems are conventionally utilized to provide network coverage in areas with complex propagation environments, and satellite links are used where terrestrial systems are unavailable.

LoS propagation is facilitated by high-altitude UAVs. These UAVs are capable of providing broadband wireless service, covering regions up to 20 kilometres in radius. This reduces the need for terrestrial BSs in suburban and remote rural locations. When compared to satellites, which require costly launches, high altitude UAVs are considered more cost-effective [70]. Consequently, the concept of an integrated network architecture combining air-based networks using UAV and GS networks has recently gained popularity among research groups. The use of UAVs in wireless communications offers cost-effective support for existing cellular networks, enabling rapid and smooth service recovery and traffic offloading in crowded locations [71].

The ability of UAVs to carry telecommunications equipment helps them to operate as a flying BSs for mobile cellular communication networks. In addition to adding extra capacity, these Ariel BSs can provide all of the features of the traditional mobile cell. UAV BSs are simple to set up and maintain; therefore, they can be helpful in the early phases of rebuilding connectivity in devastated areas. UAVs can be used to establish a connection with existing infrastructure, such as cellular networks, ensuring accurate, high-throughput, and low-latency communication with ground operators. This introduces new challenges, such as determining the optimal altitude of the UAVs to maximize coverage, minimizing the transmitted power required to cover a specified target region, and determining the optimal deployment of the UAVs [72].

Furthermore, regulators of the operators of UAVs can decide whether to deploy the UAVs based on climate conditions. Weather-tolerant drones, equipped with built-in WiFi chips to ensure uninterrupted connectivity during inclement weather, exemplify practical required characteristics of UAVs that can operate under varied weather conditions [73]. Artificial intelligence can also be employed to predict weather conditions and optimize UAVs performance [74]. As mentioned in the previous discussion, the impact of adverse weather on UAVs can be mitigated or at least managed, which is not possible with microwave links. Another advantage of UAVs is that they can be viewed as a cost-effective method to enhance coverage in rural areas lacking infrastructure [75]. UAVs can also help to sustain communication in case of unexpected emergencies such as existing infrastructure failure due to catastrophes such as earthquakes, tsunamis, flooding, or landslides [76–78].

Due to the high likelihood of UAV-ground LoS channels, the high altitude and mobility of UAVs, the swap limits of UAVs, and the need to ensure specific quality-of-service (QoS) requirements, wireless communication involving UAVs significantly differs from terrestrial counterparts. The significance of establishing an ATG network in 5G+ wireless communications is growing. However, associated challenges must be addressed, such as ATG channel modelling, resource allocation, optimal deployment, energy efficiency, path planning, and network security. In the subsequent chapters, this thesis will formulate and attempt to solve some of these crucial concerns.

2.7 Related Work

In recent years, the use of UAVs in wireless communication has attracted attention from both research and industry sectors. In [79], a method is introduced for deploying UAVs to deliver wireless services to ground users, explicitly focusing on minimizing the total transmit power needed to meet users' data rate requirements. This approach seeks to determine the optimal coverage area and UAV locations that would minimize the required transmit power.

The authors in [80] proposed an approach grounded in online learning for the dynamic assignment of transmission power. Their aim is to minimize total power consumption while QoS requirements are met within a spectrum-sharing multi-tier 5G environment. Furthermore, their scheme incorporates an approximation mechanism for the Q-value, effectively reducing the state/action space and enhancing the learning process's convergence speed. In [81], a framework was proposed for optimizing wireless networks that are powered by UAVs. The authors examined the flight time limitations of UAVs and explored two unique communication scenarios involving UAVs. Firstly, they aimed to maximize the average data service provided to ground users, taking into account the maximum hover times achievable by the UAVs. Secondly, they sought to minimize the average hover time required by UAVs to service the users while adhering to specific load requirements fully.

In [82], UAVs are leveraged to serve as a GS. This study aimed to determine the optimal positioning of the aerial GS to improve the system performance. The signal to interference and Noise Ratio (SINR) serves as a QoS metric for the system. Furthermore, in [83], the authors addressed the 3D placement and association problems of drone-BSs. They considered several constraints, including data rate, the maximum bandwidth of each drone-GS, and LoS. They proposed two scenarios, a network-centric scenario aimed to maximize the total number of served users regardless of their required rates and a user-centric scenario aimed to maximize the total sum rate.

The association problem between UAVs and users is a crucial concern when deploying UAVs in wireless communication networks. In addressing this issue, one scenario presented in [84] focused on serving the maximum possible number of users without explicitly considering the total sum rate. The study proposed two greedy solutions, a centralized solution and a distributed one. The centralized approach aimed to reduce the power consumption within the system, while the distributed aimed to minimize the latency. The choice between centralization and distribution was based on the specific optimization objective required for the system. Another approach was presented in [85], focusing on a fully distributed algorithm that aimed to maximize the number of associated users while considering QoS requirements in a Heterogeneous Networks context. This work intro-

duced a wholly distributed algorithm that operated without the need for coordination between the base stations. The algorithm sought to efficiently associate users with the available base stations, taking into account their QoS requirements.

Moreover, the association problem between UAVs and users with the objective of maximizing the total sum rate of the system was investigated in [34]. This study considered various constraints, including the maximum supported bandwidth and the maximum number of links per network flying platform (NFP)-hub. The goal was to determine the optimal associations between NFP-hubs and small cells (SCs) that would yield the highest overall sum rate while adhering to these constraints. In addition, the association problem between UAVs and users was examined in [86], with the objective of maximizing the sum data rate while minimizing inter-cell interference. This study focused on the interference between UAVs rather than between users. Moreover, a practical constraint related to the backhaul data rate was taken into account. To address this Non-deterministic polynomial time (NP)-hard problem, the authors proposed a heuristic algorithm as a solution approach. Considering the mentioned objectives and constraints, this algorithm aimed to provide efficient associations between UAVs and users.

Furthermore, it is widely recognized that the presence of HWIs has a detrimental effect on the overall system performance. Studies have demonstrated that the imbalance between the I/Q significantly impacts system performance, especially when combined with imperfect CSI [87, 88]. In related works [89, 90], researchers thoroughly examined the influence of phase noise and I/Q imbalance on multicarrier communication systems. Their investigations revealed that these physical impairments severely degrade the system performance. To mitigate these effects, the authors propose an algorithm to compensate for phase noise and I/Q imbalance. In [91], the authors specifically focused on the impact of HWIs on systems aided by large intelligent surfaces. Their findings demonstrated that HWIs impose limitations on both the spectrum efficiency and energy efficiency of the system, even when the number of transmit antennas and large intelligent surface reflectors is infinitely large. Notably, this study assumed a deterministic channel model.

In [92], the authors analyzed the performance of a reconfigurable intelligent surface in the presence of HWIs. The study concluded that the adverse effects resulting from the modeling of HWIs are particularly evident in the implementation of robust reconfigurable intelligent surface-aided systems. Furthermore, the work presented in [93] revealed a significant decrease in the capacity of large intelligent surfaces aided communication systems due to the presence of HWIs. This highlights the adverse impact that HWIs can have on the performance of communication systems employing large intelligent surfaces technology.

In [94], the authors studied the impact of hardware impairments on the performance of a UAV-based NOMA system that serves two ground users simultaneously. The outage probability and ergodic capacity expressions are derived. The results showed that HWIs can invert performance outcomes between near and far users at high transmission-power levels. This study provides valuable insights for designing and optimizing UAV-based systems under the effect of the HWIs. In [95], the performance of NOMA systems that incorporate satellite and terrestrial networks, focusing on the impact of HWIs was discussed. This study employs a UAV to relay signals from a satellite to a pair of ground users, with the goal of enhancing spectral efficiency. The results showed that the performance is affected by many parameters, such as the number of antennas on the satellite, the transmit SNR, and the level of HWIs. They also showed that increasing the number of antennas can improve the system's performance.

In [96], the authors studied the outage performance of UAV-aided NOMA technologies in downlink IoT networks under the impact of HWIs where a UAV is employed as a dynamic GS to establish communication links with two users. This work identifies several key system parameters that significantly affect the achievable ergodic capacity. These parameters include the transmit SNR at the UAV, power allocation strategies, and the level of HWIs in the system. In [97], the effects of HWIs and imperfect channel estimation were investigated on cache-enabled UAV-relaying networks. The results showed that HWIs and imperfect channel estimation introduce an error floor dependent on the channel estimation error factor, HWIs distortion factor, and QoS requirements. More-

over, the diversity order of the error floor for cached/relaying links equals the number of cached/relaying UAV nodes.

In [98], a cell-free massive mMIMO that serves UAVs and users, which are equipped with a single antenna and considering the presence of HWIs in both the UAVs and users system was studied. Consequently, these devices experience a combination of spatially-correlated Rician and Rayleigh fading channels while establishing communication links with flying BSs. A novel technique called block quadratic transformation was presented to enhance the overall energy efficiency of the system. The results demonstrated two key findings. Firstly, when UAVs experience severe HWIs, it is more beneficial to operate them at higher altitudes. Secondly, when UAVs operate at lower altitudes, they have a minimal impact on the spectral efficiency of users.

The existing literature showcases numerous works that have addressed various resource allocation problems in the context of 5G. However, it is important to note that these works often employ different system models and problem formulations, which may not directly align with the specific context and problem at hand. Additionally, the solutions proposed in these studies may not be directly applicable to the current problem being addressed. Many of these works primarily focus on utilizing Non-NFP to enhance network coverage and address other related concerns. Therefore, while these previous works provide valuable insights, a tailored approach is necessary to address the specific resource allocation problem under consideration.

It has been found that although the work in the literature has introduced exciting results, there are still some points that need to be addressed. For instance, the complexity of the proposed work remains high, and there is an opportunity to reduce it. Moreover, more practical conditions need to be considered, such as allowing each WAP to be connected to more than one UAV, dealing with WAPs distributed in different coverage areas, and ensuring fairness between WAPs, where no WAP can be left without a connection. These points have motivated us to revisit the association problem between the UAVs and WAPs.

In addition, the impact of HWIs on UAV-GS communication is still an ongoing area

of research. For instance, it is necessary to address factors such as the average ergodic capacity of the system, considering the average over a random three-dimensional trajectory movement, including the angle of arrival and the distance between the UAV and GS. Furthermore, it is important to study the effect of HWIs on the OTA. These aspects require further investigation to better understand and mitigate the impact of HWIs on UAV-GS and OTA systems and improve overall system performance.

Chapter 3

Less Complex and Higher Spectral Efficiency Resource Allocation Algorithm for Unmanned Aerial Vehicles Networks

3.1 Introduction

The vision of next-generation wireless communications must without a doubt include supporting and providing very high data rates, exceptionally low latency, a manifold increase in GS handling capacity, and significant improvements in QoS of the users' data stream relative to the existing wireless networks [99, 100].

In traditional ground network design, the fixed location of the GS is typically determined to guarantee a level of network coverage. At the same time, the users' requirements change continuously, which limits the ability of the ground network to tackle all these requirements. As such, blocking can affect the network at peak demand cases. This is because the network engineers make the design relying on the average utilization needs while overutilization can happen over and over [7, 86]. Furthermore, the fixed BSs are sig-

nificantly influenced by any dispersion and scattering weather conditions, which ultimately affect the system's transmission quality and require expensive infrastructure. On the other hand, the utilization of aerial platforms such as UAVs, balloons, and drones has recently emerged as a promising solution to overcome these challenges by offering stable, cost-effective, and efficient techniques with inherent attributes that are quite advantageous, such as versatility, flexibility, and altitude adaptability. UAVs also can support dense networks, and work in rural areas that do not have the necessary infrastructure [64, 81, 101].

There are many potential applications for UAV-assisted networks such as cellular networks, vehicular networks, device-to-device networks and disaster management. Also, the UAVs can play a critical role in building UAV-assisted network architectures for climate-induced, meteorological and geophysical disasters [102]. Moreover, the UAV-assisted wireless network can provide critical network connectivity to first responders for disaster management, which enables them to efficiently deliver emergency services. In the case of disaster forecasting applications, the interaction between the UAVs and the wireless sensor networks can be useful in developing early warning systems for areas where network infrastructure does not exist [102, 103]. There are many resource management challenges for a successful deployment of UAV-assisted wireless networks such as spectrum efficiency for subchannel allocation, user association problem, power management, deployment cost, and deployment time [104, 105].

The association problem between UAVs and WAPs has been reviewed in the literature. In [84], the authors found the solution for the association problem of SCs and UAVs to maximize the network's total sum rate and the number of users by considering UAV-related constraints. The research in [106] proposed a solution to the association problem using UAVs as hubs to support the communication between the core network and SCs. The authors analytically showed its relation to the generalized assignment problem and proved it to be NP-hard. In [81], uplink user devices' power was optimized along with their association with the GS and UAV using an iterative approach that satisfies the constraint of SINR.

The authors in [107] investigated the resource allocation problem in a multi-UAV aided IoT-NOMA system. They aimed to maximize the system capacity by jointly optimizing the channel assignment, the uplink transmits power of IoT nodes, and the altitudes of the UAVs. On the other hand, the authors in [108] applied convex relaxation to the resource allocation problem while, at the same time, considering the space-air-ground heterogeneous networks. Then, they used Lagrange dual decomposition and the convex procedure method to provide a near-optimal solution for the problem. After that, they proposed a lower-complexity algorithm to solve the problem.

In [61], an optimization approach was proposed to find the maximum radio coverage in the ground for low low-altitude platforms (LAPs). They introduced a mathematical relation for the LoS between LAPs and receivers in the ground. A unified algorithm was proposed in [109] that achieved an optimum association between the SCs and the UAVs to maximize the overall sum rate depending QoS, number of links, and bandwidth availability of the network. Their work presumed that a maximum of one UAV could be associated with each small cell (SC). However, the fairness condition where some SCs can be left without association was not considered in their work. In addition, the complexity of this work is still high and needs to be decreased, but in comparison to the related work in the literature, their work has less complexity (the comparison between their work and the previous work in the literature can be found in the complexity analysis section in [109].

Compared to the existing work in the literature, the proposed studies the association problem between the WAPs and UAVs considering more practical operational conditions such as allowing each WAP to be connected to more than one UAV, dealing with WAPs distributed in different coverage areas, and tackling fairness between WAPs, where no WAP can be left without connection. In addition, this work maximizes the total weighted sum rate of the system where each WAP can be granted a certain weight [27]. In this regard, this chapter proposes a centralized algorithm to find a suboptimal solution with very low complexity. Results show that the total weighted sum rate of the proposed algorithm outperforms the counterpart in the literature and is very close to the optimal

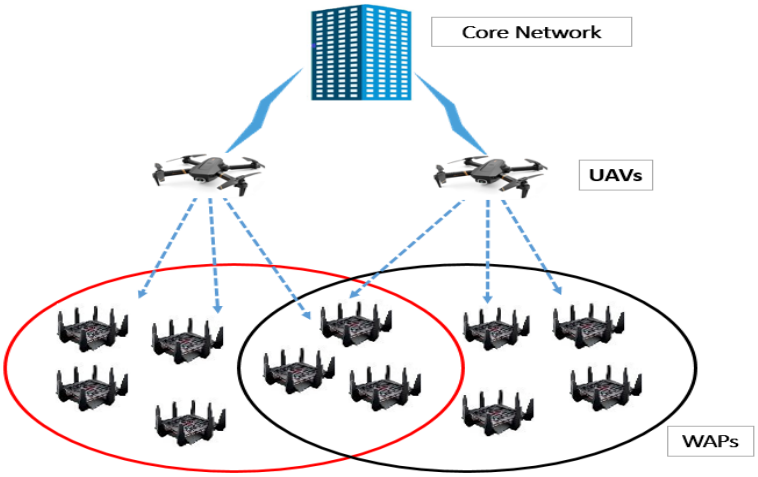

Figure 3.1: Graphical representation of UAVs, WAPs and the core network.

solution with a noticeable reduction in the system complexity.

Chapter Organization: The system model and problem formulation are described in Section 3.2. The proposed algorithm is presented in Section 3.3. Next, the time complexity analysis is given in Section 3.4. Then, the performance evaluation is discussed in Section 3.5. The chapter concludes in Section 3.6.

3.2 System Model and Problem Formulation

3.2.1 System Model

As shown in Fig. 3.1 a heterogeneous wireless network is presented. It is composed of three groups of wireless nodes: UAVs, WAPs and the core network. The UAVs are mediators that function as a hub to extend frontal connectivity between the WAPs and the core network. UAVs can be a practical solution to spread coverage in areas that do not have the required infrastructure [81]. Therefore, the association between the WAPs and UAVs is significant to enhance the overall network performance.

In this chapter, the UAVs are placed at a determined height at different locations based on the result in [61] that determines the altitude and the associated optimal coverage.

Each UAV and WAP shares the required important information such as each WAP's weight, SINR, number of links, data rate, and bandwidth with the core network. This work assumes that all UAVs and WAPs have various numbers of links (channels). This forms different coverage areas, where the channels in each coverage area are orthogonal on the other coverage areas (different frequencies for each channel).

The system has X UAVs and Y WAPs pairs with all possible cases (X <=> Y). UAVs are represented as $\mathbf{U} = \mathrm{u}_1, \mathrm{u}_2, \ldots, \mathrm{u}_x$, and WAPs are represented as $\mathbf{S} = \mathrm{s}_1, \mathrm{s}_2, \ldots, \mathrm{s}_y$. In contrast to the system model in [109], each WAP can associate with more than one UAV. Moreover, the system guarantees fairness by conditioning at least one connection for each WAP. In addition, the WAPs are distributed across different coverage areas.

To facilitate the implementation of the centralized algorithm, UAVs can share the control information (required bandwidth, required data rate, and SINR) with the core network for association purposes. Based on the control information, the system can specify the association between WAPs and UAVs. However, this does not include the data information. Finally, this work applies a weighted objective function to solve the optimization problem.

3.2.2 Problem Formulation

The proposed algorithm aims to maximize the total sum rate of the association problem between UAVs and WAPs by considering some practical constraints. This study explores the QoS, fairness, coverage, available bandwidth and the number of links supplied by each UAV.

- ***Coverage area***: This work uses the altitude constraints to determine the optimal coverage area depending on the maximum allowed PL ($PL_{\max}$) as in [61]. $PL_{\max}$ can be calculated as

$$PL_{\max} = \frac{A}{1 + a\exp\left(-b[\theta - a]\right)} + 20\log(R\sec\theta) + B, \tag{3.1}$$

where a and b are the S-curve parameters, R is the radius of the coverage zone, θ is the elevation angle between the UAV and the WAP, $A = \eta LoS - \eta NLoS$, and $B = 20\log\left(\frac{4\pi f}{c}\right) + \eta NLoS$. Here, η is the mean value of the excessive path loss, f is the carrier frequency, and c is the speed of light. Based on the UAVs altitudes and the WAPs locations, the coverage area can be defined as

$$C_{x,y} = \begin{cases} 1, & \text{if } \mathrm{s}_y \text{ in the coverage area of } \mathrm{u}_x, \\ 0, & \text{otherwise.} \end{cases} \tag{3.2}$$

Note that during the movement of WAPs and UAVs, some WAPs may fall out of coverage of certain UAVs, while others may become covered. This study targets spectral efficiency resource allocation during the coherence time, over which the channel impulse response is essentially invariant. Certainly, considering the speed of the UAV and its impact on coherence time is an interesting aspect to address in future work.

- ***Association***: If the WAP lies in the coverage area of the UAV, then the required data rate of s_y to associated with u_x is $R_{x,y}$. Shannon capacity is used to calculate $R_{x,y}$. Then, the data rate provided by each u_x can be found as $\sum_{y=1}^{Y} W_y R_{x,y} L_{x,y} C_{x,y}$ and the total sum rate over all UAVs is $\sum_{x=1}^{X}\sum_{y=1}^{Y} W_y R_{x,y} L_{x,y} C_{x,y}$. Here, W_y is the y^{th} WAP connection weight and $L_{x,y}$ is the association between s_y and u_x and can be defined as [110]

$$L_{x,y} = \begin{cases} 1, & \text{if } \mathrm{s_y} \text{ is connected with } \mathrm{u}_x, \\ 0, & \text{otherwise.} \end{cases} \tag{3.3}$$

- ***QoS***: The SINR between $\mathrm{s_y}$ and $\mathrm{u_x}$ is defined as

$$SINR_{x,y} = \frac{P_{x,y} PL(d_{x,y})}{\sum_{k=1,k\neq x}^{X} P_{k,y} PL(d_{k,y}) + \sigma_x^2}, \tag{3.4}$$

where $P_{k,y}$ is the transmitted power from u_k to s_y, and σ_x^2 represents the noise power at the u_k, $d_{x,y}$ is the distance between u_x and s_y, and PL is the total PL. The $SINR_{x,y}$ should be guaranteed to be greater than the minimum required $SINR_{min}$. Therefore, the QoS constraint can be expressed as

$$L_{x,y}C_{x,y}SINR_{\min} \leq SINR_{x,y}, \quad \forall\, x, y. \tag{3.5}$$

- ***Bandwidth***: The bandwidth constraint can be written as

$$\sum_{y=1}^{Y} L_{x,y}C_{x,y}b_{x,y} \leqslant B_x\ , \quad \forall\, x, \tag{3.6}$$

where B_x represents the maximum available bandwidth for each UAV. $b_{x,y}$ is the requested bandwidth between UAV associated with WAP.

- ***Number of links***: The number of links N_x constraint for each UAV can be written as

$$\sum_{y=1}^{Y} L_{x,y}C_{x,y} \leqslant N_x\ , \quad \forall\, x. \tag{3.7}$$

Next, the number of links N_y constraint for each WAP can be written as

$$\sum_{x=1}^{X} L_{x,y}C_{x,y} \leqslant N_y\ , \quad \forall\, y. \tag{3.8}$$

- ***Fairness***: To guarantee that each WAP has at least one association, the fairness constraint is formulated as

$$\sum_{x=1}^{X} L_{x,y}C_{x,y} \geqslant 1\ , \quad \forall\, y. \tag{3.9}$$

The final formulation for the objective function and all the previous constraints can be written as

$$\max_{L_{x,y}} \quad \sum_{x=1}^{X}\sum_{y=1}^{Y} W_y R_{x,y} L_{x,y} C_{x,y} \tag{3.10 a}$$

s. t.

$$L_{x,y} C_{x,y} SINR_{\min} \leq SINR_{x,y} \ , \quad \forall\, x, y. \tag{3.10 b}$$

$$\sum_{y=1}^{Y} L_{x,y} C_{x,y} b_{x,y} \leqslant B_x \ , \quad \forall\, x. \tag{3.10 c}$$

$$\sum_{y=1}^{Y} L_{x,y} C_{x,y} \leqslant N_x \ , \quad \forall\, x. \tag{3.10 d}$$

$$\sum_{x=1}^{X} L_{x,y} C_{x,y} \geqslant 1 \ , \quad \forall\, y. \tag{3.10 e}$$

$$\sum_{x=1}^{X} L_{x,y} C_{x,y} \leqslant N_y \ , \quad \forall\, y. \tag{3.10 f}$$

$$L_{x,y} \in \{0, 1\} \ , \quad \forall\, x, y. \tag{3.10 h}$$

$$C_{x,y} \in \{0, 1\} \ , \quad \forall\, x, y. \tag{3.10 i}$$

The formulated function is an integer linear programming problem that requires exponential time to be solved numerically [111]. This problem can be reduced to an NP-hard problem [106] or even a maximum knapsack problem [110]. The next section proposes an algorithm to obtain a suboptimal solution, which is then discussed and compared with the existing algorithm in the literature.

3.3 The Proposed Algorithm

The Hungarian method is a centralized optimization algorithm that can solve the one-to-one assignment problem (which is not the case in the studied WAPs-UAVs association problem). Moreover, it required a polynomial time to complete the matching between the elements which motivated us to exploit this algorithm in this work [33].

In this section, a suboptimal extended Hungarian algorithm with less complexity is proposed to solve the UAVs and WAPs association problem. In comparison with the existing literature, the presented algorithm is able to treat new constraints related to the practical operational conditions (as shown in the problem formulation). This section also discusses the presented algorithm performance when relaxing the bandwidth constraint.

To expedite the implementation of the centralized algorithm, the UAVs has the ability to share the required monitoring information (bandwidth, data rate, and SINR) with the core network for association purposes. Based on this information, the system determines the association between WAPs and UAVs. However, the data information is excluded in this process. The main goal of the presented algorithm is to extend the Hungarian algorithm to solve the unbalanced association problem between UAVs and WAPs when the total number of links is larger than the number of UAVs or vice versa. The centralized solution is used to move all information from the UAVs and WAPs to a central location. The proposed algorithm maximizes the total sum rate depending on the information from UAVs and WAPs, such as ($SINR_{x,y}$, $SINR_{min}$, $b_{x,y}$, N_x, N_y, B_x, $C_{x,y}$ and $R_{x,y}$).

The Hungarian algorithm achieves the optimal solution in only a one-to-one matching scenario, which is not present in this case [109]. Therefore, to make the problem compatible with the Hungarian algorithm, an unbalanced association approach is utilized. The proposed algorithm (Algorithm 1) can be briefly explained as follows:

1. Lines (4-12): The algorithm checks the constraints (coverage area, SINR, bandwidth and the number of links in UAVs), then fills the M matrix of the UAVs and WAPs with ($R_{x,y}$ or 0s) depending on the constraints.

2. Line(14): Each row of the M matrix will be repeated by the number of UAV links. i.e., UAVlink(x) times.

3. Lines (15-19) If the M matrix is not square. In this case, if the total number of UAVs' links is less than the number of WAPs, the algorithm adds the difference between the two numbers as dummy rows. On the other hand, the algorithm adds

the difference as dummy columns if the total number of UAVs' links is more than the number of WAPs. (the Hungarian algorithm works only with the square matrix, and it achieves the best path cost). It is worth mentioning that the number of WAPs is much more than the number of UAVs in real communicating systems. The proposed algorithm is applicable in either case. This advantage makes it applicable to other association problems where the number of members in each association group can take any value.

4. Line (20) Calls the Hungarian algorithm to find the association between UAVs and WAPs and then updates the M matrix with the association between UAVs and WAPs (by replacing the associated pairs by 0s).

5. Line (22) Calculates the total bandwidth(x) of the associated edges.

6. Lines (24-27) Compare the result in line (22) with the BandWidth(x). If the total bandwidth(x) is less than the BandWidth(x), then the algorithm completes the association and updates the number of available UAVs and WAPs links. On the other hand, if the total bandwidth(x) is more than BandWidth(x), then the algorithm applies lines (28-38) to find the new association.

7. Repeat starting from step 2 until all WAPs are assigned, no more available bandwidth or links at the UAVs.

The proposed algorithm calculates the maximum weighted sum rate of the association problem between UAVs and WAPs, it can be found on the last page of this chapter. Here, the obtained value is very close to the optimal one but with a noticeably reduced complexity.

3.3.1 Optimal Solution

Here, it is assumed that the bandwidth for all UAVs is very high. i.e., the bandwidth constraint is removed. In this case, the proposed algorithm achieves the performance of

the optimal exhaustive search solution. Here, lines 28-42 of the algorithm will be skipped. This would not be the case if there is a shortage of the available bandwidth at some UAVs. In that case, the associations will be revisited based on the lines 28-42 in order to maximize the total weighted sum rate.

3.3.2 The Proposed Algorithm Example

This example provides a clear depiction of the proposed algorithm's functionality. Under the premise that each WAP can create multiple connections with UAVs, and assuming that the WAPs are distributed across different coverage areas. An important aspect of this algorithm is to ensure that no WAP takes more than one connection, if there are any WAPs that have not been assigned to the connection, the goal of this initiative is to maximize the total weighted sum rate of the system. The considered scenario entails three UAVs and five WAPs, and the algorithm operates according to the following steps:

1. **Step 1:** The core network gathered essential data, encompassing factors such as coverage area, desired data rates, bandwidth requirements, SINR between UAVs and WAPs, maximum available bandwidth and links for each UAV, and the minimum SINR threshold, as demonstrated in tables 3.1-3.6 :

   Table 3.1: The coverage area.

	WAP1	WAP2	WAP3	WAP4	WAP5
UAV1	1	1	1	1	1
UAV2	1	0	1	1	1
UAV3	1	1	0	1	1

   Note: If a WAP is located within the coverage area of the UAV, it is assigned a value of 1. Otherwise, it is assigned a value of 0.

   Also, this example assumes that the maximum available bandwidth in each UAV= 60 MHz and $SINR_{min}$= 2.

2. **Setp 2:** The proposed algorithm verifies all constraints, and if they are satisfied, it updates Table 3.4 with the data rate between UAVs and WAPs. However, if any

Table 3.2: The SINR (dB) between the UAVs associated with the WAPs.

	WAP1	WAP2	WAP3	WAP4	WAP5
UAV1	3	4	6	3	2
UAV2	4	3	5	1	2
UAV3	6	7	3	2	5

Table 3.3: The requested bandwidth (MHz) between the UAVs associated with the WAPs.

	WAP1	WAP2	WAP3	WAP4	WAP5
UAV1	15	17	18	20	17
UAV2	16	61	18	15	23
UAV3	15	14	19	18	17

Table 3.4: The requested weighted data rate of the WAPs associated with the UAVs.

	WAP1	WAP2	WAP3	WAP4	WAP5
UAV1	15	18	25	20	17
UAV2	16	19	18	15	40
UAV3	15	14	19	18	17

Table 3.5: Number of links of the WAPs.

WAP1	WAP2	WAP3	WAP4	WAP5
2	1	1	1	2

Table 3.6: Number of links of the UAVs.

UAV1	4
UAV2	3
UAV3	3

constraint is not satisfied, the algorithm assigns a value of 0 to the corresponding entry in Table 3.4 that fails to meet the constraint. This can be achieved through the following:

- First, the algorithm checks the coverage area in Table 3.1 between the UAVs and WAPs. After examining the coverage area, it is observed that WAP2 is not within the coverage area of UAV2 and WAP3 is not within the coverage area of UAV3. As a result, the algorithm assigns a value of 0 to these entries in Table 3.4, as demonstrated in Table 3.7

Table 3.7: The updated data rate after coverage area check.

	WAP1	WAP2	WAP3	WAP4	WAP5
UAV1	15	18	25	20	17
UAV2	16	0	18	15	40
UAV3	15	14	0	18	17

- Second, the algorithm compares the SINR values in Table 3.2 with the minimum required $SINR_{min} = 2$ between each UAV and WAP. After examining the SINR values, it is observed that only the connection between UAV2 and WAP4 does not satisfy the minimum required SINR. As a result, the algorithm assigns a value of 0 to the data rate between UAV2 and WAP4, as demonstrated in Table 3.8

Table 3.8: The updated data rate after SINR check.

	WAP1	WAP2	WAP3	WAP4	WAP5
UAV1	15	18	25	20	17
UAV2	16	0	18	0	40
UAV3	15	14	0	18	17

- Similarly, for the maximum available bandwidth = 60 MHz and requested bandwidth between the UAVs and WAPs in Table 3.3. It can be observed that the value between UAV2 and WAP2 exceeds the maximum available value then, the algorithm replaces the data rate value between UAV2 and WAP2 with 0, as demonstrated in Table 3.9.

Table 3.9: The updated data rate after maximum available bandwidth check.

	WAP1	WAP2	WAP3	WAP4	WAP5
UAV1	15	18	25	20	17
UAV2	16	0	18	0	40
UAV3	15	14	0	18	17

3. **Setp 3:** The algorithm reconstructs Table 3.9 by adding rows for each link that the UAV has. In this example, as illustrated in Table 3.5, UAV1 has 4 links. Therefore,

the row corresponding to UAV1 will be repeated 4 times. Similarly, for UAV2, its row will be repeated 3 times, and for UAV3, its row will be repeated 3 times. The reconstructed table is presented in Table 3.10.

Table 3.10: The updated data rate after the rebuild process.

	WAP1	WAP2	WAP3	WAP4	WAP5
UAV1	15	18	25	20	17
UAV2	16	0	18	0	40
UAV3	15	14	0	18	17
UAV1	15	18	25	20	17
UAV2	16	0	18	0	40
UAV3	15	14	0	18	17
UAV1	15	18	25	20	17
UAV2	16	0	18	0	40
UAV3	15	14	0	18	17
UAV1	15	18	25	20	17

4. **Setp 4:** The Hungarian algorithm works with square matrices in order to determine the optimal path cost. However, in this example, the matrix is not square, the algorithm addresses this by converting it into a square matrix. This conversion is done by adding dummy columns based on the number of links in the UAVs and the WAPs, as demonstrated in Table 3.11.

Table 3.11: The updated data rate for Hungarian algorithm.

	WAP1	WAP2	WAP3	WAP4	WAP5					
UAV1	15	18	25	20	17	0	0	0	0	0
UAV2	16	0	18	0	40	0	0	0	0	0
UAV3	15	14	0	18	17	0	0	0	0	0
UAV1	15	18	25	20	17	0	0	0	0	0
UAV2	16	0	18	0	40	0	0	0	0	0
UAV3	15	14	0	18	17	0	0	0	0	0
UAV1	15	18	25	20	17	0	0	0	0	0
UAV2	16	0	18	0	40	0	0	0	0	0
UAV3	15	14	0	18	17	0	0	0	0	0
UAV1	15	18	25	20	17	0	0	0	0	0

Then the proposed solution calls the Hungarian algorithm to find the optimal as-

sociation between UAVs and WAPs,. Following that, the algorithm reverts the matrix back to its initial state, prior to repeating the rows, while considering the best candidates for optimal associations, as demonstrated in Table 3.12.

Table 3.12: The association candidates after applying Hungarian algorithm.

	WAP1	WAP2	WAP3	WAP4	WAP5
UAV1	15	***18***	***25***	***20***	17
UAV2	***16***	0	18	0	***40***
UAV3	15	14	0	18	17

5. **Step 5:** To complete the selection of these association candidates, the algorithm checks the available bandwidth of each UAV and compares it with the requested bandwidth for these association candidates. By referring to Table 3.3, the algorithm conducts essential computations to ensure the fulfillment of bandwidth constraints. Specifically, in this case, the maximum available bandwidth is 60 MHz. To illustrate further, the association candidates for UAV1 entail a total requested bandwidth of 55 MHz (i.e., UAV1 is associated with WAP2, WAP3 and WAP4). For UAV2, the total requested bandwidth amounts to 39 MHz (i.e., UAV2 is associated with WAP1 and WAP5).

   Afterward, the algorithm proceeds to assess the available bandwidth in each UAV. If the total requested bandwidth is lower than the available bandwidth of the UAV, the algorithm proceeds to finalize the association between the WAPs and updates both the number of available links in the UAVs and the maximum available bandwidth in each UAV. However, if the total requested bandwidth exceeds the available bandwidth, the algorithm follows alternative steps to determine the optimal rate and ensure efficient association.

   In this example, it is determined that the requested bandwidth is lower than the available bandwidth. Consequently, the algorithm successfully finalizes the association process and proceeds to update the available bandwidth in each UAV, along with the number of links for each UAV and WAP. Upon completing the association

and implementing the bandwidth updates, the summarized updates are as follows: The newly available bandwidth for UAV1 is 5 MHz, for UAV2 is 21 MHz, and for UAV3 is 60 MHz. Furthermore, the revised number of available links for each UAVs and WAPs is updated as presented in the tables 3.13-3.14.

Table 3.13: Number of links of WAPs after the update.

WAP1	WAP2	WAP3	WAP4	WAP5
1	0	0	0	1

Table 3.14: Number of links of the UAVs after the update.

UAV1	1
UAV2	1
UAV3	3

Note: If any WAP or UAV has completed their links, the corresponding data rate value will be replaced with 0, as demonstrated in Table 3.15.

Table 3.15: The updated data rate after association .

	WAP1	WAP2	WAP3	WAP4	WAP5
UAV1	15	0	0	0	17
UAV2	0	0	0	0	0
UAV3	15	0	0	0	17

6. **Step 6:** The process keeps repeating, beginning from step 2 until all WAPs are assigned successfully and there is no more unused bandwidth or available links left.

3.4 Complexity Analysis

It is known that the worst-case time complexity for the exhaustive search algorithm is exponential. For the proposed solution, the worst time complexity of the worst case is polynomial and given by $O(VX^3)$, where V is a maximum number of links in all WAPs. This can be explained as follows:

- The for loops in lines 4-12 require a complexity of $O(XY)$.
- The while loop in line 13 requires a complexity of $O(V)$.
- Repeating of the UAVs in lines 14-19 requires a complexity of $O(VXY)$.
- The Hungarian algorithm in line 20 requires a complexity of $O(VX^3)$.
- Updating the matrix and calculating the bandwidth in lines 21-22 require a complexity of $O(VXY)$.
- The for loop in lines 23-41 requires a complexity of $O(VX^2)$.

Therefore, the overall worst-case time complexity is: $O(XY) + O(V) + O(VXY) + O(VX^3) + O(VXY) + O(VX^2) = O(VX^3)$. Considering $V = 1$ as in [109] which has the lowest time complexity in the literature, then the worst case time complexity of the presented algorithm becomes $O(X^3)$. This is much less than the time [109] which is $O(X^3Y^3)$.

3.5 Performance Evaluation

The Gurobi optimization tool [112] is used to find the solution for the exhaustive search algorithm of (3.10 a). UAVs and WAPs are randomly distributed under different coverage areas. PL_{max}= 105, σ_x=1, P_t= 5 watts, $3 \leq N_x \leq 6$, $1 \leq N_y \leq 4$, $SINR_{min}$= -5 dB, $1 \leq W_y \leq 5$. f= 2 GHz, ηLoS= 1 dB, $\eta NLoS$= 20 dB, a= 9.61, b= 0.16, and R= 1000 m. Simulations were performed using three different bandwidth levels at each UAVs (high: B_x= 250MHz, medium: B_x= 120MHz, and low: B_x= 80MHz).

Fig. 3.2 shows the total sum rate of the exhaustive search and the proposed algorithms for a fixed number of 20 UAVs and the number of WAPs in the range of 50 to 120. The results are plotted for three different cases, including high, medium, and low bandwidth. As it can be seen, for a varying number of WAPs, the proposed algorithm has exactly the same performance in terms of the sum rate as the exhaustive search when removing

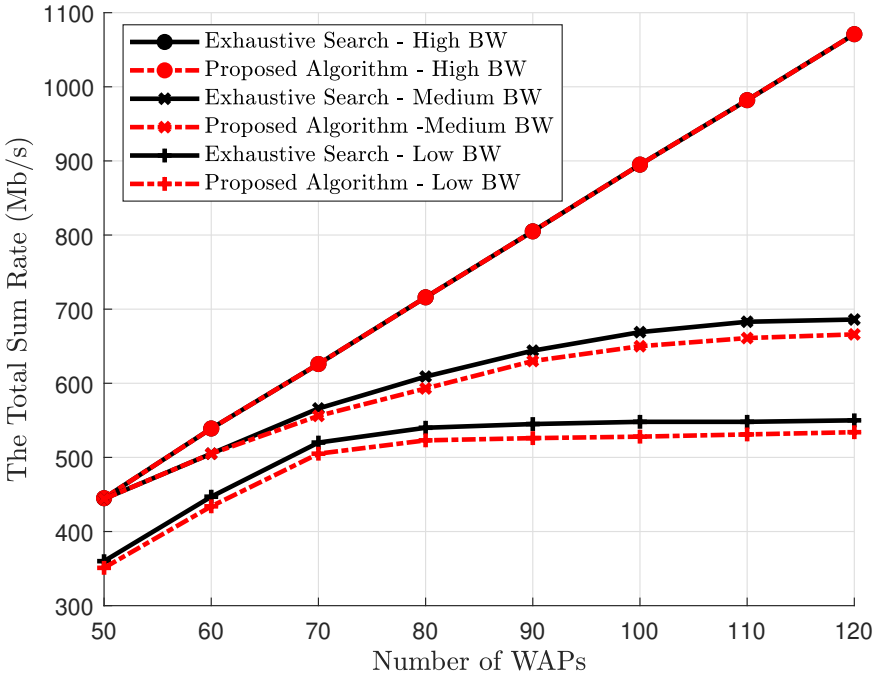

Figure 3.2: Total sum rate with different number of WAPs for exhaustive algorithm and the proposed algorithm at 20 UAVs.

the UAVs bandwidth constraints (high bandwidth level). For the remaining two levels, starting with the case where the number of WAPs range from 50 to 70, it can be noted that the proposed algorithm performance almost approaches the exhaustive search algorithm.

However, there is a slight decrease in the performance of the proposed algorithm for the medium and low level of bandwidths when the number of WAPs is above 70. This can be explained by noting that as the number of the WAPs increases, lines 28-42 will be visited more times in the proposed algorithm rather than re-running the whole process as in the exhaustive search algorithm. This ends up by reducing the complexity with only a minor reduction in the performance, which is not the case in the high bandwidth scenario. However, the weighted sum rate gap in all three cases is less for a lower number of WAPs, e.g., 50 WAPs compared with 100 WAPs. This is due to the fact that when the same bandwidth is used to associate higher numbers of WAPs, the sum rate gap becomes greater compared to the case where the same bandwidth is used to associate a smaller

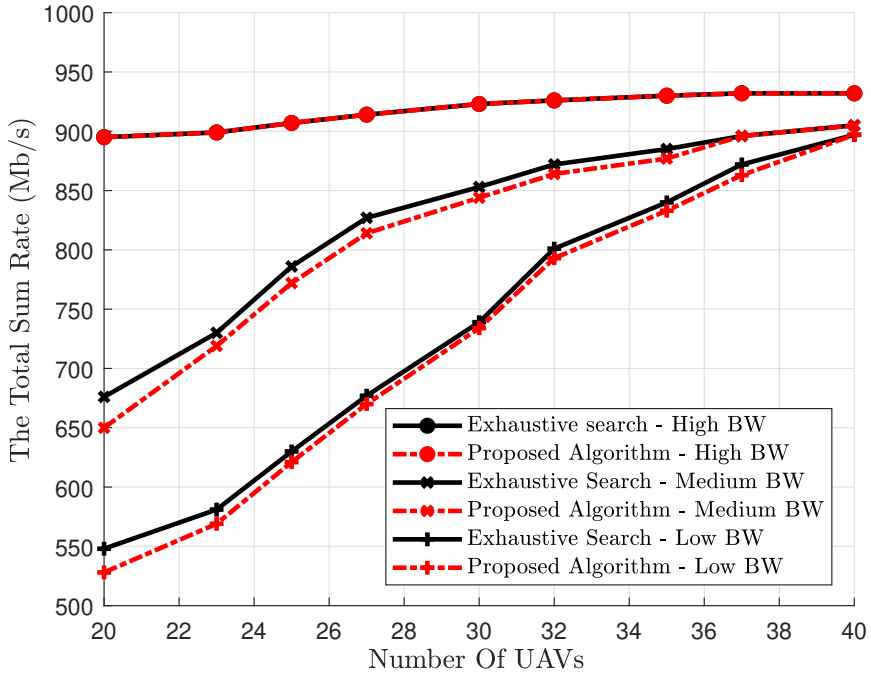

Figure 3.3: Total sum rate with different number of UAVs for exhaustive algorithm and the proposed algorithm at 120 WAPs.

number. Finally, for the medium and low bandwidth curves, the performance saturates as the number of the WAPs increases. This is because not all UAVs' links will be used due to the bandwidth constraint. Also, the saturation point shifts to the right when the bandwidth increases.

Fig. 3.3 shows the total weighted sum rate for a fixed number of 100 WAPs when the number of UAVs varies between 20 and 40. It can be noticed that for a varying number of UAVs, the proposed algorithm performance is similar to that of the optimal exhaustive search for the high bandwidth case. In contrast to the high bandwidth case, there is a slight difference in the performance of the proposed algorithm for the medium and low bandwidth levels when the number of UAVs is small. This slight degradation of performance is due to the decreased bandwidth of UAVs. However, as the number of UAVs is increased to 30 and above, the proposed solution performance approaches the optimal one in all cases. This is due to the fact that, for the fixed number of the WAPs,

the bandwidth tends to increase with the increasing number of the UAVs and attains a sufficiently large bandwidth to approach the optimal solution. Moreover, compared to Fig. 3.2, it can be observed that the sum rate gap is larger when the number of UAVs is small, and with the increasing number of UAVs, the bandwidth becomes sufficient to decrease the sum rate gap. However, in the case of 40 UAVs and 120 WAPs, the Gurobi optimization tool takes around 33672 seconds running time, which is a very long time compared to the presented algorithm (which takes around 93 second). Here, the used computer processor is Intel Xeon E3-1225V2 @ 3.20 GHz and the RAM is 8 GB.

3.6 Conclusion

This work studies the association problem of the UAVs with WAPs to maximize the sum rate with some consideration such as each UAV's bandwidth, coverage area, the minimum required SINR, the number of providing links from UAVs, the number of connections from WAPs, and fairness constraints. This work proposes an extended centralized Hungarian algorithm to find a suboptimal association between the UAVs and WAPs. The obtained results show that the proposed algorithm has noticeably lower computational complexity than the work in the literature. It even reaches the exhaustive search algorithm performance when the available bandwidth at the UAVs is very high.

Algorithm 1 The Proposed Algorithm

Input: (SINR_{min}, weight(y), UAVlink(x), UAVs(X), WAPs(Y), SINR(x, y), WAPLink(y), Coverage(x, y), BandWidth(x), bandwidth(x, y), rate(x, y)).
Let M(x, y) be a new matrix ▷ M(x, y) is the (weight(y).rate(x,y))between UAV(x) and WAP(y).
H = M.
for $i = 1$ to x **do**
    for $j = 1$ to y **do**
        if BandWidth(x) > bandwidth(x, y) and SINR(x, y) >= SINR_{min} and Coverage(x, y) == 1 **then**.
            M(x, y) = weight(y)rate(x, y).
        else
            M(x, y) = 0.
        end if
    end for
end for
while MaxLink≠ 0 **do** ▷ MaxLink : The maximum number of links in all WAPs.
    Repeat UAVs ▷ Each UAV will be repeated by the number of links it has and updates the matrix (M).
    if size(M, 2) > size(M, 1) **then**
        Make(M) as a square matrix by adding the difference value between size(M,2) and size(M,1) as dummy.
    else
        Make(M) as a square matrix by adding the difference value between size(M,1) and size(M,2) as dummy.
    end if
    Call Hungarian algorithm (M) .
    Update the matrix(H) by edge that associates
    Calculate the total bandwidth(x) in each row in edge matrix(H) that associate.
    for $x = 1$ to size(BandWidth(X) **do**
        if BandWidth(x) > total bandwidth(x) **then**
            BandWidth(x) = BandWidth(x) − total bandwidth(x)
            UAVlink(x) = UAVlink(x) − 1
            WAPLink(y) = WAPLink(y) − 1
        else
            $[x, y]$= Max value from column(x) ▷ $[x, y]$ is the element's location
            while check == false **do**
                if UAVlink(x)≠0 and BandWidth(x) > bandwidth(x, y) **then**
                    BandWidth(x) = BandWidth(x) − bandwidth(x, y)
                    UAVlink(x) = UAVlink(x) − 1
                    WAPLink(y) = WAPLink(y) − 1
                    check = True
                else
                    $[x, y]$ == 0,
                end if
            end while
        end if
    end for
    MaxLink = MaxLink − 1
end while

Chapter 4

Less Complex Algorithm to Max-Min the Resource Allocation for Unmanned Aerial Vehicles Networks

4.1 Introduction

sixth-generation (6G) wireless communication networks promise to increase network coverage, the ability to transfer large amounts of data with exceptional speed, the number of connected devices, and the network availability. It is also expected that 6G networks will enhance the spectral and energy efficiency [6, 113]. Existing terrestrial cellular systems provide communication services using BSs at fixed locations. Building a complete cellular infrastructure in some regions and countries can be very expensive. In some situations, ground BSs suffer from limited coverage, which leads to poor communication quality. Furthermore, weather conditions reduce the communication quality of the ground BSs [114, 115].

In 6G wireless communication, new technologies can be applied to overcome the exist-

ing terrestrial cellular systems limitations and satisfy the performance expectations of the communication system. UAVs are one of these technologies, which can be used as flying BSs. Low power networks, in which devices use low power to communicate over a short distance, can efficiently utilize the UAVs. i.e., when there is no need to increase network coverage. As a result, UAVs can be used as wireless relays to increase the coverage of a network and the connectivity of ground-based wireless devices [21, 23]. Thus, these flying BSs can be used to provide connectivity for the terrestrial networks. Due to UAVs' mobility, flexibility, cost-effectiveness, and ability to adapt their altitude, UAV-BSs are able to avoid the obstacles and provide additional capacity for urban areas. Also, they can provide network coverage in hard-to-reach rural areas [100, 114]. Moreover, due to the high altitude at which UAVs are found, LoS communication is greatly facilitated. For example, in vertical or slant-free space optic links, the effect of atmospheric turbulence decreases with altitude [116].

There are many resource management challenges for a successful deployment of UAV-assisted wireless networks such as spectrum efficiency for sub-channel allocation, user association problem, power management, deployment cost, and deployment time [104, 105]. The association problem between UAVs and WAPs has been studied in the literature. The authors in [86] studied the users-UAVs association problem to maximize the sum data rate along with minimizing the inter-cell interference. They considered the re-usable channel pool to solve the association problem while taking into account the interference with neighboring cells. The authors in [106] formulated the association problem of SCs and UAVs to maximize the sum data rate while taking into consideration the UAVs' data rate, bandwidth and the number of links. They also showed that the SCs-UAVs association problem is an NP-hard problem.

Centralized and distributed algorithms were proposed in [109] to optimize the SCs - UAVs association with the objective of maximizing the total sum rate. The authors took into consideration the QoS constraint, the UAV's number of links, and available bandwidth. One of this work's limitations is that it did not consider the fairness condition, where some SCs can be associated with the minimum data rate. Another limitation is the

fixed number of links for each UAV. Additionally, the complexity of the work in [109] is still high and ought to be decreased, but in comparison to related work in the literature, this work has less complexity (the comparison between their work and the nearest previous work in the literature can be found in the complexity analysis section in [109]).

Compared to the existing work in the literature, this chapter examines the association problem between WAPs and UAVs, considering more practical operational conditions, such as dealing with WAPs distributed in different coverage areas. This study also tackles the issue of fairness between WAPs by formulating a max-min optimization problem. In addition, this work maximizes the total weighted sum rate of the system, and so each WAP can be granted a certain weight. In this regard, this chapter proposes a centralized algorithm to find a sub-optimal solution at very low complexity. Moreover, the proposed algorithm assigns the channels among the pool of channels provided by the main core network. The obtained result results show that the proposed algorithm outperforms its counterparts in the literature and that it approaches the optimal solution with a noticeable reduction in system complexity.

Chapter Organization: The system model and problem formulation are described in Section 4.2. The proposed algorithm is presented in Section 4.3. After that, time complexity analysis is provided in Section 4.4. Then, the system performance is evaluated in Section 4.5. Finally, this work is concluded in Section 4.6.

4.2 System Model and Problem Formulation

4.2.1 System Model

As shown in Fig. 4.1, a heterogeneous wireless network is studied, which contains WAPs, UAVs and a core network. Each UAV works as a flying BSs to provide connectivity to the WAPs. This work assumes that the UAVs are deployed at the best pre-defined altitude, and they are distributed at different locations in a specific coverage area [61]. To facilitate the implementation of the centralized algorithm, UAVs can share the control

information (required bandwidth, required data rate, and SINR) with the core network for association purposes. Based on the control information, the system can specify the association between WAPs and UAVs. However, this does not include the data. Finally, the proposed work applies a weighted objective function to solve the optimization problem.

This work investigates a system with Y UAVs and X WAPs ($X <=> Y$) where the set of UAVs are represented as a vector $\mathbf{U} = [u_1, u_2, \ldots, u_y]$, and the set of WAPs are represented as vector $\mathbf{S} = [s_1, s_2, \ldots, s_x]$. This system model can be considered as a similar model to the one in [109]. However, the main difference between the used system model and the one in [109], The difference is that this approach applies channel assignments from the channel pool provided by the core network and distributes them to UAVs depending on the number of users and the maximum data rate between UAVs and WAPs. The system also tackles the fairness between the WAPs through finding the max-min total sum data.

4.2.2 Problem Formulation

The proposed algorithm aims to find the best association between UAVs and WAPs. This work enables the core network (while utilizing the best channel assignment) to distribute links between UAVs to maximize the minimum total sum rate subject to some practical constraints. These constraints are the QoS, the maximum number of links, and the available bandwidth of each UAV.

- ***Association***: Assuming that the s_x WAP is in the coverage area of the u_y UAV, then the data rate $R_{x,y}$ between s_x and u_y can be calculated using the Shannon's capacity. Therefore, the provided data rate by each u_y can be found as $\sum_{x=1}^{X} W_x R_{x,y} L_{x,y}$. Also, the total sum-rate over all UAVs can be calculated as $\sum_{x=1}^{X} \sum_{y=1}^{Y} W_x R_{x,y} L_{x,y}$. Here, W_x is the x^{th} WAP connection weight and $L_{x,y}$ de-

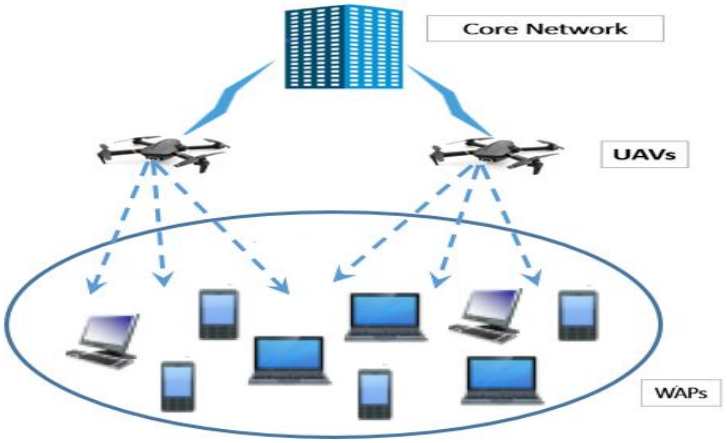

Figure 4.1: Graphical representation of UAVs, WAPs and the core network.

notes the association between s_x, and u_y that can be defined as

$$L_{x,y} = \begin{cases} 1, & \text{if } s_x \text{ is connected with } u_y, \\ 0, & \text{otherwise.} \end{cases} \tag{4.1}$$

- ***QoS***: The SNR between s_x and u_y can be defined as

$$SNR_{x,y} = \frac{P_{x,y} PL(d_{x,y})}{\sigma_y^2}, \tag{4.2}$$

where $P_{x,y}$ is the transmit power from u_y to s_x, σ_y^2 is the noise power at u_y, $d_{x,y}$ is the distance between u_y and s_x, and PL is the path loss (function of $d_{x,y}$). The $SNR_{x,y}$ should be greater than the minimum required SNR_{min}. Therefore, the QoS constraint can be defined as

$$L_{x,y} SNR_{\min} \leq SNR_{x,y}, \quad \forall\, x, y. \tag{4.3}$$

- ***Bandwidth***: The bandwidth constraint can be written as

$$\sum_{x=1}^{X} L_{x,y} b_{x,y} \leqslant B_y\ , \quad \forall\, y, \tag{4.4}$$

where B_y represents the maximum available bandwidth for u_y, and $b_{x,y}$ denotes the s_x requested bandwidth from u_y.

- ***Number of links***: Let N denotes the total number of available links (channels) at the core network. Thus, the total number of associations can not exceed N as

$$\sum_{y=1}^{Y}\sum_{x=1}^{X} L_{x,y} \leqslant N. \tag{4.5}$$

Moreover, each WAP can only be associated to a single UAV. This constraint can be written as

$$\sum_{y=1}^{Y} L_{x,y} \leqslant 1\ , \quad \forall\ x. \tag{4.6}$$

Taking into consideration the previously mentioned constraint, the association problem between the WAPs and UAVs can be written as

$$\text{Objective:} \quad \max \min_{L_{x,y}} \quad \sum_{x=1}^{X}\sum_{y=1}^{Y} W_x R_{x,y} L_{x,y}. \tag{4.7a}$$

$$\text{Subject to:} \quad L_{x,y} SNR_{\min} \leq SNR_{x,y}\ , \quad \forall\ x, y. \tag{4.7b}$$

$$\sum_{x=1}^{X} L_{x,y} b_{x,y} \leqslant B_y\ , \quad \forall\ y. \tag{4.7c}$$

$$\sum_{y=1}^{Y}\sum_{x=1}^{X} L_{x,y} \leqslant N. \tag{4.7d}$$

$$\sum_{y=1}^{Y} L_{x,y} \leqslant 1\ , \quad \forall\ x. \tag{4.7e}$$

$$L_{x,y} \in \{0, 1\}\ , \quad \forall\ x, y. \tag{4.7f}$$

This problem is an ILP that can be solved numerically to get the optimal solution with an exponential upper-bound computational complexity [111]. Hence, this problem is an NP-hard problem as explained in [106, 109]. The proposed work in [106, 109] shows that the formulated problem is equivalent to the generalized assignment problem. This equivalent

relation along with the fact that the formulated problem can be reduced to a maximum knapsack problem [110] proves the NP-hard complexity of the formulated problem. The following section explains the proposed algorithm that obtains a sub-optimal solution but with much less complexity.

4.3 The Proposed Algorithm

This section proposes a channel assignment centralized algorithm with low complexity to find a sub-optimal solution to the association problem in 4.7. The proposed algorithm aims to solve the unbalanced association problem between the UAVs and the WAPs. More specifically, this algorithm does the best assignment of the available channel pool at the core network (i.e., distributes them between the UAVs), and calculates the total sum rate by maximizing the minimum data rate at each WAP. The channel assignment centralized algorithm (Algorithm 2) can be explained as follows:

1. Line(1): The UAVs share some control information (SNR_{min}, W, N, $\mathbf{U}$, $\mathbf{S}$, SNR, B, b, R) with the core network.

2. Lines (3-4): The algorithm calculates the average value for each row in matrix M, then it finds the minimum average which is used as a threshold to keep the entries of M or replace them by 0s.

3. Lines (5-13): The algorithm checks if all constraints are satisfied for each entry in M, if not, then $M_{x,y} = 0$.

4. Lines (14-15): The algorithm calculates the maximum value of each row in the matrix M and reorders its rows in descending order depending on the maximum values.

5. Lines (17-20): The algorithm checks if the UAVs have free links or all WAPs are connected. Thus, if any of the UAVs has free links and not all the WAPs are

connected, then the lines (22-41) will be applied. Otherwise, the algorithm will stop.

6. Lines (22-32): The algorithm calculates the total sum rate by taking the maximum value on each matrix M row, and comparing the requested WAP bandwidth of the selected value with the bandwidth of the candidate UAV. If the WAP bandwidth is less than the candidate UAV bandwidth, then the algorithm completes the association and updates the number of available UAVs, the number of links, and the total sum rate. Otherwise, the algorithm applies lines (33-37).

7. Repeat points 5 and 6 until all WAPs are assigned, no more available bandwidth, or all UAVs links are used.

It is worth mentioning that if the available bandwidth at all UAVs is high (i.e., when removing the bandwidth constraint). The lines 30-39 of the algorithm will be ignored. In this case, the presented algorithm achieves the exact optimal exhaustive solution. The proposed algorithm 2.

4.3.1 The Proposed Algorithm Example

This section presents an illustrative example to clarify the methodology of the proposed algorithm. Assuming 4 UAVs and 4 WAPs, the algorithm follows the following steps to find the best association :

1. **Step 1:** The core network acquired the necessary data including SNR_{min}, required data rates, bandwidth and SNR between UAVs and WAPs, and maximum available bandwidth at each UAV. Additionally, it determined the number of available links within the core network that can support the connection, as demonstrated in the tables 4.1-4.3:

Table 4.1: The SNR (dB) between the WAPs associated with the UAVs.

	UAV1	UAV2	UAV3	UAV4
WAP1	3	4	6	3
WAP2	4	1	5	2
WAP3	6	7	3	2
WAP4	3	4	6	3

Table 4.2: The requested bandwidth (MHz) of the WAPs associated with the UAVs.

	UAV1	UAV2	UAV3	UAV4
WAP1	15	17	18	20
WAP2	16	41	18	15
WAP3	15	14	19	18
WAP4	15	17	18	20

Table 4.3: The requested weighted data rate of the WAPs associated with the UAVs.

	UAV1	UAV2	UAV3	UAV4
WAP1	15	18	25	20
WAP2	20	14	13	15
WAP3	15	14	24	16
WAP4	3	3	7	4

Also, this example assumes that the maximum available bandwidth for each UAV= 40 MHz, SNR_{min}= 2 and the maximum number of links at the core network = 8.

2. **Step 2:** Firstly, the algorithm calculates the average value for each row in Table 4.3 as demonstrated in Table 4.4.

Table 4.4: The average data rate of the WAPs associated with the UAVs.

	UAV1	UAV2	UAV3	UAV4	The average
WAP1	15	18	25	20	19.50
WAP2	20	14	13	15	15.50
WAP3	15	14	24	16	17.25
WAP4	3	3	7	4	04.25

Next, it finds the minimum value from the average column and designates it as the threshold value. If any value in Table 4.4 is less than the threshold value, the algorithm replaces it with 0. In this example, the minimum value is **4.25**, resulting in a threshold of **4.25**. Upon examination, it is observed that the rates between WAP4 and UAV1, UAV2, and UAV4 are below the threshold. Consequently, the algorithm replaces these rates with 0 as demonstrated in Table 4.5, while keeping the other values unchanged.

Table 4.5: The updated data rate of the WAPs associated with the UAVs.

	UAV1	UAV2	UAV3	UAV4
WAP1	15	18	25	20
WAP2	20	14	13	15
WAP3	15	14	24	16
WAP4	0	0	7	0

3. **Setp 3:** The proposed algorithm will now verify all the constraints and update Table 4.5 with the data rate between UAV and WAP if the constraints are met. If the constraints are not satisfied, the algorithm will assign a value of 0 to the corresponding entry in Table 4.5. This can be achieved through the following:

   - First, the algorithm compares the SNR values in Table 4.1 with the $\text{SNR}_{min} = 2$ between each WAP and UAV. Based on the SNR values in Table 4.1, it is clear that only the connection between WAP2 and UAV2 does not meet the minimum required SNR. Consequently, the algorithm assigns a value of 0 to the data rate between UAV2 and WAP2, as demonstrated in Table 4.6.

Table 4.6: The updated data rate of the WAPs associated with the UAVs.

	UAV1	UAV2	UAV3	UAV4
WAP1	15	18	25	20
WAP2	20	0	13	15
WAP3	15	14	24	16
WAP4	0	0	7	0

- Second, for the maximum available bandwidth = 40 MHz and requested bandwidth between the WAP and UAV in Table 4.2. It can be observed that the value between UAV2 and WAP3 is above the maximum available value, then, the algorithm replaces the data rate value between UAV2 and WAP2 with 0 as demonstrated in Table 4.7.

Table 4.7: The updated data rate of the WAPs associated with the UAVs.

	UAV1	UAV2	UAV3	UAV4
WAP1	15	18	25	20
WAP2	20	0	0	15
WAP3	15	14	16	24
WAP4	0	0	7	0

4. **Step 4:** The algorithm finds the maximum value for each row in Table 4.7. It is observed that the maximum value in row 1 is 25, in row 2 is 20, in row 3 is 24, and in row 4 is 7 as demonstrated in Table 4.8.

Table 4.8: The updated data rate considering the maximum values.

	UAV1	UAV2	UAV3	UAV4	The Max
WAP1	15	18	25	20	25
WAP2	20	0	0	15	20
WAP3	15	14	16	24	24
WAP4	0	0	7	0	7

Subsequently, the algorithm proceeds to rearrange the rows of Table 4.8 in descending order based on their respective maximum values as demonstrated in Table 4.9.

Table 4.9: The updated data rate after rearranging the rows.

	UAV1	UAV2	UAV3	UAV4
WAP1	15	18	25	20
WAP3	15	14	16	24
WAP2	20	0	0	15
WAP4	0	0	7	0

5. **Step 5:** In order to guarantee the assignment of all WAPs, the algorithm examines the associations of each WAP. If any WAP is found to have only one candidate

association, such as WAP4 in this case, the algorithm prioritizes the association with that particular WAP. Consequently, the algorithm reorganizes Table 4.9 based on this update. As a result, WAP4 is moved to the top of Table 4.9, as demonstrated in Table 4.10.

Table 4.10: The updated data rate after guaranteeing the assignment.

	UAV1	UAV2	UAV3	UAV4
WAP4	0	0	7	0
WAP1	15	18	25	20
WAP3	15	14	16	24
WAP2	20	0	13	15

6. **Step 6:** In order to finalize these association candidates, the algorithm must assess the available bandwidth for each UAV in relation to the requested bandwidth for the UAV associated with the WAP.

   Using Table 4.2, the algorithm performs the necessary calculations to guarantee bandwidth constraint satisfaction, in this case, the maximum available bandwidth =40 MHz. In this example, the total requested bandwidth for the candidate associations with UAV1 is 16 MHz (i.e., UAV1 is associated with WAP2). In UAV3, the total requested bandwidth is 36 MHz (i.e., UAV3 is associated with WAP1 and WAP4), while in UAV4 it is 18 MHz (i.e., UAV4 is associated with WAP3).

   Following that, the algorithm proceeds to examine the available bandwidth for each UAV. If the total requested bandwidth is less than the available bandwidth, the algorithm will finalize the association of WAPs and update both the number of available links in the core network and the maximum available bandwidth for each UAV. Otherwise, the algorithm applies the steps in lines (22-41) again. In this example, the requested bandwidth is found to be less than the available bandwidth. As a result, the algorithm successfully completes the association process and proceeds to update the available bandwidth for each UAV, as well as the number of links in the core network. After completing the association and updating the bandwidth, the updates are summarized as follows: The new available bandwidth for UAV1

is 24 MHz, for UAV2 is 40 MHz, for UAV3 is 4 MHz, and for UAV4 is 22 MHz. Additionally, the revised number of available links in the core network is now 4.

7. The algorithm continues to repeat, starting from step 3, until all WAPs are successfully assigned, and there is no remaining available bandwidth or links. This approach ensures the efficient allocation of resources and guarantees the assignment of all WAPs.

4.4 Complexity Analysis

It is well known that the worst-case time complexity of the exhaustive solution is exponential. For the presented algorithm, the worst-case time complexity is polynomial and given by $O(NXY^2)$. This can be explained as follows:

- Calculating the average value in lines 3-4 requires a complexity of $O(XY)$.
- The loops in lines 5-13 require a complexity of $O(XY)$.
- Calculating the maximum value in lines 14-15 requires a complexity of $O(XY)$.
- The loop in line 17 requires a complexity of $O(N)$.
- The loop in lines 22-39 requires a complexity of $O(XY^2)$.

Therefore, the overall worst-case time complexity of the proposed algorithm can be calculated as $O(XY)+O(XY)+O(XY)+O(NXY^2) = O(NXY^2)$ which is much less than the exponential time complexity.

4.5 Performance Evaluation

This section compares the performance of the presented algorithm with an exhaustive search. The work assumes that the UAVs and WAPs are randomly distributed in the

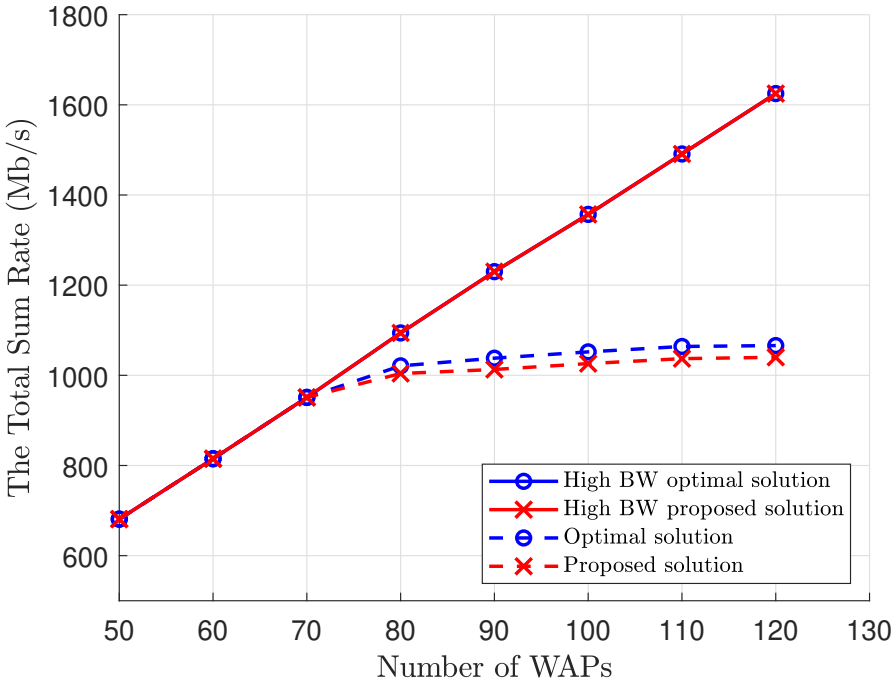

Figure 4.2: Total sum rate with different number of WAPs for exhaustive algorithm and the proposed algorithm at 10 UAVs.

same coverage area. $\sigma_y^2 = 1$, P_t= 5 watts, SNR_{min}= -5 dB. Simulations were performed using two different bandwidth levels at each UAVs (high: B_x= 250 MHz, and low: B_x= 80 MHz). The fminimax function in Matlab [117] is used to find the solution for the exhaustive search algorithm solution of (4.7a).

In Fig. 4.2, the total sum rate of the proposed algorithm is plotted and compared against the exhaustive search method. Here, the number of UAVs is fixed to 10, and the number WAPs varies from 50 to 120. Two different cases are considered that are the high and low bandwidth. As the figure shows, the performance of the proposed algorithm is exactly the same as the exhaustive search for the high bandwidth case (i.e., without considering the UAVs bandwidth constraints). For the low bandwidth case, it can be clearly seen that the solution of the proposed algorithm approximately approaches the exhaustive search algorithm when the number of WAPs ranges from 50 to 70. On the other hand, considering the case in which the number of WAPs is more than 70, the performance of the proposed

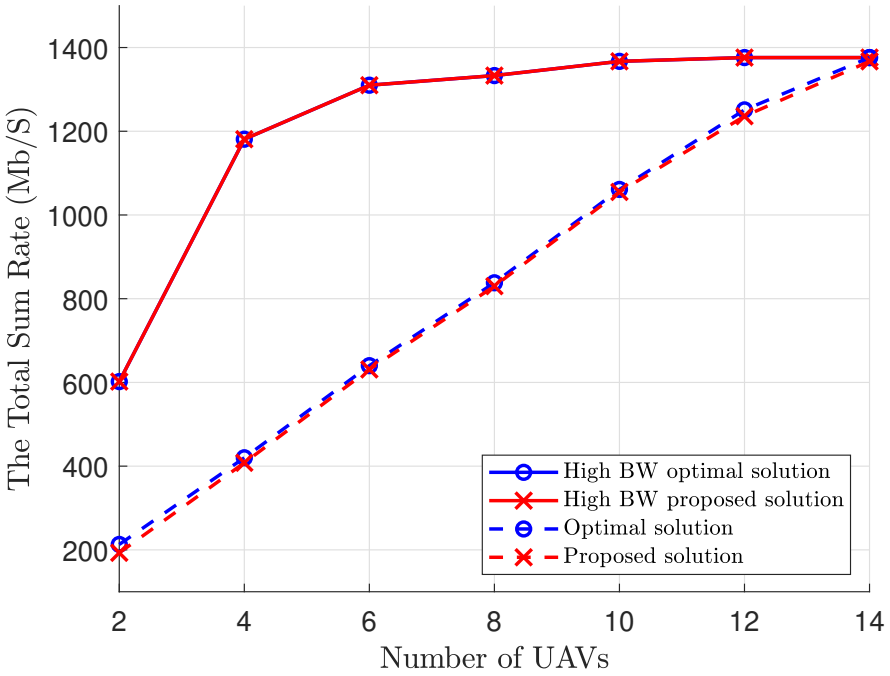

Figure 4.3: Total sum rate with different number of UAVs for exhaustive algorithm and the proposed algorithm at 100 WAPs.

algorithm slightly decreases for the low bandwidth case. This can be understood by noticing that as the number of the WAPs increases, lines 33-37 of the proposed algorithm will be executed more times rather than re-running the whole process as in the exhaustive search algorithm. As a result, the complexity of the system is reduced without much degradation in the system performance. Finally, the performance saturates for the low bandwidth curve as the number of the WAPs increases. Fig. 4.3 shows the total sum rate for a fixed number of WAPs when the number of UAVs varies between 2 and 14. The result here agrees with the result in Fig. 4.2 where for a varying number of UAVs, the proposed algorithm performance is similar to that of the optimal exhaustive search for the high bandwidth case. In contrast to the high bandwidth case, there is a slight difference in the performance of the proposed algorithm for the low bandwidth case. On the other hand, the performance saturates in the high bandwidth case for both the proposed and the exhaustive algorithms when the number of UAVs reaches 10. This is because for a fixed number of WAPs, the bandwidth tends to increase when the number UAVs is increased

and it achieves a sufficient large amount to reach the optimal solution. Finally, to show the reduction in the system complexity, the simulation is run when the system has 10 UAVs and 120 WAPs. The exhaustive algorithm takes around 41253 seconds running time, which is a very long time compared to the proposed algorithm which takes around 17 seconds. Here, the used computer processor used is Intel Xeon E3-1225V2 @ 3.20 GHz and the RAM is 8 GB.

4.6 Conclusion

This work proposed a simplified algorithm that jointly optimizes the channel assignment from the pool of channels and max-min the total sum rate. The obtained results show that the proposed algorithm approaches the performance of the exhaustive search with much lower computational complexity. Moreover, it can reach the performance of the exhaustive search algorithm when the available bandwidth at the UAVs is very high. More practical operation conditions such as the movement of the UAVs and the power constraints will be considered in future work.

Algorithm 2 The Proposed Algorithm

1: Input: $\big(SNR_{min}, W, N, \mathbf{U}, \mathbf{S}, SNR, B, b, R\big)$.
2: Let $M_{X,Y}$ be a new weighted matrix such that $M_{x,y} = W_x R_{x,y}$.
3: Let Z_X be a new vector such that z_x is the average value of each row on the matrix M
4: Let A be a new variable such that A is the minimum value of the vector Z
5: **for** $x = 1$ to X **do**
6: **for** $y = 1$ to Y **do**
7: **if** $B_y > b_{x,y}$ && $SNR_{x,y} >= SNR_{min}$ && $M_{x,y} > A$ **then**.
8: The value of $M_{x,y}$ Unchanged
9: **else**
10: $M_{x,y} = 0$.
11: **end if**
12: **end for**
13: **end for**
14: Let K be a new vector such that k_x is the max value of each row in M
15: Rearrange the M matrix rows descending based on the descending sort of the K vector values.
16: $Improve = true$
17: **while** $Improve$ **do**
18: Let T be a new variable such that T is the summation of all element in matrix M
19: **if** $N == 0 \parallel T == 0$ **then**
20: $Improve = false$
21: **end if**
22: **for** $x = 1$ to X **do**
23: Let c be a new variable such that c is the location of the maximum value in row x
24: **if** $B_c > b_{x,c}$ **then**
25: $B_c = B_c$- $b_{x,c}$
26: N=$N-1$
27: Let TSM be a new variable such that TSM is the total sum rate
28: TSM=TSM+ $Max(M_{x,:})$
29: $M(x,:) = 0$
30: **if** $N == 0$ **then**
31: $Improve = false$
32: **end if**
33: **else**
34: $M_{x,c} = 0$
35: Repeat lines 14-15
36: $Improve = true$
37: $break$;
38: **end if**
39: **end for**
40: **end while**
41: $Display\ TSM$

Chapter 5

Capacity Analysis of UAV Communications Under the Non-ideal Transceiver Effects

5.1 Introduction

Compared to current wireless networks, 6G wireless communication networks need to support lower latency, higher data rate, and greater QoS for all data streams [6, 113]. In conventional terrestrial network architectures, the fixed locations of the BSs are usually determined to guarantee a certain level of network coverage. However, static BSs are greatly affected by blockage, dispersion, and unpredictable weather conditions, which ultimately affect the system performance [81]. In contrast, aerial technologies like drones, balloons, and UAVs have demonstrated promising potential in addressing these challenges by offering reliable, economical, and environmentally-friendly solutions with built-in advantages, including versatility, adaptability, and altitude flexibility. UAVs can also assist dense networks and operate in rural areas with a lack of adequate infrastructure [86]. In particular, cellular-connected UAVs hold enormous potential in achieving genuinely remote UAV operations with indefinite range, practical UAV monitoring and control,

high-capacity payload transmission, and cellular-enhanced positioning [118].

The work in [119] designed a UAV-assisted IoT system that relies on the shortest flight trajectory of the UAVs in order to maximize the amount of information gathered from IoT nodes. Additionally, the optimum trajectory and throughput within a specific coverage region were determined using a deep reinforcement learning-based method. The work in [120] provided a projectile motion trajectory for the communication between the UAV and GS. The optimal data rate was obtained using the Genetic algorithm, and the effect of the projection angle on the transmission rate was analyzed. The work in [121] analyzed the UAVs-GS cooperative network in which each communication link has unique channel conditions. It showed the height-dependent outage performance of the network when implementing the decode and forward protocol at the ground relays, and they derived the lower bound for the end-to-end outage probability.

However, these works sidestepped the HWIs at the transmitters and receivers, while in practical communication systems, HWIs have a significant effect on system performance. The HWIs are caused by a variety of factors, including power amplifier non-linearity, in-phase quadrature-phase imbalance, analog imperfections, phase noise, and timing and frequency synchronization issues [122,123]. The work in [124] studied the impacts of HWIs on intelligent reflecting surfaces enabled multiple-input single-output (MISO) wireless communication system. This work showed that the ergodic capacity always reaches a finite limit, which depends only on the levels of transceiver HWIs. The work in [125] studied the performance of intelligent reflecting surfaces-assisted integrated satellite-UAV -terrestrial networks under the effects of the HWIs. This work obtained a closed-form expression for the outage probability and concluded that a higher level of impairment would result in worse system performance.

After reviewing the literature, it found that no work has studied the effects of the HWIs on UAV-GS communication. Motivated by the importance of this topic, this work studies the effect of the HWIs on the ergodic capacity. This work provides an analytical derivation for the average ergodic capacity considering the averaging over the Rician

parameter, the distance between the UAV and the GS. This work also assumes that the GS has multiple antennas. This work also provides an asymptotic analysis of the system performance when the transmitted power and the number of GS antennas become very large.

Chapter Organization: Section 5.2 presents the system model. Section 5.3 discusses the system performance analyses. Section 5.4 discusses the simulation results. Finally, Section 5.5 concludes the work.

Notations: Scalar, column vector, and matrix are represented using a normal letter, lower-case bold-face, and capital-case bold-face, respectively. $\mathbb{E}\{\cdot\}$, $\|\cdot\|$, and $(\cdot)^{\mathrm{H}}$ are used for statistical expectations, Euclidean second norm, and Hermitian, respectively. An identity matrix and a zero vector are represented by $\mathbf{I}$ and $\mathbf{0}$, respectively. A circularly symmetric complex Gaussian vector with $\mathbf{0}$ mean vector and $\boldsymbol{\epsilon}$ covariance matrix is represented by $\mathbf{z} \sim \mathcal{CN}(\mathbf{0}, \boldsymbol{\epsilon})$.

5.2 System Model

5.2.1 Channel Model

This work considers a single-antenna UAV transmitting data to a GS equipped with M-antennas as illustrated in Fig. 5.1. The assumption is that theUAV moves in a random 3D trajectory within a spherical space with radius r, and this is done such that the GS is fixed on the surface of the 3D sphere while the UAV flies within this domain. The channel vector between the GS and the UAV is $\boldsymbol{g} = \sqrt{\beta}\boldsymbol{h}$, where $\beta = l^{-\alpha}$, l is the distance between the UAV and the GS , α[1] is the path loss exponent, and $\mathbf{h} \in \mathbb{C}^{\mathrm{M}\times 1}$ is the fast fading channel. The fast fading channel realizations are modeled as Rician fading channels consisting of two components: The deterministic component corresponds to the LoS signal and the Rayleigh distribution of the scattered signal. The Rician parameter K

[1] α can be modeled as a non-increasing function of θ, and the latter has a slight effect on α. Based on that, α can be considered independent of θ, depending only on the environmental conditions [121, 126].

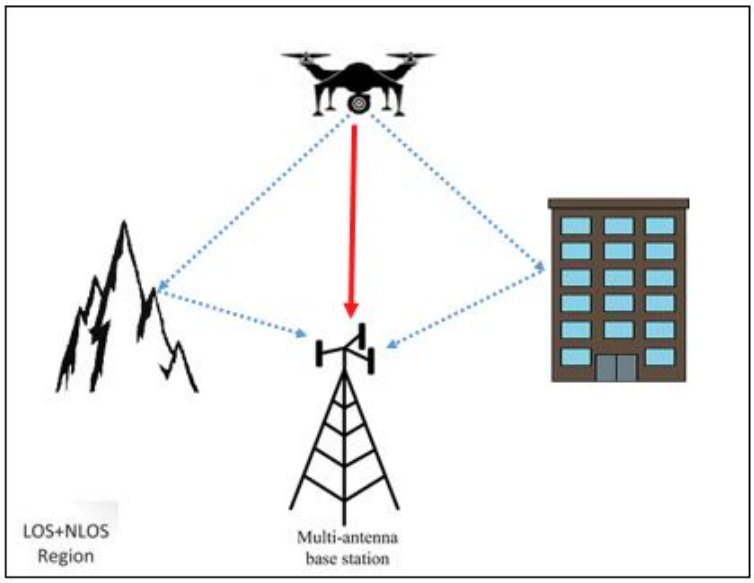

Figure 5.1: System model: single-antenna UAV communicates with a GS equipped with M-antennas.

represents the ratio of the LoS component power to the Rayleigh-distributed component power.

The fading channel is given as in [55–57]

$$\mathbf{h} = \sqrt{\frac{K}{K+1}}\bar{\mathbf{h}} + \sqrt{\frac{1}{K+1}}\mathbf{h}_w, \tag{5.1}$$

where $\bar{\mathbf{h}} = [1, e^{-j\frac{2\pi d}{\lambda}\sin(\theta)}, \cdots, e^{-j(M-1)\frac{2\pi d}{\lambda}\sin(\theta)}]$, is the LoS channel component, and $\mathbf{h}_w \sim \mathcal{CN}(\mathbf{0}, \mathbf{I}_\mathrm{M})$ is the diffused channel component. Here d represents the antenna spacing, λ represents the wavelength, and θ represents the angle of arrival.For simplicity, $d = \lambda/2$ is set in this chapter. The altitude of the UAV can significantly influence the propagation characteristics of the U2G link. This is because the LoS path condition and the environment between the UAV and the GS change with θ. It is worth mentioning that this work assumes that the UAV moves in a random three-dimensional trajectory, and therefore, the K parameter is a random variable and not a constant. Moreover, α is also a random variable and not a constant. Both K and α are random variables that depend on each

other. The performance analysis section discusses this in detail.

5.2.2 Hardware Impairments Model

The HWIs are caused by a variety of factors, including power amplifier non-linearity, in- I/Q - phase imbalance, analog imperfections, phase noise, as well as timing and frequency synchronization issues. The aggregate effects of these factors can be modeled as additive Gaussian noises at both the transmitter and receiver based on the analytical tractability and experimental validation done in [5, 127, 128]. Having established the origins of HWIs, their effects can be discussed on the system model in greater detail.

The transmitted signal is $\tilde{x}$ instead of the intended signal x, and it can be written as

$$\tilde{x} = \sqrt{P\kappa_t}\; x + \zeta_t, \tag{5.2}$$

where x has a normalized power , P represents the transmitted power, $\kappa_t \in (0, 1]$ represents the transmitter's HWIs parameter and $\zeta_t \sim \mathcal{CN}(0, (1-\kappa_t)P)$ represents the transmitter's complex HWIs noise.

The impaired signal at the receiver can be given as

$$y = \underbrace{\sqrt{P\kappa_r\kappa_t}\; g\; x}_{\text{designated signal}} + \underbrace{\sqrt{\kappa_r}\; g\; \zeta_t + \zeta_r}_{\text{HWIs noise}} + \underbrace{w}_{\text{AWGN}}, \tag{5.3}$$

where g is the channel between the transmitter and the receiver, $\kappa_r \in (0, 1]$ is the receiver's HWI parameter, $\zeta_r \sim \mathcal{CN}\big(0, (1-\kappa_r)P\,|g|^2\big)$ is the complex receiver additive HWIs noise, and $w \sim \mathcal{CN}(0, \sigma_w^2)$ is the receiver AWGN. The distortion power is therefore proportional to the input power P. This makes the additive HWIs term different from typical receiver noise, which is independent of the input power. The terms κ_t and κ_r refer to the hardware quality factors that can be effectively measured using the EVM stated on the data sheets of the RF transceivers [5], as well as references therein. In the case of ideal hardware, $\kappa_r = \kappa_t = 1$ and $\zeta_r = \zeta_t = 0$.

5.3 Performance Analysis

This section analyzes how the HWIs affect the system's performance. The received signal at the GS from the UAV can be written as:

$$\mathbf{r} = \sqrt{\kappa_r \beta}\mathbf{h}\tilde{x} + \boldsymbol{\zeta}_r + \mathbf{n}, \tag{5.4}$$

where, $\mathbf{r} \in \mathbb{C}^{\mathrm{M}\times 1}$, $\mathbf{n} \sim \mathcal{CN}(\mathbf{0}, \sigma_n^2 \mathbf{I}_{\mathrm{M}})$ is the AWGN at the GS receive antennas, $\boldsymbol{\zeta}_r \sim \mathcal{CN}(\mathbf{0}_{\mathrm{M}}, \mathbf{C}_{\boldsymbol{\zeta}})$ is HWIs noise at the GS, the parameter $\kappa_r \in (0, 1]$ determines the quality of the GS hardware, and the covariance matrix $\mathbf{C}_{\boldsymbol{\zeta}}$ can be given as

$$\mathbf{C}_{\boldsymbol{\zeta}} = (1-\kappa_r) P\beta \mathrm{diag}\left(|h^{(1)}|^2, |h^{(2)}|^2, \cdots, |h^{(M)}|^2\right), \tag{5.5}$$

where $h^{(m)}$ denotes the m^{th} element of $\mathbf{h}$. By substituting $\tilde{x}$ in (5.4) the following result is obtained

$$\mathbf{r} = \underbrace{\sqrt{\kappa_r \kappa_t P\beta}\ \mathbf{h}x}_{\text{designated signal}} + \underbrace{\sqrt{\kappa_r \beta}\mathbf{h}\zeta_t + \boldsymbol{\zeta}_r}_{\text{HWIs noise}=\boldsymbol{\zeta}^c} + \underbrace{\mathbf{n}}_{\text{AWGN}}. \tag{5.6}$$

The transmitter and receiver HWI noises in (5.6) can be added together as

$$\boldsymbol{\zeta}^c \sim \mathcal{CN}(\mathbf{0}_{\mathrm{M}}, \mathbf{C}_{\boldsymbol{\zeta}^c}), \tag{5.7}$$

where the covariance matrix can be given as

$$\mathbf{C}_{\boldsymbol{\zeta}^c} = (1-\kappa_r\kappa_t) P\beta \mathrm{diag}\left(|h^{(1)}|^2, |h^{(2)}|^2, \cdots, |h^{(M)}|^2\right). \tag{5.8}$$

Now, to detect the transmitted signal, a liner maximum ratio combining detector is applied at the GS. From (5.6), and using the receive combining vector $\mathbf{w} = \mathbf{h} \in \mathbb{C}^{\mathrm{M}\times 1}$, the received signal $r = \mathbf{w}^{\mathrm{H}}\mathbf{r}$ can be given as :

$$r = \underbrace{\sqrt{\kappa_r \kappa_t P \beta}\mathbf{w}^{\mathrm{H}}\mathbf{h}x}_{\text{designated signal}} + \underbrace{\sqrt{\kappa_r \beta}\mathbf{w}^{\mathrm{H}}\mathbf{h}\zeta_t + \mathbf{w}^{\mathrm{H}}\boldsymbol{\zeta}_r}_{\text{HWI noise}} + \underbrace{\mathbf{w}^{\mathrm{H}}\mathbf{n}}_{\text{AWGN}}. \tag{5.9}$$

Based on this, the received signal-to-distortion plus noise ratio (SDNR) Γ at the GS can be calculated as

$$\Gamma = \frac{\kappa_r \kappa_t P \beta \|\mathbf{h}\|^4}{\mathbf{h}^{\mathrm{H}}\mathbf{C}_{\boldsymbol{\zeta}^c}\mathbf{h} + \|\mathbf{h}\|^2 \sigma_n^2}. \tag{5.10}$$

Accordingly, the instantaneous ergodic capacity can be written as

$$\mathcal{R}(\mathbf{h}, K, l) = \log_2\left(1 + \frac{\kappa_r \kappa_t P \beta \|\mathbf{h}\|^4}{\mathbf{h}^{\mathrm{H}}\mathbf{C}_{\boldsymbol{\zeta}^c}\mathbf{h} + \|\mathbf{h}\|^2 \sigma_n^2}\right). \tag{5.11}$$

As (5.11) shows, increasing the level of HWIs causes a noticeable degradation in the instantaneous ergodic capacity level. This can be explained by noting that smaller values of κ_r and κ_t minimize the numerator and at the same time maximize the denominator. The term $(1 - \kappa_r \kappa_t)$ is included in $\mathbf{h}^{\mathrm{H}}\mathbf{C}_{\boldsymbol{\zeta}^c}\mathbf{h}$.

Lemma 5.3.1 *Assuming Rician fading conditions with a given Rician factor, impaired UAV and GS transceivers, and fixed UAV-GS distance, the average ergodic capacity of the UAV-GS communication can be approximated as*

$$\bar{\mathcal{R}}(K, l) \approx \log_2\left(1 + \frac{\kappa_t \kappa_r P \beta \left(MK^2 + 4(M+1)(K+1)\right)}{(K^2 + 3K + 2)\sigma_n^2 + P\beta(1 - \kappa_t \kappa_r)(K^2 + 8K + 8)}\right). \tag{5.12}$$

Proof: Using Jensen's inequality [56], the average capacity in (5.11) can be further approximated as

$$\mathbb{E}\left\{\log_2(1+\Gamma)\right\} \approx \log_2\left(1 + \frac{\kappa_r \kappa_t P \beta \mathbb{E}\left\{\|\mathbf{h}\|^4\right\}}{\mathbb{E}\left\{\mathbf{h}^{\mathrm{H}}\mathbf{C}_{\boldsymbol{\zeta}^c}\mathbf{h} + \|\mathbf{h}\|^2 \sigma_n^2\right\}}\right). \tag{5.13}$$

Now, the second and fourth moment-generating functions of the Rician random variable will be obtained. From [129], $\mathbb{E}\{|h|^2\} = (K+2)/(K+1)$ and $\mathbb{E}\{|h|^4\} = (K^2+8K+8)/(K+1)^2$.

The numerator can be obtained as follows

$$\mathbb{E}\left\{\|\mathbf{h}\|^4\right\} = M\left(M\left(\frac{K}{K+1}\right)^2 + 4\frac{M+1}{K+1}\right). \tag{5.14}$$

Next, the denominator can be expressed as follows

$$\begin{aligned}\mathbb{E}\left\{\mathbf{h}^{\mathrm{H}}\mathbf{C}_{\boldsymbol{\zeta}^c}\mathbf{h}\right\} &= (1-\kappa_r\kappa_t)\, P\, \beta \times\ \mathbb{E}\left\{\mathbf{h}^{\mathrm{H}}\mathrm{diag}\left(|h^{(1)}|^2, |h^{(2)}|^2, \cdots, |h^{(M)}|^2\right)\mathbf{h}\right\} \\ &= (1-\kappa_r\kappa_t)\, P\beta M\left(\frac{K^2+8K+8}{(K+1)^2}\right). \qquad (5.15)\\ \mathbb{E}\left\{\|\mathbf{h}\|^2\right\} &= M\,(K+2)/(K+1)\,. \qquad (5.16)\end{aligned}$$

Substituting (5.14) and (5.15) in (5.13) results in (5.12) and this concludes the proof.

From [130], the probability density function (PDF) of a random distance l between UAV and the GS when the UAV moves within a spherical space with radius r is given as $f_L(l) = \frac{3l^2}{r^3} - \frac{9l^3}{4r^4} + \frac{3l^5}{16r^6},\ 0 \le l \le 2r$. Based on this, the expected value of $\mathbb{E}[\beta^{-1}] = \mathbb{E}[l^\alpha]$ can be calculated as

$$\begin{aligned}\mathbb{E}[l^\alpha] &= \int_0^{2r} l^\alpha\left(\frac{3l^2}{r^3} - \frac{9l^3}{4r^4} + \frac{3l^5}{16r^6}\right) dl \\ &= 12(2r)^\alpha\left(\frac{2}{3+\alpha} - \frac{3}{4+\alpha} + \frac{1}{6+\alpha}\right). \qquad (5.17)\end{aligned}$$

Now, considering the average distance between the UAV and the GS over a sphere of radius r, the capacity in (5.12) can be rewritten as

$$\bar{\mathcal{R}}(K) \approx \log_2\left(1+\frac{\kappa_t\kappa_r P\left(MK^2+4(M+1)(K+1)\right)}{\left(12(2r)^\alpha\left(\frac{2}{3+\alpha}-\frac{3}{4+\alpha}+\frac{1}{6+\alpha}\right)(K^2+3K+2)\sigma_n^2+P(1-\kappa_t\kappa_r)(K^2+8K+8)\right)}\right). \tag{5.18}$$

The LoS conditions between UAV and GS change as the angle of arrival θ changes. This means that the height of the UAV affects the propagation characteristics of the LoS communication link (i.e., the Rician parameter is heavily influenced by the UAV's

elevation angle relative to the GS) [131,132]. It is apparent that a larger K is accompanied by a higher LoS contribution and fewer multipath scatters at the receiver when $\theta = \frac{\pi}{2}$. Furthermore, when $\theta = 0$ the communication link encounters the worst multipath conditions. The Rician parameter can be modeled as in [2] [121]

$$K(\theta) = k_0 \cdot \exp\left[\frac{2}{\pi} \ln\left(\frac{k_{\frac{\pi}{2}}}{k_0}\right) \theta\right], \tag{5.19}$$

where the parameters k_0 and $k_{\frac{\pi}{2}}$ depend on the frequency and environmental conditions.

Assuming that θ has a uniform PDF distribution in the interval $[0, \frac{\pi}{2}]$ and considering (5.19), the PDF of K can be given as

$$f_K(k) = \begin{cases} \frac{1}{k \ln\left(\frac{k_{\frac{\pi}{2}}}{k_0}\right)} & k_0 < k < k_{\frac{\pi}{2}} \\ 0 & k < k_0 \text{ or } k > k_{\frac{\pi}{2}}. \end{cases}, \tag{5.20}$$

Based on that, the first moment-generating function of K can be calculated as

$$\bar{K} = \mathbb{E}[k] = \int_{k_0}^{k_{\frac{\pi}{2}}} \frac{1}{\ln\left(\frac{k_{\frac{\pi}{2}}}{k_0}\right)} dk = \frac{k_{\frac{\pi}{2}} - k_0}{\ln\left(\frac{k_{\frac{\pi}{2}}}{k_0}\right)}. \tag{5.21}$$

The second moment can then be calculated as

$$\bar{K}_2 = \mathbb{E}[k^2] = \int_{k_0}^{k_{\frac{\pi}{2}}} \frac{k}{\ln\left(\frac{k_{\frac{\pi}{2}}}{k_0}\right)} dk = \frac{k_{\frac{\pi}{2}}^2 - k_0^2}{2 \ln\left(\frac{k_{\frac{\pi}{2}}}{k_0}\right)}. \tag{5.22}$$

Now, the dependency of the Rician fading parameter on the evaluation angle in (5.18) is discussed.

Lemma 5.3.2 *When the system faces hardware impairments, the Rician fading conditions, and the trajectory variables of the UAV the average ergodic capacity of the UAV -GS communication can be approximated as in* (5.23).

[2] The normal range of the Rician parameter $k_0 = 1 \leq K \leq k_{\frac{\pi}{2}} = 10$ (this depends on the frequency and environmental conditions).

$$\bar{\mathcal{R}} \approx \log_2\left(1+\frac{\kappa_t\kappa_r P\left(M\bar{K}_2+4(M+1)(\bar{K}+1)\right)}{\left(12(2r)^{\alpha}\left(\frac{2}{3+\alpha}-\frac{3}{4+\alpha}+\frac{1}{6+\alpha}\right)(\bar{K}_2+3\bar{K}+2)\sigma_n^2+P(1-\kappa_t\kappa_r)(\bar{K}_2+8\bar{K}+8)\right)}\right). \tag{5.23}$$

Now, as (5.18) and (5.23) show, increasing the level of HWIs causes a noticeable degradation to the ergodic capacity level. This can be explained by noting that smaller values of κ_r and κ_t minimize the numerator, maximizing at the same time the value of the denominator. Also, the effect of the HWIs appears clearer at shorter distances because it has an exponential effect on the system performance.

5.3.1 Asymptotic Analysis

This section shows the asymptotic behavior of the ergodic capacity in (5.23).

- Transmit power: When $P \to \infty$, the ergodic capacity enters the saturation region and can be given as

$$\bar{\mathcal{R}} \approx \log_2\left(1+\frac{\kappa_t\kappa_r\left(M\bar{K}_2+4(M+1)(\bar{K}+1)\right)}{(1-\kappa_t\kappa_r)(\bar{K}_2+8\bar{K}+8)}\right). \tag{5.24}$$

  Now, if the system has perfect hardware conditions (i.e., $\kappa_t = \kappa_r = 1$), the system does not enter the saturation region and $\bar{\mathcal{R}} \to \infty$ when $P \to \infty$.

- Number of antennas at the GS: It is apparent that when $M \to \infty$ then $\bar{\mathcal{R}} \to \infty$ and the system does not enter the saturation region as in the case of increasing the power. This means that if the system is under the effect of the HWIs, increasing the number of antennas might be a better solution than increasing the transmitting power to boost the ergodic capacity. However, when applying the power scaling law where the transmitted power $P = \frac{P_t}{M}$, the system performance is upper bounded as (P_t is the transmitted power in this case)

$$\bar{\mathcal{R}} \approx \log_2 \left(1 + \frac{\kappa_t \kappa_r P_t \left(\bar{K}_2 + 4(\bar{K}+1) \right)}{12(2r)^{\alpha} \left(\frac{2}{3+\alpha} - \frac{3}{4+\alpha} + \frac{1}{6+\alpha} \right) \times (\bar{K}_2 + 3\bar{K} + 2)\sigma_n^2} \right). \tag{5.25}$$

- HWIs level: When $\kappa_t = 0$ or $\kappa_r = 0$, the ergodic capacity $\bar{\mathcal{R}} \to 0$. If the system has perfect hardware conditions (i.e., $\kappa_t \kappa_r \to 1$), the ergodic capacity can be given as

$$\bar{\mathcal{R}} \approx \log_2 \left(1 + \frac{P \left(M\bar{K}_2 + 4(M+1)(\bar{K}+1) \right)}{12(2r)^{\alpha} \left(\frac{2}{3+\alpha} - \frac{3}{4+\alpha} + \frac{1}{6+\alpha} \right) \times (\bar{K}_2 + 3\bar{K} + 2)\sigma_n^2} \right). \tag{5.26}$$

5.4 Results and Analysis

In this section, extensive computer simulations were conducted to validate the presented analytical results. This section uses the first and second moments of the Rician factor ($\bar{K}$ and $\bar{K}_2$), and the average of the channel factor $\mathbb{E}[\beta^{-1}]$ between the UAV and the GS over a sphere with radius r. Unless otherwise specified, the UAV transmit power $P = 30$ dBm, the noise power $\sigma_n^2 = -40$ dBm, and the path loss exponent $\alpha = 2.5$. However, the analyses are general and not restricted to these particulars.

Fig. 5.2 plots the ergodic capacity against the transmitted power at different levels of HWI. The curves prove that the presented analytical results obtained in (5.23) align well with the simulation results. It shows that, due to the HWIs, the performance saturates in the high-power region and that there can be no further improvement upon increasing the transmitted power. This can be explained by noting that the term $(\bar{K}_2 + 3\bar{K} + 2)\sigma_n^2$ in (5.23) vanishes in the high-power region. Consequently, the average ergodic capacity saturates at $\bar{\mathcal{R}} \approx \left(1 + \frac{\kappa_t \kappa_r \left(M\bar{K}_2 + 4(M+1)(\bar{K}+1) \right)}{(1-\kappa_t\kappa_r)(\bar{K}_2 + 8\bar{K} + 8)} \right)$. In contrast, the capacity increases without limit for an ideal system.

Fig. 5.3 plots the ergodic capacity against HWI levels at different numbers of GS

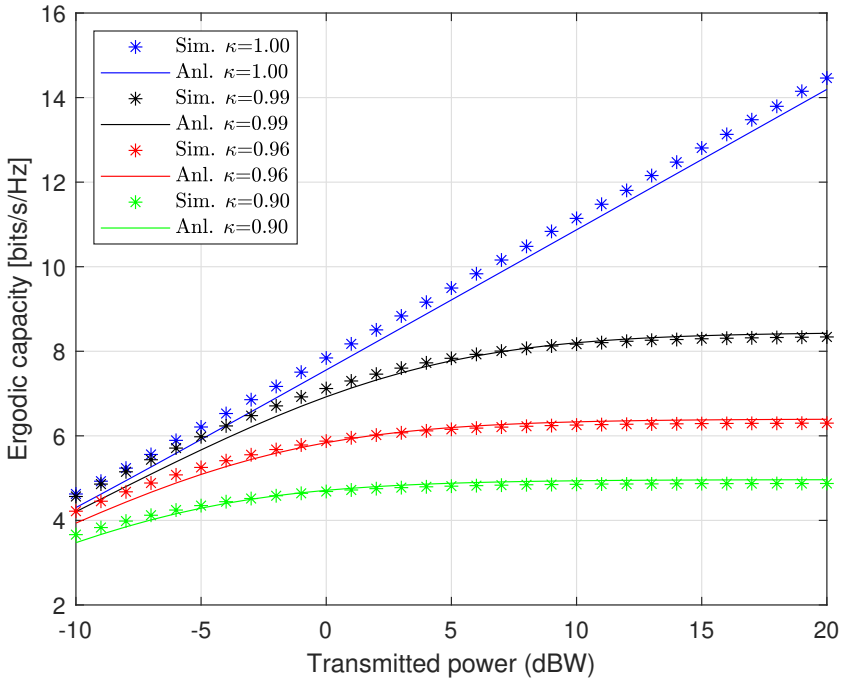

Figure 5.2: The ergodic capacity vs. the transmitted power when M= 10, $\sigma_n^2 = 10^{-6}$ and r = 75 m at different levels of HWIs.

antennas. As in Fig. 5.2, the accuracy of the presented analysis is also confirmed here since the simulation results match strongly with the analytical ones. This figure shows the negative impact of the HWIs on the system performance. Fortunately, increasing the number of GS antennas can alleviate the HWI effects. For example, the ergodic capacity decreases from 14.2 to 6.5 when M=32 (this is 54% degradation), while it decreases from 11 to 3.9 when M=4 (this is 65%). This can be interpreted from (5.18) and (5.23), where increasing the level of HWIs causes a noticeable degradation to the ergodic capacity level. In this case, the smaller values of κ_r and κ_t minimize the numerator while maximizing the value of the denominator. It is worth mentioning that this degradation can be compensated by adding more antennas since $\bar{\mathcal{R}} \to \infty$ when $M \to \infty$, and the system does not enter the saturation region as it does when increasing the power, as explained in the asymptotic analysis section.

Fig. 5.4 shows the effect of the HWIs when considering spherical regions with different

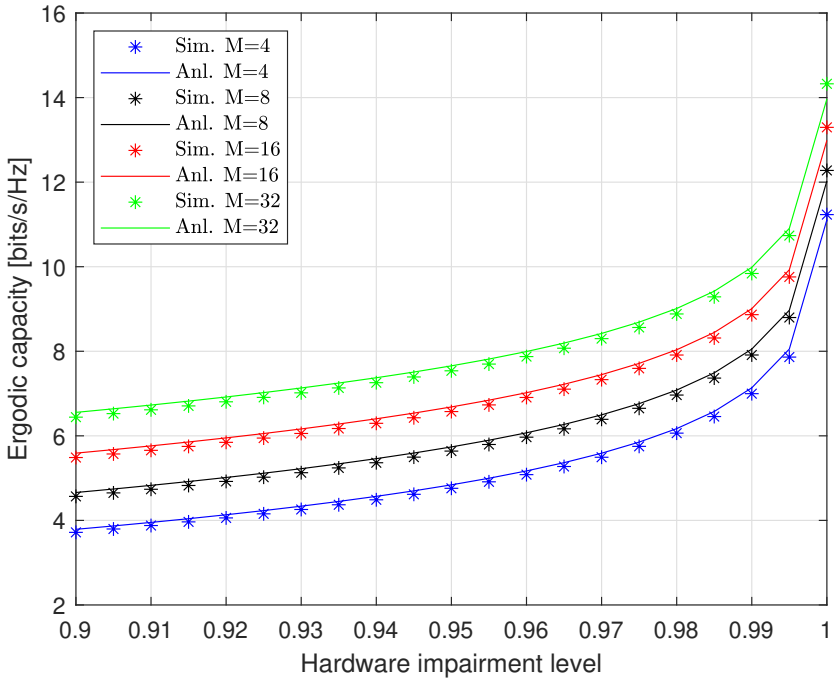

Figure 5.3: The ergodic capacity vs. the transmitted power when $r = 50$ at different levels of HWIs .

radii. As the figure shows, increasing the level of the HWIs causes more degradation to the system performance for all radius values; this can be explained by (5.23) where $2r$ is raised to the power of α. The degradation is more noticeable in smaller radius values. This is because the distances have an exponential effect on the system performance. For example, when $r = 50$ the capacity decreases from 12.4 to 6 at $\kappa = 0.95$ while it decreases from 7.5 to 5.5 when $r = 200$.

Fig. 5.5 plots the ergodic capacity against the number of GS antennas at different levels of HWIs. The result in this figure agrees with the ones in Fig. 5.2, where increasing the level of the HWIs causes more degradation to the system performance. However, increasing the number of transmitting antennas does not lead to performance saturation as in the case of increasing power. Moreover, as expected from the analytical analysis, increasing the number of GS antennas improves system performance.

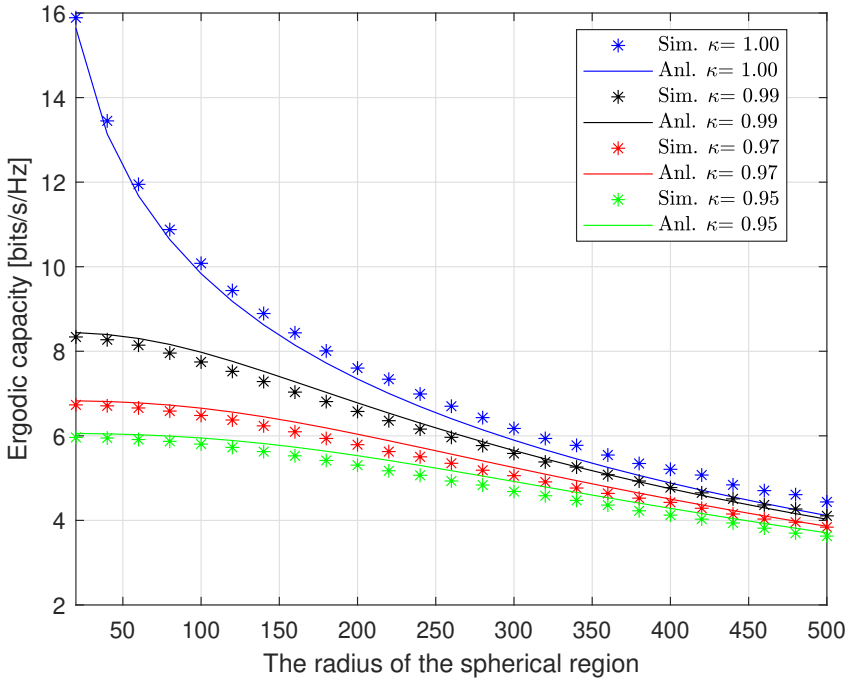

Figure 5.4: The ergodic capacity vs. HWIs level at different trajectory radii when $P = 10$ dBW, $\sigma_n^2 = 10^{-6}$, and $M = 10$.

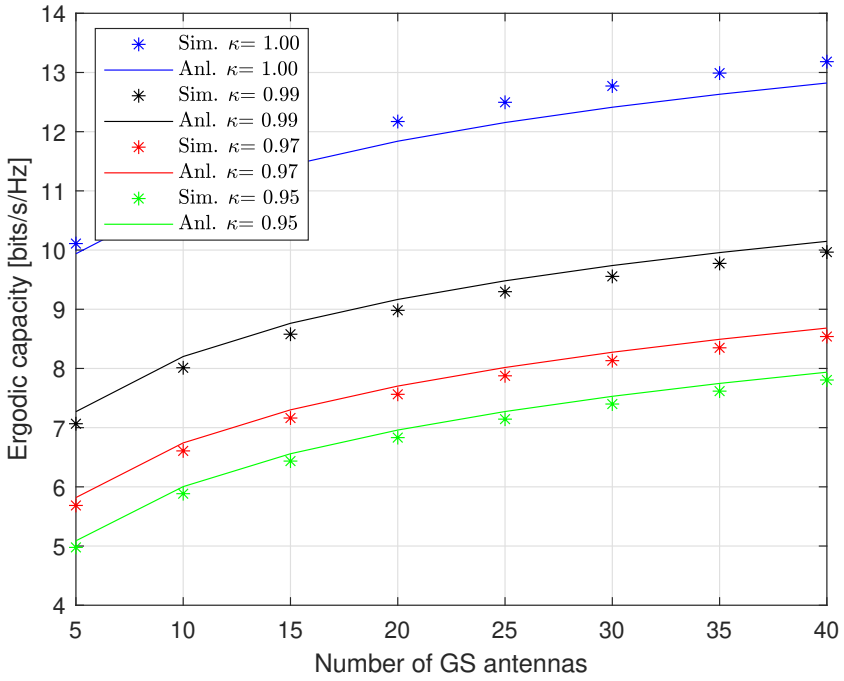

Figure 5.5: The ergodic capacity vs. the number of GS antennas when $P = 30$ dBm and $r = 75$ at different levels of HWIs.

5.5 Conclusions

This work analyzes the average ergodic capacity of UAV-GS communication in the presence of HWIs, specifically when the UAV moves in a random three-dimension trajectory. This work derives an approximate expression for the ergodic capacity and validated the obtained results using simulations. The obtained results demonstrated that the HWIs can dramatically affect the system's performance and lead the system to enter a saturation region where no more improvement can be obtained when the transmitted power is increased. This saturation region can be alleviated by increasing the number of transmitting antennas at the GS. This work assumed perfect knowledge of the channel's state information; future works can consider imperfect channels' state information conditions and other metrics of the system performance such as the bit error rate.

Chapter 6

Hardware Impairments Effects on Over the Air System Assisted by Unmanned Aerial Vehicles

6.1 Introduction

OAC has attracted attention due to its efficient data aggregation capabilities across a massive number of distributed sensor nodes with finite bandwidth [133, 134]. This technique utilizes the superposition property of wireless channels to calculate the sensing data by simultaneous transmissions from the sensors. As such, OAC can provide an effective solution for the IoT and machine-to-machine technologies by tackling the latency and bandwidth consumption issues [135]. In this context, UAVs can be utilized as fusion centers (FCs), enabling ultrafast data collection from numerous sensor nodes and paving the way for widespread sensing and environmental monitoring applications e.g., disaster alarms [136]. Here, smart sensors can send their readings over a wireless channel to the UAV, which reconstructs each sensor reading and calculates the desired measurements.

Nevertheless, in practical communication systems, channel estimation is a significant challenge when it comes to deploying OAC. The reason for this is that data fusion experi-

ences heightened MSE due to the estimation error. In addition, HWIs affect the channel estimation accuracy [87]. As a result, the combined data is distorted due to amplitude errors in CSI, and synchronization issues in the signals transmitted from multiple nodes occur due to phase errors. The effect of channel estimation errors on OAC systems was discussed when using the random sequence-based synchronization approach [137]. However, this approach forces nodes to transmit identical data several times, resulting in a reduction in the achievable sum rate. In the same context, it was shown in [138] that the performance of OAC systems is degraded due to the unfavorable channel conditions of wireless devices.

However, these studies overlooked the impact of HWIs at both transmitters and receivers. In reality, HWIs significantly influence the performance of communication systems. These impairments can be attributed to a range of factors, including power amplifier non-linearity, in-phase quadrature-phase imbalance, analog imperfections, phase noise, and timing and frequency synchronization issues [139]. The work in [140] examined the performance of reconfigurable intelligent surface assisted integrated satellite- UAV-terrestrial networks under the influence of HWIs. This research derived a closed-form expression for the outage probability, concluding that a higher level of impairment leads to a noticeable decline in the system performance.

In practical communication systems, both transmitters and receivers need to create carrier signals with precise and consistent frequencies. Typically, these frequencies are generated by a local crystal, producing a low-frequency sine wave or a reference clock, which is then amplified to the required carrier frequency by a circuit called a phase-locked loop. However, due to inherent differences in these crystals, slight frequency variations occur across different devices, resulting in frequency offsets. These offsets fluctuate due to environmental factors like temperature and induce a rotational effect on transmitted signals, leading to phase drift over time and potentially adverse impacts on intended transmission. Thus, it is of critical importance to consider phase errors caused by frequency offsets when examining system performance under imperfect CSI conditions [141, 142].

In contrast to current work in the literature, this chapter discusses the performance degradation in data fusion within UAV-assisted OAC systems caused by imperfect CSI and non-ideal transceivers. Motivated by the importance of this topic, this study investigates the combined impact of HWIs and imperfect CSI on the performance of UAV-assisted OAC. As a result, mathematical frameworks are developed to calculate the average MSE for both perfect and imperfect CSI of the impaired signal. The obtained results are then validated through computer simulations.

6.2 System Model

6.2.1 Channel Model

This work studies a UAV-assisted-OAC wireless communication system as illustrated in Fig. 6.1, where the UAV serves as an fusion center (FC) that communicates with M sensors, each equipped with one antenna. The sensors gather time-varying measurements and transmit them to the FC, which then calculates the average of the data received from the sensors. The i^{th} sensor coordinates at the t^{th} time slot are represented by $(r_i[t], \theta_i[t], 0)$. Here, $r_i[t]$ is the distance between the i^{th} sensor and the zero point Q, and $\theta_i[t]$ is the angle considering the x-coordinate line on the xy-coordinate plane. The FC's coordinates are represented by (ρ, Θ, L) where L is the UAV altitude, and hence, the distance between the origin and the FC is $d = \sqrt{\rho^2 + L^2}$. The further presumption is that the FC is situated in the far-field region. (i.e., $d > \rho \gg R$), and that the nodes are evenly and arbitrarily positioned inside a circular area with a radius R. Moreover, during any time slot t, a group of active nodes, K, is chosen at random to simultaneously transmit operating OAC. As a result, the PDFs for $r_i[t]$ and $\theta_i[t]$ can be described as $f_{r_i[t]}(r) = \frac{2r}{R^2}$ and $f_{\theta_i[t]}(\theta) = \frac{1}{2\pi}$, with $r \in [0, R]$ and $\theta \in [-\pi, \pi]$.

The desired function at the FC at instant t is $f[t] = \frac{1}{K}\sum_{i=1}^{K} s_i[t]$ where $\mathbb{E}\{s_i[t]\} = 0$ and $\mathbb{V}\text{ar}\{s_i[t]\} = 1$. The sensing data $s_i[t]$ is presumed to be independent for various i

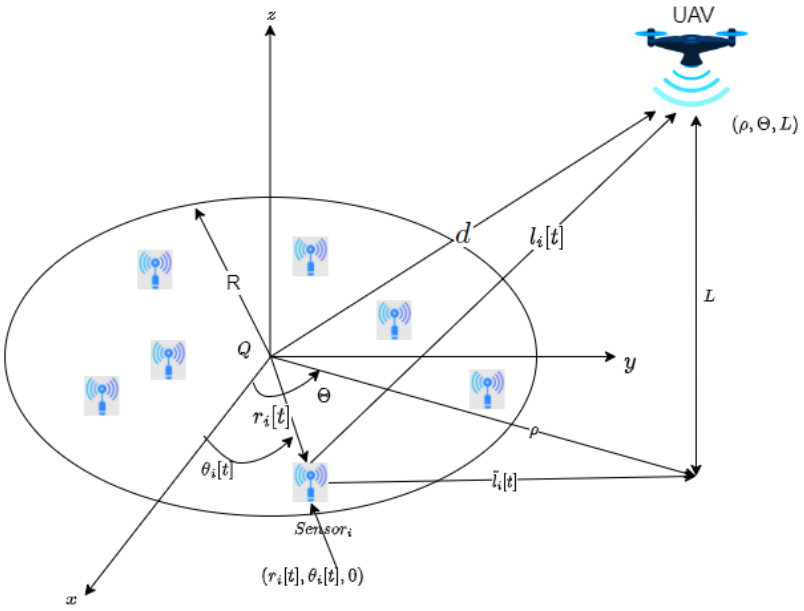

Figure 6.1: System model: UAV-Assisted over-the-air computation system.

and t. Now, the incoming signal at the FC can be given as

$$y[t] = \sum_{i=1}^{K} h_i[t] b_i[t] s_i[t] + w[t], \tag{6.1}$$

where $h_i[t]$ is the complex channel between i^{th} sensor and the FC at t time slot. $h_i[t]$ is influenced by ground-to-air channels that are predominantly line-of-sight (LoS) [143]. Therefore, $h_i[t]$ can be represented as $h_i[t] = \frac{1}{l_i[t]} e^{-j\frac{2\pi l_i[t]}{\lambda}}$ where $l_i[t]$ is the distance from the i^{th} sensor to the FC at time slot t. Due to the assumption of LoS channels, the path-loss exponent of 2 is used for the squared envelope. The distance $l_i[t]$ is computed as $l_i[t] = \sqrt{\rho^2 + r_i^2[t] - 2\rho r_i[t]\cos(\varphi - \theta_i[t]) + L^2}$. Additionally, $b_i[t]$ represents the i^{th} sensor transmit coefficient, and $w[t]$ is the receiver AWGN following a complex normal distribution with a zero mean and σ^2 variance.

Given that the group of active nodes, K, is arbitrarily chosen for every time slot, $h_i[t]$ is independent for various i and t. The channel $h_i[t]$ is a composite random variable that encompasses path loss and phase difference based on the distance $l_i[t]$ [144]. Without loss of generality, it is assumed that $|h_1[t]| \leq |h_2[t]| \leq \cdots \leq |h_{K-1}[t]| \leq |h_K[t]|$. In reference

to [145], the OAC transmit coefficient is determined by $b_i[t] = \sqrt{p_i[t]}(\hat{h}_i^*[t]/|\hat{h}_i[t]|)$ where $p_i[t]$ stands for the i^{th} sensor transmit power. Additionally, $\hat{h}_i[t]$ represents the i^{th} sensor estimated version of $h_i[t]$, while $(\cdot)^*$ indicates the complex conjugate. By employing the channel inversion technique [145], [146], the transmit power for the i^{th} sensor is calculated as $p_i[t] = P|\hat{h}_1[t]|^2/|\hat{h}_i[t]|^2$ where P is a constant and $|\hat{h}_1[t]| = \min_{i\in K}|\hat{h}_i[t]|$. The FC retrieves the mean of the desired data, expressed as [145]

$$\hat{f}[t] = \frac{y[t]}{K\sqrt{\alpha[t]}} = \frac{\sum_{i=1}^{K} h_i[t]b_i[t]s_i[t]}{K\sqrt{\alpha[t]}} + \frac{w[t]}{K\sqrt{\alpha[t]}}, \tag{6.2}$$

where $\alpha[t] = P|\hat{h}_1[t]|^2$ is the denoising factor.

6.2.2 Hardware Impairments Model

Many factors contribute towards HWIs, such as non-linear power amplifiers, imbalanced in-phase and quadrature phases, phase noises, and synchronization problems related to timing and frequency. These factors collectively result in the addition of Gaussian noises at transceivers. With the sources of HWIs now established, it allows for a more comprehensive analysis of their impact on the system model [5]. The transmitted signal is represented by $\tilde{s}$, which deviates from the intended signal s. It can be expressed as [5]

$$\tilde{s} = \sqrt{E\kappa_t}\ s + \zeta_t, \tag{6.3}$$

where s has normalized power, E denotes the transmitted power, $\kappa_t \in (0, 1]$ represents HWIs parameter of the transmitter, and ζ_t signifies the transmitter's complex HWIs noise which follows a complex normal distribution with a mean of 0 and a variance of $CN(0, (1-\kappa_t)E)$. The impaired signal at the receiver can be described as

$$y = \underbrace{\sqrt{E\kappa_r\kappa_t}\ g\ x}_{\text{designated signal}} + \underbrace{\sqrt{\kappa_r}\ g\ \zeta_t + \zeta_r}_{\text{HWIs noise}} + \underbrace{n}_{\text{AWGN}}, \tag{6.4}$$

where g represents the channel between the transmitter and receiver, $\kappa_r \in (0, 1]$ is the receiver's HWI parameter, ζ_r is the complex receiver additive HWIs noise following a complex normal distribution with a mean of 0 and a variance of $\sim \mathcal{CN}\big(0, (1-\kappa_r)E\,|g|^2\big)$, and n is the receiver AWGN following a complex normal distribution with a zero mean and σ_n^2) variance.

The distortion power is directly proportional to the input power E, making the additive HWIs term distinct from the typical receiver noise, which is independent of input power. The terms κ_t and κ_r factors refer to the hardware quality at the transmitter and the receiver, respectively. In the case of ideal hardware, $\kappa_r = \kappa_t = 1$ and $\zeta_r = \zeta_t = 0$. Considering the HWI model at the transmitter and receiver, the FC retrieves the average desired data as

$$\hat{f}[t] = \frac{\sqrt{\kappa_t\kappa_r}\sum_{i=1}^{K} h_i[t]b_i[t]s_i[t]}{K\sqrt{\alpha[t]}} + \frac{\chi[t]}{K\sqrt{\alpha[t]}} + \frac{w[t]}{K\sqrt{\alpha[t]}}, \tag{6.5}$$

where $\chi[t] \sim \text{CN}\left(0, (1-\kappa_t\kappa_r)\sum_{i=1}^{K}\left|(h_i[t]b_i[t]s_i[t])\right|^2\right)$. Here, $\text{CN}(\mu, \sigma)$ is a complex Gaussian random variable with μ mean and σ^2 variance.

6.3 Performance Analysis

6.3.1 Mean Square Error under HWIs and Perfect CSI

This section examines the MSE assuming perfect CSI when the transmitter and receiver are under the effect of HWIs. As per equation (6.5), the instantaneous MSE for a given time slot t can be obtained as

$$\begin{aligned}\texttt{MSE}[t] =& \mathbb{E}\left[\left|\hat{f}[t] - f[t]\right|^2\right] = \frac{1}{K^2}\mathbb{E}\left[\left|\frac{y[t]}{\sqrt{\alpha[t]}} - \sum_{i=1}^{K} s_i[t]\right|^2\right] \\ =& \frac{1}{K^2}\left(\sum_{i=1}^{K}\left|\frac{\sqrt{\kappa_t\kappa_r}h_i[t]b_i[t]}{\sqrt{\alpha[t]}} - 1\right|^2 \frac{K(1-\kappa_t\kappa_r)\sum_{i\in K}\left|(h_i[t]b_i[t])\right|^2}{\alpha[t]} + \frac{\sigma^2}{\alpha[t]}\right).\end{aligned} \tag{6.6}$$

Now, by noting that the nodes fading channels $h_i[t]$ are independent, the average error in (6.6) can be calculated as

$$\begin{aligned}\overline{\texttt{MSE}} =& \frac{1}{K} + \frac{\kappa_t\kappa_r}{K}\mathbb{E}\left[\left|\frac{h_i[t]b_i[t]}{\sqrt{\alpha[t]}}\right|^2\right] - \frac{\sqrt{\kappa_t\kappa_r}}{K}\mathbb{E}\left[\frac{h_i[t]b_i[t]}{\sqrt{\alpha[t]}} + \frac{h_i^*[t]b_i^*[t]}{\sqrt{\alpha[t]}}\right] \\ &+ \frac{(1-\kappa_t\kappa_r)}{K}\mathbb{E}\left[\left|\frac{h_i[t]b_i[t]}{\sqrt{\alpha[t]}}\right|^2\right] + \frac{\sigma^2}{K^2}\mathbb{E}\left[\frac{1}{\alpha[t]}\right]. \end{aligned} \tag{6.7}$$

After some tedious mathematical manipulations, the $\overline{\texttt{MSE}}$ can be rewritten as

$$\overline{\texttt{MSE}} = \frac{1}{K} - \frac{\sqrt{\kappa_t\kappa_r}}{K}\mathbb{E}\left[\frac{h_i[t]\hat{h}_i^*[t]}{|\hat{h}_i[t]|^2} + \frac{h_i^*[t]\hat{h}_i[t]}{|\hat{h}_i[t]|^2}\right] + \frac{1}{K}\mathbb{E}\left[\frac{|h_i[t]|^2}{|\hat{h}_i[t]|^2}\right] + \frac{\sigma^2}{PK^2}\mathbb{E}\left[\frac{1}{|\hat{h}_1[t]|^2}\right]. \tag{6.8}$$

Now, considering perfect CSI (i.e., $\hat{h}_i[t] = h_i[t]$) and assuming the far-field scenario, the $\overline{\texttt{MSE}}$ can be calculated as

$$\overline{\texttt{MSE}} = \frac{2\left(1-\sqrt{\kappa_t\kappa_r}\right)}{K} + \frac{\sigma^2}{PK^2}\mathbb{E}\left[\frac{1}{|h_1[t]|^2}\right], \tag{6.9}$$

where it is not easy to calculate the exact value of the expectation in the second term. Fortunately, an approximation can be computed using the Taylor expansion and exploiting some facts in [147–149]. By assuming that $\zeta_1 = |h_1[t]| = \min_{i\in K}\zeta_i$, the following approximations for the expectation and variance of ζ_i can be obtained:

$$\mathbb{E}[\zeta_i] \approx \frac{8d^4 - R^2d^2 + 3R^2\rho^2}{8d^5}, \quad \mathbb{V}\text{ar}[\zeta_i] \approx \frac{R^2\rho^2}{4d^6}. \tag{6.10}$$

In addition, $\mathbb{E}\left[\frac{1}{\zeta_1^2}\right] = \mathbb{E}\left[\frac{1}{|h_1[t]|^2}\right] \overset{(a)}{\approx} \frac{1}{(\mathbb{E}[\zeta_1])^2}$, where (a) follows from $\mathbb{V}\text{ar}[\zeta_1] < \mathbb{V}\text{ar}[\zeta_i] \approx 0$ and assuming the far-field scenario where $d \gg R$, and considering $\zeta_1 = |h_1[t]| = \min_{i\in K}|h[t]|_i$

[148]. By utilizing these approximations $\mathbb{E}[\zeta_1]$ can be given as

$$\begin{aligned}\mathbb{E}[\zeta_1] &\approx \mathbb{E}[\zeta_i] + \Phi^{-1}\left(\frac{1}{K+1}\right)\sqrt{\mathbb{V}\mathrm{ar}[\zeta_i]}, \\ &\approx \frac{8d^4 - R^2d^2 + 3R^2\rho^2}{8d^5} + \Phi^{-1}\left(\frac{1}{K+1}\right)\frac{R\rho}{2d^3}.\end{aligned} \tag{6.11}$$

Finally, using (6.9) and (6.11), the $\overline{\texttt{MSE}}$ can be approximated as

$$\overline{\texttt{MSE}} \approx \frac{2(1-\sqrt{\kappa_t\kappa_r})}{K} + \frac{\sigma^2}{PK^2}\left[\frac{8d^4 - R^2d^2 + 3R^2\rho^2}{8d^5} + \Phi^{-1}\left(\frac{1}{K+1}\right)\frac{R\rho}{2d^3}\right]^{-2}. \tag{6.12}$$

The result in (6.12) shows that, in the impaired system, there is a floor in the $\overline{\texttt{MSE}}$ even if the transmit power grows immense due to the effect of the HWIs. This error increases with higher levels of HWIs. On the other hand, in the case of the ideal system, the $\overline{\texttt{MSE}}$ approaches zero.

6.3.2 Mean Square Error under HWIs and Imperfect CSI

Achieving perfect CSI is not feasible in practical communication systems. This work assumes that each node estimates its channel with the FC based on a pilot signal transmitted from the FC. The i^{th} node estimated channel at time slot t can be obtained as

$$\hat{h}_i[t] = (|h_i[t]| + \delta_i[t])e^{j(\angle h_i[t] + \boldsymbol{\epsilon}_i[t])}, \tag{6.13}$$

where $\delta_i[t]$ is the amplitude error, and $\boldsymbol{\epsilon}_i[t]$ is the phase error. The amplitude error introduces distortion to the amplitude of the i^{th} signal received by the FC, while the phase error introduces a synchronization discrepancy between the sensors.

Conditional on the amplitude and phase errors, the $\overline{\texttt{MSE}}$ in the presence of HWIs can

be represented as

$$\overline{\mathtt{MSE}}(\delta_i[t], \boldsymbol{\epsilon}_i[t]) = \frac{1}{K} + \frac{1}{K}\,\mathbb{E}\left[\frac{|h_i[t]|^2}{(|h_i[t]| + \delta_i[t])^2}\middle|\delta_i[t]\right]$$
$$- \frac{\sqrt{\kappa_t \kappa_r}}{K}\,\mathbb{E}\left[\frac{|h_i[t]|}{|h_i[t]| + \delta_i[t]}\middle|\delta_i[t]\right]\mathbb{E}[e^{j\,\boldsymbol{\epsilon}_i[t]} + e^{-j\,\boldsymbol{\epsilon}_i[t]}|\,\boldsymbol{\epsilon}_i[t]] + \frac{\sigma^2}{PK^2}\,\mathbb{E}\left[\frac{1}{|\hat{h}_1[t]|^2}\middle|\delta_i[t]\right]. \quad (6.14)$$

The amplitude errors $\delta_i[t] \in (-\Delta, \Delta)$ can be modeled as independent uniform random variables [150], and the phase errors $\boldsymbol{\epsilon}_i[t] \in [-\pi, \pi]$ can be modeled as Tikhonov distributions expressed as [151]

$$f_{\boldsymbol{\epsilon}_i[t]}(\boldsymbol{\epsilon}) = \frac{1}{2\pi I_0\left(\gamma_L\right)} \exp\left(\gamma_L \cos \boldsymbol{\epsilon}\right), \quad (6.15)$$

where γ_L depends on the PLL circuit, and I_0 is an order zero modified first kind Bessel function.

Now, considering the PDF of $\delta_i[t]$ and assuming the far-field scenario, the $\overline{\mathtt{MSE}}$ can be obtained by using the Taylor expansion and by exploiting some facts in [147–149] as

$$\mathbb{E}\left[\frac{|h_i[t]|^2}{(|h_i[t]| + \delta_i[t])^2}\right] \approx \int_{-\Delta}^{\Delta} \beta(\delta_i[t]) \frac{1}{2\Delta} \mathrm{d}\delta_i[t] = \mathcal{A}, \quad (6.16)$$

where $\beta(\delta_i[t])$ is the conditional expectation and can be calculated as

$$\mathbb{E}\left[\frac{|h_i[t]|^2}{(|h_i[t]| + \delta_i[t])^2}\middle|\delta_i[t]\right] \approx \frac{1}{4d^4\left((\delta_i[t])d + 1\right)^4} \times$$
$$\left[4H^6(\delta_i[t])^2 + H^2\left(2\rho^2\left(8\delta_i[t]d + R^2(\delta_i[t])^2 + 4\right) - R^2\delta_i[t]d + 12(\delta_i[t])^2\rho^4\right) +\right.$$
$$\left.\rho^4\left(8\delta_i[t]d + 3R^2(\delta_i[t])^2 + 4(\delta_i[t])^2\rho^2 + 4\right) + H^4\left(8\delta_i[t]d - R^2(\delta_i[t])^2 + 12(\delta_i[t])^2\rho^2 + 4\right)\right]. \quad (6.17)$$

and $\mathcal{A}$ can be given as

$$\mathcal{A} = \frac{\Delta^2(4L^4\Delta^2 - L^2(\Delta^2(R^2 - 8\rho^2) + 8) + \rho^2(3\Delta^2R^2 - 8) + 4\Delta^2\rho^4 + R^2) + 4}{4(1 - \Delta^2d^2)^3}. \quad (6.18)$$

Following the same context, the expectation related to the magnitude in the third term in (6.14) can be given as

$$\mathbb{E}\left[\frac{|h_i[t]|}{|h_i[t]|+\delta_i[t]}\right] \approx \int_{-\Delta}^{\Delta} \xi(\delta_i[t])\frac{1}{2\Delta}\mathrm{d}\delta_i[t] = \mathcal{B}, \tag{6.19}$$

where $\xi(\delta_i[t])$ is the conditional expectation which can be calculated as

$$\begin{aligned}\mathbb{E}\left[\frac{|h_i[t]|}{|h_i[t]|+\delta_i[t]}\middle|\delta_i[t]\right] \approx \frac{1}{8d^4\left(\delta_i[t]d+1\right)^3}&\left[8L^6(\delta_i[t])^2 + L^2\left(\rho^2\left(32\delta_i[t]d + R^2(\delta_i[t])^2+16\right)\right.\right.\\ &- R^2\delta_i[t]d + 24(\delta_i[t])^2\rho^4\big) + 2\rho^4\left(8\delta_i[t]d + R^2(\delta_i[t])^2 + 4(\delta_i[t])^2\rho^2+4\right)\\ &\left.+ L^4\left(16\delta_i[t]d - R^2(\delta_i[t])^2 + 24(\delta_i[t])^2\rho^2+8\right)\right].\end{aligned} \tag{6.20}$$

and $\mathcal{B}$ can be given as

$$\begin{aligned}\mathcal{B} =& \frac{\Delta R^2(-L^4\Delta^2 + L^2(3\Delta^2\rho^2+1) + 4\Delta^2\rho^4 - 2\rho^2)}{8\Delta d^4(\Delta^2 d-1)^2} + \\ &\frac{(8L^4 + 2\rho^2(8L^2+R^2) - L^2R^2 + 8\rho^4)\tanh^{-1}(\Delta d)}{8\Delta d^5}.\end{aligned} \tag{6.21}$$

Moreover, the expectation related to the phase error $\boldsymbol{\epsilon}_i[t]$ in the third term in (6.14) can be given as

$$\begin{aligned}\mathbb{E}[e^{j\,\boldsymbol{\epsilon}_i[t]} + e^{-j\,\boldsymbol{\epsilon}_i[t]}] =& 2\mathop{\mathbb{E}}_{\boldsymbol{\epsilon}_i[t]}\left[\mathbb{E}[e^{j\,\boldsymbol{\epsilon}_i[t]} + e^{-j\,\boldsymbol{\epsilon}_i[t]}|\,\boldsymbol{\epsilon}_i[t]]\right]\\ =& \int_{-\pi}^{\pi}\frac{\cos(\boldsymbol{\epsilon})}{\pi I_0(\gamma_L)}\exp(\gamma_L\cos\boldsymbol{\epsilon})\,\mathrm{d}\,\boldsymbol{\epsilon} = 2\frac{I_1(\gamma_L)}{I_0(\gamma_L)},\end{aligned} \tag{6.22}$$

where I_1 is an order one modified first kind Bessel function.

The expectation in the fourth term in (6.14) can be given as

$$\mathbb{E}\left[\frac{1}{|\hat{h}_1[t]|^2}\right] = \frac{1}{\left[\frac{8d^4 - R^2d^2 + 3R^2\rho^2}{8d^5} + \Phi^{-1}\left(\frac{1}{K+1}\right)\sqrt{\frac{R^2\rho^2}{4d^6} + \frac{\Delta^2}{3}}\right]^2}. \tag{6.23}$$

The result in (6.23) is obtained by assuming that $\hat{\zeta}_1 = |\hat{h}_1[t]| = \min_{i\in K}(|h_i[t]| + \delta_i[t]) =$

$\min_{i\in K} \hat{\zeta}_i$, and following the same procedures in Section 6.3.1. Hence, the following approximations are obtained

$$\mathbb{E}[\hat{\zeta}_i] = \mathbb{E}[|h_i[t]|] + \mathbb{E}[\delta_i[t]] \approx \frac{8d^4 - R^2d^2 + 3R^2\rho^2}{8d^5}. \tag{6.24}$$

$$\mathbb{V}\text{ar}[\hat{\zeta}_i] = \mathbb{V}\text{ar}[|h_i[t]|] + \mathbb{V}\text{ar}[\delta_i[t]] \approx \frac{R^2\rho^2}{4d^6} + \frac{\Delta^2}{3}. \tag{6.25}$$

Combining the previous terms, the $\overline{\texttt{MSE}}$ can be approximated as

$$\begin{aligned}\overline{\texttt{MSE}} \approx & \frac{1}{K}(1 + \mathcal{A} - 2\sqrt{\kappa_r\kappa_t}\,\mathcal{B}\,\frac{I_1(\gamma_L)}{I_0(\gamma_L)}) + \\ & \frac{1}{K^2}\frac{\sigma^2}{P}\left[\frac{8d^4 - R^2d^2 + 3R^2\rho^2}{8d^5} + \Phi^{-1}\left(\frac{1}{K+1}\right)\sqrt{\frac{R^2\rho^2}{4d^6} + \frac{\Delta^2}{3}}\right]^{-2}.\end{aligned} \tag{6.26}$$

6.4 Results and Analysis

Extensive computer simulations were carried out in this section to confirm the accuracy of the presented analytical results. Additionally, this section examines the impact of the HWIs and the imperfect CSI channel estimation on $\overline{\texttt{MSE}}$. The wavelength is set at 0.3 m. The simulation results assume random sensor locations, uniformly distributed on a circle with radius R = 80 m. The sensors send the data through OAC. The FC positioned at (d, L) = (1 km, 200 m). Furthermore, the simulations assume that $\kappa_r = \kappa_t$, $\kappa = \sqrt{\kappa_t\kappa_r}$, $\Delta = 10^{-5}$, and $\gamma_L = 15$ dB.

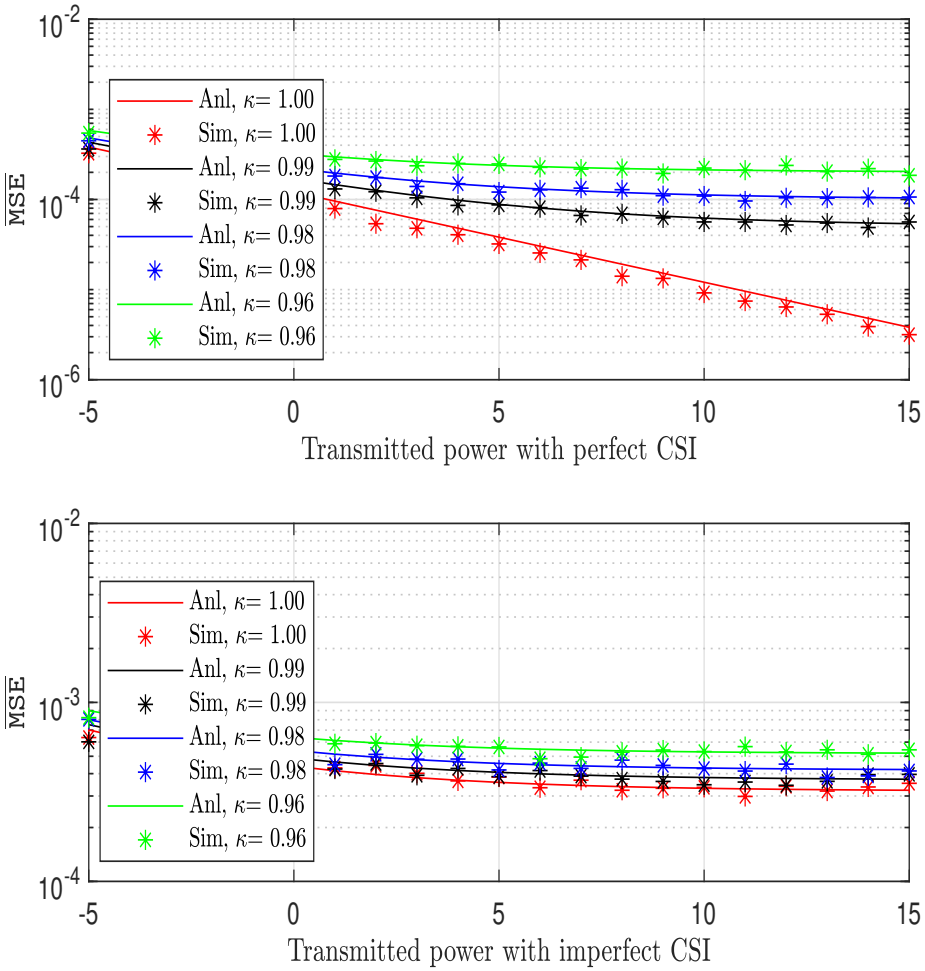

Figure 6.2: $\overline{\text{MSE}}$ versus power with perfect and imperfect CSI, when number of nodes = 100.

Fig. 6.2 illustrates the relationship between the $\overline{\texttt{MSE}}$ and the transmitted power under various levels of HWIs. The plotted curves demonstrate a strong agreement between the simulation and analytical results obtained from (6.12) and (6.26). It is evident that the performance reaches a saturation point in the high-power region due to the presence of HWIs and the imperfect CSI, indicating that further enhancements cannot be achieved by increasing the transmitted power. In the case of perfect CSI, this saturation can be attributed to the term $\frac{2\,(1-\sqrt{\kappa_t\kappa_r})}{K}$, which becomes dominant for smaller values of κ_t and κ_r. In contrast, the performance of the ideal system increases without any constraints.

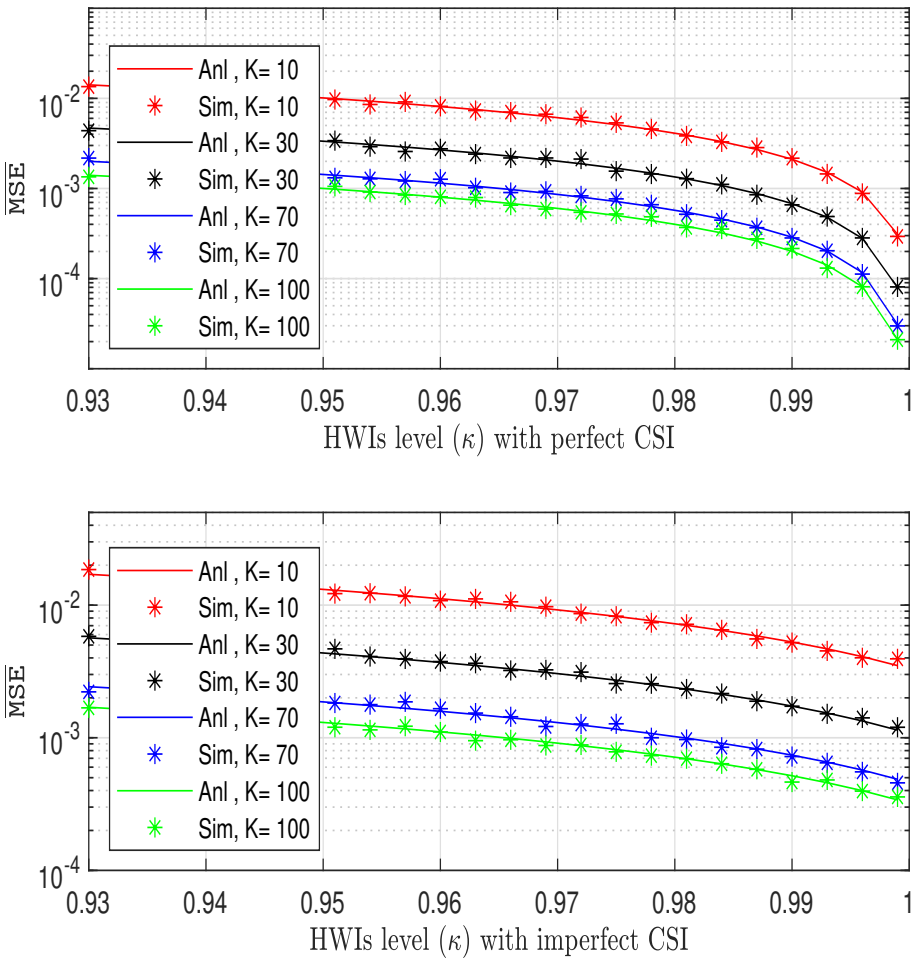

Figure 6.3: $\overline{\text{MSE}}$ at different levels of HWIs with perfect and imperfect CSI, when power = 20 dB.

Fig. 6.3 illustrates the relationship between HWI levels and the $\overline{\text{MSE}}$ for various numbers of nodes for both perfect and imperfect CSI. Similar to Fig. 6.2, the simulation results strongly corroborate the analytical findings, affirming the accuracy of the presented analysis. The figure highlights the detrimental impact of HWIs on system performance. However, there is a silver lining: increasing the number of nodes mitigates the effects of HWIs. For instance, considering the perfect CSI, when the number of nodes is 10, the $\overline{\text{MSE}}$ increases from 0.0003 to 0.0135, representing a degradation of 97% when the HWIs level becomes 0.93. Similarly, when the number of nodes is 100, the $\overline{\text{MSE}}$ increases from

0.000021 to 0.00135, indicating a 63% degradation. These findings align with (6.12) where higher HWI levels noticeably degrade the $\overline{\text{MSE}}$ for the small number of nodes. Importantly, it should be noted that this degradation can be compensated by adding more nodes, as indicated by the fact that $\overline{\text{MSE}}$ approaches zero as K increases. The same trend can be seen in case of the imperfect CSI.

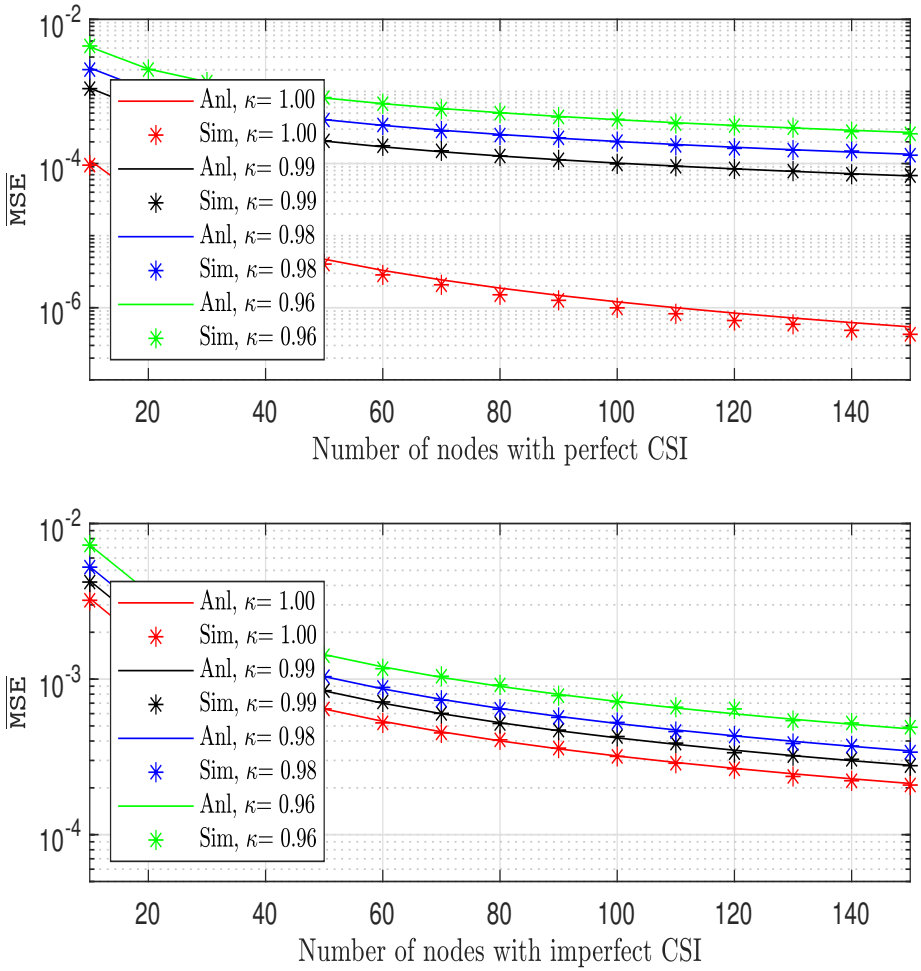

Figure 6.4: $\overline{\text{MSE}}$ versus number of nodes with perfect and imperfect CSI, when power = 20 dB.

In Fig. 6.4, the $\overline{\text{MSE}}$ is plotted as a function of the number of nodes across different levels of HWIs. The results in this graph are consistent with those shown in previous ones, demonstrating that higher levels of HWIs lead to a greater decline in system performance.

However, unlike the scenario with increased power, increasing the number of nodes does not result in performance saturation. The performance of the system can be significantly improved by serving more nodes. However, this improvement is decreased in the case of imperfect CSI.

6.5 Conclusions

This study investigated the $\overline{\texttt{MSE}}$ of UAV-Assisted- OAC communication under the joint effects of HWIs and imperfect CSI. This work looked in particular at the way UAVs can function as the FC and communicate with K nodes. By deriving approximate expressions for the $\overline{\texttt{MSE}}$ and conducting simulations, the obtained findings were validated. These findings emphasize the significant impact of HWIs on the system's performance, revealing the presence of a saturation region where increasing the transmitted power no longer leads to improvements. Furthermore, it was observed that the system's performance degraded more severely in the case of imperfect CSI. Notably, it is discovered that enhancing the system's performance is possible by increasing the number of nodes. It is important to mention that this study assumed one antenna per node. Future research could explore scenarios with multiple antennas at the nodes and consider other performance metrics, such as bit error rate.

Chapter 7

Conclusions and Future Work

7.1 Conclusions

In summary, this thesis studies UAVs systems as a viable solution for the next wireless communication networks. The study evaluates various factors that dictate the system's performance, including aspects such as total sum rates, ergodic capacity, and MSE. A significant emphasis is placed on addressing the association problem between UAVs and WAPs to optimize the system performance. The thesis also provides a detailed examination of the performance of UAV-assisted systems under different scenarios, especially in the presence of HWIs. These investigations consider both perfect and imperfect CSI by offering an in-depth exploration, the thesis illuminates both the potentials and restrictions of UAVs in improving wireless communication networks and establishes a strong foundation for further study and innovation in this area.

Specifically, this study explores the problem of associating UAVs with WAPs with the goal of maximizing the total sum rate. Various factors are considered in this process, including the individual bandwidth of each UAV, the coverage area, the minimum required SINR, the number of links provided by UAVs, the number of connections at WAPs, and fairness constraints. To address this, an extension of the centralized Hungarian algorithm was proposed, which facilitates a suboptimal association between the UAVs and

WAPs. The results of the study indicate that this proposed algorithm significantly reduced computational complexity compared to other methods in the literature. Remarkably, the performance of the proposed algorithm aligns with the exhaustive search one when the available bandwidth at the UAVs is high.

Furthermore, this work introduces a simplified algorithm that optimizes channel assignment from a pool of channels while maximizing the total sum rate with a max-min approach. The results demonstrate that this algorithm is capable of approaching the performance of the exhaustive search algorithm, again with much lower computational complexity. Additionally, this thesis evaluated the average ergodic capacity of UAV-GS communication systems, specifically under the influence of HWIs and while the UAV is navigating in an arbitrary three-dimensional trajectory. The analytical derivation incorporated the averaging over the Rician parameter and the distance between the UAV and the GS. It obtained an approximate formula for the ergodic capacity and then validated the obtained results through simulations.

The findings highlight that HWIs can critically degrade the system's performance, pushing it into a saturation zone where increasing the transmitted power yields no further improvements. This saturation region can be mitigated by augmenting the number of transmitting antennas at the GS. Furthermore, it conducted an asymptotic analysis to investigate the system's performance when the transmitted power and the number of GS antennas are significantly large. Finally, this thesis studied a new communication system known as OAC assisted with UAV. Particularly, it examined the $\overline{\texttt{MSE}}$ of UAV-Assisted-OAC, considering the combined effects of HWIs and imperfect CSI. The focus was on scenarios where the UAV serves as the FC and communicates with K nodes. The results emphasized the significant influence of HWIs on the system's performance, revealing the existence of a saturation region where increasing the transmitted power no longer yields improvements. Additionally, it is noticed that imperfect CSI led to more severe degradation in system performance. Remarkably, it was observed that enhancing the system's performance can be achieved by increasing the number of nodes.

7.2 Future Work

A significant amount of work still needs to be completed, and more challenges need to be solved for UAVs deployments. One such challenge is resource management. This poses a significant issue in UAV networks due to various factors, including the complex interplay between UAV flight duration, energy consumption, path planning, and spectral efficiency. Additional challenges arise from the high mobility of UAVs and the LoS interference originating from ATG.

The optimization of three-dimensional UAVs trajectory presents a significant and complex challenge. To determine the path of UAVs in three dimensions, several crucial factors must be carefully considered. These factors encompass variations in the communication channel due to mobility, the dynamics of the UAVs themselves, the energy consumption of the UAVs, and the constraints imposed by flight regulations.

Moreover, it is vital to study interference management techniques to effectively minimize both ATG and air-to-air interference. This can be achieved through the development of more accurate models of interference in UAV-assisted wireless communication scenarios.

Additionally, exploring the potential of machine learning in enhancing wireless communication systems that rely on UAVs is essential. Machine learning techniques can enable UAVs to dynamically adjust their trajectories, thereby improving the QoS for ground users. Furthermore, the application of machine learning could facilitate the support of a large number of UAVs and WAPs with manageable computational complexity. Similarly, by leveraging neural network techniques and data analysis, UAVs can be strategically deployed based on predictions of ground users' behavior, such as their mobility patterns and traffic distribution.

It is also crucial to conduct comprehensive research on security and privacy concerns within UAV networks. This involves investigating scenarios where UAVs collect and transmit data to users. However, this process carries inherent risks, as malicious individuals could exploit UAV to gain unauthorized access to sensitive information. They may em-

ploy tactics such as obstructing network connections, intercepting transmitted data, or utilizing devices to interfere with the UAV's communication system.

Therefore, an efficient security management system is necessary to counteract malicious cyber-attacks in UAV networks. In addition to this, the application of quantum cryptography as a service can be explored for fortified UAVs communication. Given the limitations of conventional cryptography in ensuring secure communication, quantum cryptography has emerged as a proficient method for cohesive communication across air and ground networks. By utilizing a quantum connection, data can be protected with superior security protocols. Consequently, research focusing on quantum wireless networks is expected to witness substantial growth in both academic and industry sectors, propelled by the potential advantages it provides.

Bibliography

[1] G. T. Specification, "LTE; evolved universal terrestrial radio access (E-UTRA); base station (BS) radio transmission and reception," 2017.

[2] H. Holma and A. Toskala, *LTE for UMTS: Evolution to LTE-Advanced*. John Wiley & Sons, 2011.

[3] E. TS, "5G; NR; base station (BS) radio transmission and reception (3GPP TS 38.104 version 16.4.0 release 16)," *URL: https://www.etsi.org/deliver/etsi_ts/138100_138199/138104/16.04.00_60/ts_138104v160400p.pdf*, 2020.

[4] K. K. Vaigandla, S. Bolla, and R. Karne, "A survey on future generation wireless communications-6G: Requirements, technologies, challenges and applications," *International Journal*, vol. 10, no. 5, 2021.

[5] E. Björnson, J. Hoydis, and L. Sanguinetti, "Massive MIMO networks: Spectral, energy, and hardware efficiency," *Foundations and Trends in Signal Processing*, vol. 11, no. 3-4, pp. 154–655, 2017.

[6] X. You, C.-X. Wang, J. Huang, X. Gao, Z. Zhang, M. Wang, Y. Huang, C. Zhang, Y. Jiang, J. Wang, *et al.*, "Towards 6G wireless communication networks: Vision, enabling technologies, and new paradigm shifts," *Science China Information Sciences*, vol. 64, no. 1, pp. 1–74, 2021.

[7] J. G. Andrews, S. Buzzi, W. Choi, S. V. Hanly, A. Lozano, A. C. K. Soong, and J. C. Zhang, "What Will 5G Be?," *IEEE Journal on Selected Areas in Communications*, vol. 32, no. 6, pp. 1065–1082, Jun. 2014.

[8] S. Eswaran and P. Honnavalli, "Private 5G networks: a survey on enabling technologies, deployment models, use cases and research directions," *Telecommunication Systems*, vol. 82, no. 1, pp. 3–26, 2023.

[9] H. Q. Ngo, E. G. Larsson, and T. L. Marzetta, "Energy and spectral efficiency of very large multiuser MIMO systems," *IEEE Transactions on Communications*, vol. 61, no. 4, pp. 1436–1449, 2013.

[10] C. Kong, A. Mezghani, C. Zhong, A. L. Swindlehurst, and Z. Zhang, "Multipair massive MIMO relaying systems with one-bit ADCs and DACs," *IEEE Transactions on Signal Processing*, vol. 66, no. 11, pp. 2984–2997, 2018.

[11] F. Boccardi, R. W. Heath, A. Lozano, T. L. Marzetta, and P. Popovski, "Five disruptive technology directions for 5G," *IEEE Communications Magazine*, vol. 52, no. 2, pp. 74–80, 2014.

[12] A. E. Canbilen, S. S. Ikki, E. Basar, S. S. Gultekin, and I. Develi, "Joint impact of I/Q imbalance and imperfect CSI on SM-MIMO systems over generalized beckmann fading channels: Optimal detection and cramer-rao bound," *IEEE Trans. Wireless Commun.*, vol. 19, no. 5, pp. 3034–3046, 2020.

[13] Q. Wu and R. Zhang, "Intelligent reflecting surface enhanced wireless network via joint active and passive beamforming," *IEEE Transactions on Wireless Communications*, vol. 18, no. 11, pp. 5394–5409, 2019.

[14] S. A. H. Mohsan, M. A. Khan, F. Noor, I. Ullah, and M. H. Alsharif, "Towards the unmanned aerial vehicles (uavs): A comprehensive review," *Drones*, vol. 6, no. 6, p. 147, 2022.

[15] M. Alzenad, M. Z. Shakir, H. Yanikomeroglu, and M. Alouini, "FSO-Based Vertical Backhaul/Fronthaul Framework for 5G+ Wireless Networks," *IEEE Communications Magazine*, vol. 56, no. 1, pp. 218–224, Jan. 2018.

[16] A. Merwaday and I. Guvenc, "UAV assisted heterogeneous networks for public safety communications," in *2015 IEEE Wireless Communications and Networking Conference Workshops (WCNCW)*, pp. 329–334, 2015.

[17] I. Bucaille, S. Héthuin, A. Munari, R. Hermenier, T. Rasheed, and S. Allsopp, "Rapidly Deployable Network for Tactical Applications: Aerial Base Station with

Opportunistic Links for Unattended and Temporary Events ABSOLUTE Example," in *MILCOM 2013 - 2013 IEEE Military Communications Conference*, pp. 1116–1120, Nov. 2013.

[18] H. Ahmadi, K. Katzis, and M. Z. Shakir, "A Novel Airborne Self-Organising Architecture for 5G+ Networks," in *2017 IEEE 86th Vehicular Technology Conference (VTC-Fall)*, pp. 1–5, Sep. 2017.

[19] S. Meng, X. Su, Z. Wen, X. Dai, Y. Zhou, and W. Yang, "Robust drones formation control in 5G wireless sensor network using mmWave," *Wireless Communications and Mobile Computing*, May 2018.

[20] A. Al-Fuqaha, M. Guizani, M. Mohammadi, M. Aledhari, and M. Ayyash, "Internet of things: A survey on enabling technologies, protocols, and applications," *IEEE communications surveys & tutorials*, vol. 17, no. 4, pp. 2347–2376, Jun. 2015.

[21] T. Park, N. Abuzainab, and W. Saad, "Learning How to Communicate in the Internet of Things: Finite Resources and Heterogeneity," *IEEE Access*, vol. 4, pp. 7063–7073, 2016.

[22] A. Zanella, N. Bui, A. Castellani, L. Vangelista, and M. Zorzi, "Internet of Things for Smart Cities," *IEEE Internet of Things Journal*, vol. 1, no. 1, pp. 22–32, Feb. 2014.

[23] A. Ferdowsi and W. Saad, "Deep Learning-Based Dynamic Watermarking for Secure Signal Authentication in the Internet of Things," in *2018 IEEE International Conference on Communications (ICC)*, pp. 1–6, May 2018.

[24] K. Meng, Q. Wu, J. Xu, W. Chen, Z. Feng, R. Schober, and A. L. Swindlehurst, "UAV-enabled integrated sensing and communication: Opportunities and challenges," *IEEE Wireless Communications*, pp. 1–9, 2023.

[25] X. Wang, Z. Fei, J. A. Zhang, J. Huang, and J. Yuan, "Constrained utility maximization in dual-functional radar-communication multi-UAV networks," *IEEE Transactions on Communications*, vol. 69, no. 4, pp. 2660–2672, 2020.

[26] A. Liu, Z. Huang, M. Li, Y. Wan, W. Li, T. X. Han, C. Liu, R. Du, D. K. P. Tan, J. Lu, *et al.*, "A survey on fundamental limits of integrated sensing and communication," *IEEE Communications Surveys & Tutorials*, vol. 24, no. 2, pp. 994–1034, 2022.

[27] H. ALsmadi, H. Alsheyab, M. Alsmadi, E. Mohammed, Y. Alomari, and S. Ikki, "Less complex and higher spectral efficiency resource allocation algorithm for unmanned aerial vehicles networks," *IEEE Canadian Journal of Electrical and Computer Engineering*, vol. 45, no. 3, pp. 279–284, 2022.

[28] H. Alsmadi, H. Alsheyab, M. Alsmadi, and S. Ikki, "Less complex algorithm to max-min the resource allocation for unmanned aerial vehicles networks," in *2022 IEEE 95th Vehicular Technology Conference: (VTC2022-Spring)*, pp. 1–5, 2022.

[29] H. Alsmadi, E. Saleh, M. Alsmadi, and S. Ikki, "Capacity analysis of uav communications under the non-ideal transceiver effects," *IEEE Communications Letters*, pp. 1–1, 2023.

[30] L. A. Wolsey, *Integer programming*, vol. 52. John Wiley & Sons, Sep. 1998.

[31] J. Clausen, "Branch and bound algorithms-principles and examples," *Department of Computer Science, University of Copenhagen*, pp. 1–30, 1999.

[32] M. Fischetti and D. P. Williamson, *Integer Programming and Combinatorial Optimization*, vol. 4513. Springer, Jun. 2007.

[33] W. Kuhn, "The Hungarian method for the assignment problem," *Naval research logistics quarterly*, vol. 2, no. 1-2, pp. 83–97, Mar. 1955.

[34] S. A. W. Shah, T. Khattab, M. Z. Shakir, and M. O. Hasna, "A Distributed Approach for Networked Flying Platform Association with Small Cells in 5G+ Networks," in *GLOBECOM 2017-2017 IEEE Global Communications Conference*, pp. 1–7, Dec. 2017.

[35] E. Saleh, M. Alsmadi, and S. Ikki, "Energy efficiency and power allocation optimization in hardware-impaired full-duplex access point," in *GLOBECOM 2022-2022 IEEE Global Communications Conference*, pp. 3815–3820, IEEE, 2022.

[36] J. Qi and S. Aissa, "Analysis and compensation of power amplifier nonlinearity in MIMO transmit diversity systems," *IEEE Transactions on Vehicular Technology*, vol. 59, no. 6, pp. 2921–2931, 2010.

[37] M. H. N. Shaikh, V. A. Bohara, A. Srivastava, and G. Ghatak, "Performance analysis of intelligent reflecting surface-assisted wireless system with non-ideal

transceiver," *IEEE Open Journal of the Communications Society*, vol. 2, pp. 671–686, 2021.

[38] H. E. Rowe, "Memoryless nonlinearities with gaussian inputs: Elementary results," *The Bell System Technical Journal*, vol. 61, no. 7, pp. 1519–1525, 1982.

[39] O. T. Demir and E. Bjornson, "The Bussgang decomposition of nonlinear systems: Basic theory and MIMO extensions [lecture notes]," *IEEE Signal Processing Magazine*, vol. 38, no. 1, pp. 131–136, 2021.

[40] T. Schenk, *RF imperfections in high-rate wireless systems: impact and digital compensation*. Springer Science & Business Media, 2008.

[41] P. Zetterberg, "Experimental investigation of TDD reciprocity-based zero-forcing transmit precoding," *EURASIP Journal on Advances in Signal Processing*, vol. 2011, pp. 1–10, 2011.

[42] M. Wenk, *MIMO-OFDM-testbed: challenges, implementations, and measurement results: challenges, implementations, and measurement results*. PhD thesis, ETH Zurich, 2010.

[43] T. Aulin, "Characteristics of a digital mobile radio channel," *IEEE Transactions on Vehicular Technology*, vol. 30, no. 2, pp. 45–53, 1981.

[44] H. Suzuki, "A statistical model for urban radio propogation," *IEEE Transactions on Communications*, vol. 25, no. 7, pp. 673–680, 1977.

[45] M. Nakagami, "The m-distribution: a general formula of intensity distribution of rapid fading," in *Statistical methods in radio wave propagation*, pp. 3–36, Elsevier, 1960.

[46] Nakagami, "Some considerations on random phase problems from the standpoint of fading," *The Institute of Electrical and Communication Engineers Proceedings*, vol. 36, no. 11, pp. 595–602, 1953.

[47] M. A. Taneda, J.-I. Takada, and K. Araki, "The problem of the fading model selection," *IEICE Transactions on Communications*, vol. 84, no. 3, pp. 660–666, 2001.

[48] M. Yacoub, G. Fraidenraich, and J. Santos Filho, "Nakagami-m phase-envelope joint distribution," *Electronics Letters*, vol. 41, no. 5, pp. 259–261, 2005.

[49] M. D. Yacoub, "Nakagami-m phase-envelope joint distribution: A new model," *IEEE Transactions on Vehicular Technology*, vol. 59, no. 3, pp. 1552–1557, 2010.

[50] N. C. Sagias and G. K. Karagiannidis, "Effects of carrier phase error on EGC receivers in correlated Nakagami-m fading," *IEEE Communications Letters*, vol. 9, no. 7, pp. 580–582, 2005.

[51] R. K. Mallik, "A new statistical model of the complex Nakagami-m fading gain," *IEEE Transactions on Communications*, vol. 58, no. 9, pp. 2611–2620, 2010.

[52] L. Rayleigh, "XII. on the resultant of a large number of vibrations of the same pitch and of arbitrary phase," *The London, Edinburgh, and Dublin Philosophical Magazine and Journal of Science*, vol. 10, no. 60, pp. 73–78, 1880.

[53] S. Rice and N. Wax, "Statistical properties of random noise currents," 1954.

[54] M. K. Simon and M. Alouini, *Digital communication over fading channels: A Unified Approach to Performance Analysis*. New York: Wiley, 2001.

[55] J. Liu, J. Dai, J.-Y. Wang, J. Zhao, and C. Cheng, "Achievable rates for full-duplex massive MIMO systems over Rician fading channels," *IEEE Access*, vol. 6, pp. 30208–30216, 2018.

[56] Q. Zhang, S. Jin, K.-K. Wong, H. Zhu, and M. Matthaiou, "Power scaling of uplink massive MIMO systems with arbitrary-rank channel means," *IEEE Journal of Selected Topics in Signal Processing*, vol. 8, no. 5, pp. 966–981, 2014.

[57] Q. Ding, Y. Lian, and Y. Jing, "Performance analysis of full-duplex massive MIMO systems with low-resolution ADCs/DACs over Rician fading channels," *IEEE Transactions on Vehicular Technology*, vol. 69, no. 7, pp. 7389–7403, 2020.

[58] W. Wongtrairat and P. Supnithi, "New simple form for pdf and mgf of rician fading distribution," in *2011 International Symposium on Intelligent Signal Processing and Communications Systems (ISPACS)*, pp. 1–4, 2011.

[59] K. Nonami, F. Kendoul, S. Suzuki, W. Wang, and D. Nakazawa, *Autonomous flying robots: unmanned aerial vehicles and micro aerial vehicles*. Springer Science & Business Media, 2010.

[60] P. Basset, A. Tremolet, and T. Lefebvre, "Rotary wing UAV pre-sizing: past and present methodological approaches at onera," *Aerospace Lab*, no. 8, pp. 1–12, 2014.

[61] A. Al-Hourani, S. Kandeepan, and S. Lardner, "Optimal LAP Altitude for Maximum Coverage," *IEEE Wireless Communications Letters*, vol. 3, no. 6, pp. 569–572, Dec. 2014.

[62] F. A. d'Oliveira, F. C. L. d. Melo, and T. C. Devezas, "High-altitude platforms—present situation and technology trends," *Journal of Aerospace Technology and Management*, vol. 8, pp. 249–262, 2016.

[63] T. Lagkas, V. Argyriou, S. Bibi, and P. Sarigiannidis, "UAV iot framework views and challenges: Towards protecting drones as "things"," *Sensors*, vol. 18, no. 11, p. 4015, 2018.

[64] Y. Zeng, R. Zhang, and T. J. Lim, "Wireless communications with unmanned aerial vehicles: opportunities and challenges," *IEEE Communications Magazine*, vol. 54, no. 5, pp. 36–42, May 2016.

[65] M. Ding, P. Wang, D. López-Pérez, G. Mao, and Z. Lin, "Performance Impact of LoS and NLoS Transmissions in Dense Cellular Networks," *IEEE Transactions on Wireless Communications*, vol. 15, no. 3, pp. 2365–2380, Mar. 2016.

[66] T. Ding, M. Ding, G. Mao, Z. Lin, D. López-Pérez, and A. Y. Zomaya, "Uplink Performance Analysis of Dense Cellular Networks With LoS and NLoS Transmissions," *IEEE Transactions on Wireless Communications*, vol. 16, no. 4, pp. 2601–2613, Apr. 2017.

[67] M. Ding and D. Lopez Perez, "Please Lower Small Cell Antenna Heights in 5G," in *2016 IEEE Global Communications Conference (GLOBECOM)*, pp. 1–6, Dec. 2016.

[68] "Performance Impact of Base Station Antenna Heights in Dense Cellular Networks," *IEEE Transactions on Wireless Communications*, vol. 16, no. 12, pp. 8147–8161, Dec. 2017.

[69] I. H. Cihan, *Optimal path planning of an unmanned combat aerial vehicle with obstacle avoidance*. PhD thesis, University of Missouri–Columbia, 2016.

[70] G. Ding, Q. Wu, L. Zhang, Y. Lin, T. A. Tsiftsis, and Y. Yao, "An Amateur Drone Surveillance System Based on the Cognitive Internet of Things," *IEEE Communications Magazine*, vol. 56, no. 1, pp. 29–35, Jan. 2018.

[71] X. Liu, M. Qiu, X. Wang, W. Liu, and K. Cai, "Energy efficiency optimization for communication of air-based information network with guaranteed timing constraints," *Journal of Signal Processing Systems*, vol. 86, no. 2-3, pp. 299–312, Apr. 2016.

[72] M. Mozaffari, W. Saad, M. Bennis, and M. Debbah, "Drone Small Cells in the Clouds: Design, Deployment and Performance Analysis," pp. 1–6, Dec. 2015.

[73] M. S. Boosters, "DRONES vs BAD WEATHER,www.thatsclever.co.uk/drones-vs-bad-weather.."

[74] M. T. Linaza, J. Posada, J. Bund, P. Eisert, M. Quartulli, J. Döllner, A. Pagani, I. G. Olaizola, A. Barriguinha, T. Moysiadis, *et al.*, "Data-driven artificial intelligence applications for sustainable precision agriculture," *Agronomy*, vol. 11, no. 6, p. 1227, 2021.

[75] M. Mozaffari, W. Saad, M. Bennis, Y. Nam, and M. Debbah, "A Tutorial on UAVs for Wireless Networks: Applications, Challenges, and Open Problems," *IEEE Communications Surveys Tutorials*, vol. 21, no. 3, pp. 2334–2360, Mar. 2019.

[76] M. Erdelj and E. Natalizio, "UAV-assisted disaster management: Applications and open issues,"

[77] A. Restas, "Drone applications for supporting disaster management," *World Journal of Engineering and Technology*, vol. 3, no. 03, p. 316, Oct. 2015.

[78] T. J. Tanzi, M. Chandra, D. C. J. Isnard, O. Sébastien, and F. Harivelo, "Towards" drone-borne" disaster management: future application scenarios," in *XXIII ISPRS Congress, Commission VIII (Volume III-8)*, vol. 3, pp. 181–189, Copernicus GmbH, Jul. 2016.

[79] M. Mozaffari, W. Saad, M. Bennis, and M. Debbah, "Optimal transport theory for power-efficient deployment of unmanned aerial vehicles," in *2016 IEEE International Conference on Communications (ICC)*, pp. 1–6, May 2016.

[80] I. AlQerm and B. Shihada, "Energy-Efficient Power Allocation in Multitier 5G Networks Using Enhanced Online Learning," *IEEE Transactions on Vehicular Technology*, vol. 66, no. 12, pp. 11086–11097, Jul. 2017.

[81] M. Mozaffari, W. Saad, M. Bennis, and M. Debbah, "Wireless Communication Using Unmanned Aerial Vehicles UAVs: Optimal Transport Theory for Hover time Optimization, year=2017," *IEEE Transactions on Wireless Communications*, vol. 16, no. 12, pp. 8052–8066.

[82] R. Ghanavi, E. Kalantari, M. Sabbaghian, H. Yanikomeroglu, and A. Yongacoglu, "Efficient 3D aerial base station placement considering users mobility by reinforcement learning," in *2018 IEEE Wireless Communications and Networking Conference (WCNC)*, pp. 1–6, 2018.

[83] E. Kalantari, M. Z. Shakir, H. Yanikomeroglu, and A. Yongacoglu, "Backhaul-aware robust 3D drone placement in 5G+ wireless networks," in *2017 IEEE International Conference on Communications Workshops (ICC Workshops)*, pp. 109–114, 2017.

[84] S. A. W. Shah, T. Khattab, M. Z. Shakir, and M. O. Hasna, "Association of networked flying platforms with small cells for network centric 5G+ C-RAN," in *2017 IEEE 28th Annual International Symposium on Personal, Indoor, and Mobile Radio Communications (PIMRC)*, pp. 1–7, Oct. 2017.

[85] Z. Mlika, E. Driouch, W. Ajib, and H. Elbiaze, "A completely distributed algorithm for user association in HetSNets," in *2015 IEEE International Conference on Communications (ICC)*, pp. 2172–2177, Jun. 2015.

[86] S. A. W. Shah, M. G. Khafagy, T. Khattab, M. O. Hasna, and K. Abualsaud, "ICIC-Enabled Association and Channel Selection for UAV-BSs Based on User Locations and Demands," in *2019 IEEE Wireless Communications and Networking Conference Workshop (WCNCW)*, pp. 1–7, 2019.

[87] M. M. Alsmadi, A. E. Canbilen, N. Abu Ali, S. S. Ikki, and E. Basar, "Cognitive networks in the presence of I/Q imbalance and imperfect CSI: Receiver design and performance analysis," *IEEE Access*, vol. 7, pp. 49765–49777, 2019.

[88] M. Alsmadi, *The effects of I/Q imbalance and improper Gaussian noise on different wireless communication systems*. PhD thesis, Lakehead University, 2020.

[89] L. D. Le *et al.*, *Compensation of Physical Impairments in Multi-Carrier Communications*. PhD thesis, University of Saskatchewan, 2021.

[90] L. D. Le and H. H. Nguyen, "Compensation of phase noise and IQ imbalance in multi-carrier systems," *IEEE Access*, vol. 8, pp. 191263–191277, 2020.

[91] S. Zhou, W. Xu, K. Wang, M. Di Renzo, and M. Alouini, "Spectral and energy efficiency of IRS-assisted MISO communication with hardware impairments," *IEEE Wireless Communications Letters*, pp. 1–1, 2020.

[92] A. Bouhlel, , M. Alsmadi, E. Saleh, and S. Ikki, "Performance analysis of RIS-SSK in the presence of hardware impairments," in *2021 IEEE PIMRC Commun. Conf.*, pp. 1–6, 2021.

[93] E. Saleh, M. M. Alsmadi, A. Bouhlel, A. E. Canbilen, N. A. Ali, and S. Ikki, "Impact of channel correlation and hardware impairments on large intelligent surfaces-aided communication systems," in *2021 IEEE 32nd Annual International Symposium on Personal, Indoor and Mobile Radio Communications (PIMRC)*, pp. 805–810, 2021.

[94] C. H. Duc, S. Q. Nguyen, C.-B. Le, and N. T. V. Khanh, "Performance evaluation of UAV-based noma networks with hardware impairment," *Electronics*, vol. 11, no. 1, p. 94, 2022.

[95] N.-L. Nguyen, S.-P. Le, A.-T. Le, N. D. Nguyen, D.-T. Do, and M. Voznak, "UAV based satellite-terrestrial systems with hardware impairment and imperfect sic: Performance analysis of user pairs," *IEEE Access*, vol. 9, pp. 117925–117937, 2021.

[96] N. D. Nguyen and A.-T. Le, "Improving ergodic capacity of imperfect IoT system relying on UAV and noma," in *2021 10th International Conference on Information and Automation for Sustainability (ICIAfS)*, pp. 352–356, 2021.

[97] D. Deng, Y. Rao, and F. Zhu, "Impact of hardware impairments with imperfect channel estimation for cache-enabled UAV relaying networks," *Wireless Communications and Mobile Computing*, vol. 2020, pp. 1–12, 2020.

[98] V. Tentu, E. Sharma, D. N. Amudala, and R. Budhiraja, "UAV-enabled hardware-impaired spatially correlated cell-free massive mimo systems: Analysis and energy efficiency optimization," *IEEE Transactions on Communications*, vol. 70, no. 4, pp. 2722–2741, 2022.

[99] M. Agiwal, A. Roy, and N. Saxena, "Next generation 5G wireless networks: A comprehensive survey," *IEEE Communications Surveys & Tutorials*, vol. 18, no. 3, pp. 1617–1655, 2016.

[100] M. Z. Noohani and K. U. Magsi, "A review of 5G technology: Architecture, security and wide applications," vol. 07, pp. 3440–3471, 05 2020.

[101] J. Wang, C. Jiang, Z. Han, Y. Ren, R. G. Maunder, and L. Hanzo, "Taking drones to the next level: Cooperative distributed unmanned-aerial-vehicular networks for small and mini drones," *IEEE Vehicular Technology Magazine*, vol. 12, no. 3, pp. 73–82, 2017.

[102] M. Erdelj, E. Natalizio, K. R. Chowdhury, and I. F. Akyildiz, "Help from the sky: Leveraging UAVs for disaster management," *IEEE Pervasive Computing*, vol. 16, no. 1, pp. 24–32, 2017.

[103] B. Alzahrani, O. S. Oubbati, A. Barnawi, M. Atiquzzaman, and D. Alghazzawi, "UAV assistance paradigm: State-of-the-art in applications and challenges," *Journal of Network and Computer Applications*, vol. 166, p. 102706, 2020.

[104] R. Masroor, M. Naeem, and W. Ejaz, "Resource management in UAV-assisted wireless networks: An optimization perspective," *Ad Hoc Networks*, vol. 121, p. 102596, 06 2021.

[105] J. Hu, H. Zhang, L. Song, Z. Han, and H. V. Poor, "Reinforcement learning for a cellular internet of UAVs: Protocol design, trajectory control, and resource management," *IEEE Wireless Communications*, vol. 27, no. 1, pp. 116–123, 2020.

[106] S. Shah, T. Khattab, M. Shakir, M. Khafagy, and M. Hasna, "Small cell association with networked flying platforms: Novel algorithms and performance bounds," *arXiv preprint arXiv:1802.01117*, Feb. 2018.

[107] R. Duan, J. Wang, C. Jiang, H. Yao, Y. Ren, and Y. Qian, "Resource allocation for multi-UAV aided iot noma uplink transmission systems," *IEEE Internet of Things Journal*, vol. 6, no. 4, pp. 7025–7037, 2019.

[108] J. Wang, C. Jiang, Z. Wei, C. Pan, H. Zhang, and Y. Ren, "Joint UAV hovering altitude and power control for space-air-ground iot networks," *IEEE Internet of Things Journal*, vol. 6, no. 2, pp. 1741–1753, 2019.

[109] H. Y. Alsheyab, S. Choudhury, E. Bedeer, and S. S. Ikki, "Near-Optimal Resource Allocation Algorithms for 5G+ Cellular Networks," *IEEE Tran. on Veh. Tech.*, vol. 68, no. 7, pp. 6578–6592, Jul. 2019.

[110] E. Balas and E. Zemel, "An algorithm for large zero-one knapsack problems," *operations Research*, vol. 28, no. 5, pp. 1130–1154, Oct. 1980.

[111] M. R. Garey and D. S. Johnson, *Computers and intractability*, vol. 174. freeman San Francisco, 1990.

[112] Gurobi, "Gurobi Optimizer." http://www.gurobi.com/products/gurobi-optimizer.

[113] W. S. H. M. W. Ahmad, N. A. M. Radzi, F. S. Samidi, A. Ismail, F. Abdullah, M. Z. Jamaludin, and M. N. Zakaria, "5G technology: Towards dynamic spectrum sharing using cognitive radio networks," *IEEE Access*, vol. 8, pp. 14460–14488, 2020.

[114] H. Peng, C. Chen, C. C. Lai, L. C. Wang, and Z. Han, "A Predictive On-Demand Placement of UAV Base Stations Using Echo State Network," in *2019 IEEE/CIC International Conference on Communications in China (ICCC)*, pp. 36–41, 2019.

[115] M. Mozaffari, W. Saad, M. Bennis, and M. Debbah, "Optimal transport theory for cell association in UAV-enabled cellular networks," *IEEE Communications Letters*, vol. 21, no. 9, pp. 2053–2056, 2017.

[116] H. S. Khallaf and M. Uysal, "UAV-based fso communications for high speed train backhauling," in *2019 IEEE Wireless Communications and Networking Conference (WCNC)*, pp. 1–6, 2019.

[117] Matlab, "Matlab Optimizer." https://www.mathworks.com/help/optim/ug/fminimax.html.

[118] Y. Zeng, X. Xu, S. Jin, and R. Zhang, "Simultaneous navigation and radio mapping for cellular-connected UAV with deep reinforcement learning," *IEEE Transactions on Wireless Communications*, vol. 20, no. 7, pp. 4205–4220, 2021.

[119] O. J. Faqir, E. C. Kerrigan, and D. Gündüz, "Information transmission bounds between moving terminals," *IEEE Communications Letters*, vol. 24, no. 7, pp. 1410–1413, 2020.

[120] Indu, R. P. Singh, H. R. Choudhary, and A. K. Dubey, "Trajectory design for UAV-to-ground communication with energy optimization using genetic algorithm for agriculture application," *IEEE Sensors Journal*, vol. 21, no. 16, pp. 17548–17555, 2021.

[121] M. M. Azari, F. Rosas, K.-C. Chen, and S. Pollin, "Ultra reliable UAV communication using altitude and cooperation diversity," *IEEE Transactions on Communications*, vol. 66, no. 1, pp. 330–344, 2018.

[122] P. K. Sharma and P. K. Upadhyay, "Cognitive relaying with transceiver hardware impairments under interference constraints," *IEEE Commun. Lett.*, vol. 20, pp. 820–823, April 2016.

[123] D. K. Nguyen and H. Ochi, "On the impact of transceiver impairments to cognitive DF relay networks," in *2014 IEEE Asia Pacific Conf. on Cir.and Sys. (APCCAS)*, pp. 125–128, Nov 2014.

[124] A. M. Tota Khel and K. A. Hamdi, "Effects of hardware impairments on IRS-enabled MISO wireless communication systems," *IEEE Communications Letters*, vol. 26, no. 2, pp. 259–263, 2022.

[125] K. Guo and K. An, "On the performance of RIS-assisted integrated satellite-UAV-terrestrial networks with hardware impairments and interference," *IEEE Wireless Communications Letters*, vol. 11, no. 1, pp. 131–135, 2022.

[126] T. Shafique, H. Tabassum, and E. Hossain, "End-to-end energy-efficiency and reliability of UAV-assisted wireless data ferrying," *IEEE Transactions on Communications*, vol. 68, no. 3, pp. 1822–1837, 2020.

[127] C. Studer, M. Wenk, and A. Burg, "Mimo transmission with residual transmit-rf impairments," in *2010 International ITG Workshop on Smart Antennas (WSA)*, pp. 189–196, 2010.

[128] T. Schenk, *RF imperfections in high-rate wireless systems: impact and digital compensation*. Springer Science & Business Media, 2008.

[129] J.-M. Nicolas and F. Tupin, "A new parameterization for the Rician distribution," *IEEE Geoscience and Remote Sensing Letters*, vol. 17, no. 11, pp. 2011–2015, 2020.

[130] S.-J. Tu and E. Fischbach, "Random distance distribution for spherical objects: general theory and applications to physics," *Journal of Physics A: Mathematical and General*, vol. 35, pp. 6557–6570, jul 2002.

[131] J. Hagenauer, F. Dolainsky, E. Lutz, W. Papke, and R. Schweikert, "The maritime satellite communication channel–channel model, performance of modulation and coding," *IEEE Journal on Selected Areas in Communications*, vol. 5, no. 4, pp. 701–713, 1987.

[132] Iskandar and S. Shimamoto, "The channel characterization and performance evaluation of mobile communication employing stratospheric platform," in *IEEE/ACES International Conference on Wireless Communications and Applied Computational Electromagnetics, 2005.*, pp. 828–831, 2005.

[133] G. Zhu, J. Xu, K. Huang, and S. Cui, "Over-the-air computing for wireless data aggregation in massive IoT," *IEEE Wireless Communications*, vol. 28, no. 4, pp. 57–65, 2021.

[134] Z. Chen and Y. Malitsky, "Over-the-air computation with multiple receivers: A space-time approach," *IEEE Wireless Communications Letters*, pp. 1–1, 2023.

[135] W. Liu, X. Zang, Y. Li, and B. Vucetic, "Over-the-air computation systems: Optimization, analysis and scaling laws," *IEEE Transactions on Wireless Communications*, vol. 19, no. 8, pp. 5488–5502, 2020.

[136] G. Zhu and K. Huang, "MIMO over-the-air computation for high-mobility multimodal sensing," *IEEE Internet of Things journal*, vol. 6, no. 4, pp. 6089–6103, 2018.

[137] M. Goldenbaum and S. Stanczak, "On the channel estimation effort for analog computation over wireless multiple-access channels," *IEEE Wireless Communications Letters*, vol. 3, no. 3, pp. 261–264, 2014.

[138] X. Zhai, G. Han, Y. Cai, Y. Liu, and L. Hanzo, "Simultaneously transmitting and reflecting (STAR) RIS assisted over-the-air computation systems," *IEEE Transactions on Communications*, vol. 71, no. 3, pp. 1309–1322, 2023.

[139] E. Saleh, M. M. Alsmadi, and S. Ikki, "Spectral-Energy efficiency and power allocation in full-duplex networks: The effects of hardware impairment and Nakagami-

m fading channels," *IEEE Transactions on Vehicular Technology*, vol. 72, no. 1, pp. 772–788, 2023.

[140] K. Guo and K. An, "On the performance of RIS-assisted integrated satellite-UAV-terrestrial networks with hardware impairments and interference," *IEEE Wireless Communications Letters*, vol. 11, no. 1, pp. 131–135, 2022.

[141] H. V. Balan, R. Rogalin, A. Michaloliakos, K. Psounis, and G. Caire, "AirSync: Enabling distributed multiuser MIMO with full spatial multiplexing," *IEEE/ACM Transactions on Networking*, vol. 21, no. 6, pp. 1681–1695, 2013.

[142] K. Chintalapudi, B. Radunovic, H. V. Balan, M. Buettener, S. Yerramalli, V. Navda, and R. Ramjee, "WiFi-NC: WiFi over narrow channels.," in *NSDI*, vol. 12, pp. 4–4, 2012.

[143] W. Khawaja, I. Guvenc, D. W. Matolak, U.-C. Fiebig, and N. Schneckenburger, "A survey of air-to-ground propagation channel modeling for unmanned aerial vehicles," *IEEE Communications Surveys and Tutorials*, vol. 21, no. 3, pp. 2361–2391, 2019.

[144] K. Buchanan and G. H. Huff, "A stochastic mathematical framework for the analysis of spherically-bound random arrays," *IEEE transactions on antennas and propagation*, vol. 62, no. 6, pp. 3002–3011, 2014.

[145] X. Cao, G. Zhu, J. Xu, and K. Huang, "Optimized power control for over-the-air computation in fading channels," *IEEE Transactions on Wireless Communications*, vol. 19, no. 11, pp. 7498–7513, 2020.

[146] W. Liu, X. Zang, Y. Li, and B. Vucetic, "Over-the-air computation systems: Optimization, analysis and scaling laws," *IEEE Transactions on Wireless Communications*, vol. 19, no. 8, pp. 5488–5502, 2020.

[147] H. Jung and I.-H. Lee, "Outage analysis of millimeter-Wave wireless backhaul in the presence of blockage," *IEEE Communications Letters*, vol. 20, no. 11, pp. 2268–2271, 2016.

[148] N. Papadatos, "Maximum variance of order statistics," *Annals of the Institute of Statistical Mathematics*, vol. 47, pp. 185–193, 1995.

[149] J. Royston *et al.*, "Expected normal order statistics (exact and approximate)," *Journal of the Royal Statistical Society Series C (Applied Statistics)*, vol. 31, no. 2, pp. 161–165, 1982.

[150] R. Rogalin, O. Y. Bursalioglu, H. Papadopoulos, G. Caire, A. F. Molisch, A. Michaloliakos, V. Balan, and K. Psounis, "Scalable synchronization and reciprocity calibration for distributed multiuser MIMO," *IEEE Transactions on Wireless Communications*, vol. 13, no. 4, pp. 1815–1831, 2014.

[151] N. C. Beaulieu, M. Naseri, and J. Cheng, "Novel theoretical performance comparisons of open-loop and closed-loop timing recovery in Rayleigh fading channels with and without a receiver outage condition," *IEEE Wireless Communications Letters*, vol. 8, no. 5, pp. 1448–1451, 2019.